Coordination Chemistry Reviews 365 (2018) 75–102

Contents lists available at ScienceDirect

Coordination Chemistry Reviews

journal homepage: www.elsevier.com/locate/ccr

Review

Rationally designed mimics of antioxidant manganoenzymes: Role of structural features in the quest for catalysts with catalase and superoxide dismutase activity

Sandra Signorella *, Claudia Palopoli, Gabriela Ledesma

IQUIR (Instituto de Química Rosario), Consejo Nacional de Investigaciones Científicas y Técnicas (CONICET), Facultad de Ciencias Bioquímicas y Farmacéuticas, Universidad Nacional de Rosario, Suipacha 531, S2002LRK Rosario, Argentina

ARTICLE INFO

Article history:
Received 2 January 2018
Accepted 5 March 2018

ABSTRACT

Manganese catalases (MnCAT) and superoxide dismutases (MnSOD) deplete hydrogen peroxide and superoxide in cells through a ping-pong mechanism involving cyclic oxidation and reduction of the metal cofactor. In a variety of pathological situations, the generation of reactive oxygen species overwhelms the capacity of endogenous scavengers and tissues become vulnerable to damage. Due to the limited success of the use of exogenous SOD and CAT as therapeutic agents to reduce oxidative stress damage,

Abbreviations: Adpa, bis(2-pyridylmethyl)amino-2-propionic acid; [15]aneN$_5$, 1,4,7,10,13-pentaazacyclopentadecane; baba, bis(*N*-allylbenzimidazol-2-ylmethyl)aniline; Bbzimpy, 2,6-bis(1-butyl-1H-benzo[*d*]imidazol-2-yl)pyridine; BIG, *N*,*N*-bis[(1-methyl-2-imidazolyl)methyl]glycinate; Bimtacn, 1,4-bis(benzimidazol-2-ylmethyl)-1,4,7-triazacyclononane; BimindH, 1,3-bis(2′-benzimidazolylimino)isoindoline; BMPG, *N*,*N*-bis[(6-methyl-2-pyridyl)methyl]glycinate; BSA, bovine serum albumin; 2-(CH$_2$)$_2$OHpy, 2-hydroxyethylpyridine; 2-CH$_2$OHpy, 2-hydroxymethylpyridine; CDL, 6^A-deoxy-6^A[(*S*-cysteamidobenzoyl(3,4-diamino)-*N*,*N*′-bis(salicylidene))]-β-cyclodextrin; CM-PVIm, carboxymethylpoly(1-vinylimidazole); Cy[15]aneN$_5$, 2,3,8,9-bis-cyclohexano-1,4,7,10,13-pentaazacyclopentadecane; CySalen, *N*,*N*′-bis(salicylidene)-1,2-diaminocyclohexane; CySalenSO$_3$, *N*,*N*′-bis(5-sulfonatosalicylidene)-(*R*,*R*)-1,2-diaminocyclohexane; Csalophen, *N*,*N*′-bis(salicylidene)-3,4-diaminobenzoic acid; Etobb, 1,3-bis(1-ethylbenzimidazol-2-yl)-2-oxopropane; EUK-108, [Mn(III)salen(OAc)]; EUK-113, [Mn(III)(3-OMe-salen)(OAc)]; EUK-172, [Mn(III)(salophen)(OAc)]; EUK-207, Mn(III) complex of a cyclic salen-crown ether; Hbpg, bis-2-picolylglycylamine; H$_2$dapsox, 2,6-diacetylpyridinebis(semioxamazide); H$_2$Daphp, 2,6-bis((2-(pyridin-2-yl)hydrazono)ethyl)pyridine; H$_2$Dcphp, *N*′^{2}, *N*′^{6}-di(pyridin-2-yl)pyridine-2,6-dicarbohydrazide; HEPES, 4-(2-hydroxyethyl)piperazine-1-ethanesulfonic acid; H$_3$L6, 1-[*N*-(2-pyridylmethyl),*N*-(2-hydroxybenzyl)amino]-3-[*N*′-(2-hydroxybenzyl),*N*′-(4-methylbenzyl)amino]propan-2-ol; HL12, 2-{[[di(2-pyridyl)methyl](methyl)amino]methyl}phenol; HL13, Bis(pyrazol-1-yl)acetic acid; HPBMPA, *N*-propanoate-*N*,*N*-bis-(2-pyridylmethyl)amine; HPClNOL, 1-[bis(pyridin-2-ylmethyl)amino]-3-chloropropan-2-ol; H$_2$pda, 2-picolyldiglycylamine; Hptp1, *N*-(2-hydroxy-5-methylbenzyl)-*N*,*N*′,*N*′-tris(2-pyridinylmethyl)-1,2-ethanediamine; H$_2$qtp1, *N*-(2,5-dihydroxybenzyl)-*N*,*N*′,*N*′-tris(2-pyridinylmethyl)-1,2-ethanediamine; H$_2$pyr$_2$en, 1,2-bis(pyridoxylidenamino)ethane; H$_2$pyr$_2$pn, 1,3-bis(pyridoxylidenamino)propane; HSA, human serum albumin; HSJ-0017, manganese(III) 5,10,15,20-tetrakis[3-(2-(2-methoxy)-ethoxy)ethoxy]phenyl porphyrin chloride; HSM, hollow silica microspheres; HSX-salophOMe, Hangman salophen xanthene ligand; HSX, ^{t}Bu-Cysalen, Hangman salen xanthene ligand; Imtacn, 1-(benzimidazol-2-ylmethyl)-1,4,7-triazacyclononane; IndH, 1,3-bis(2′-pyridylimino)isoindoline; IPG, *N*-[(1-methyl-2-imidazolyl)methyl]-*N*-(2-pyridylmethyl)glycinate; L1, [*N*-(3,5-di-*tert*-butyl-4-hydroxybenzyl)-*N*,*N*-di(2-pyridylmethyl)]amine; L2H, 2-(benzyl(2-(bis(pyridin-2-ylmethyl)amino)ethyl)amino)acetic acid; L3, *N*,*N*′-dimethyl-*N*,*N*′-bis(2-pyridylmethyl)ethane-1,2-diamine; L4H, *N*-(2-hydroxybenzyl)-*N*,*N*′-bis[2-(N-methylimidazolyl)methyl]ethane-1,2-diamine; L5, *N*-methyl-*N*,*N*′,*N*′-tris(2-pyridylmethyl)ethane-1,2-diamine; L7, pyridine pentaazamacrocyclic ligand with acid/base auxiliary; L8–10, Me$_2$-pyane functionalized with alkyl ether chains: C$_{12}$H$_{25}$ (L8), C$_{16}$H$_{33}$ (L9), C$_{22}$H$_{45}$ (L10); L11, 4,10-dimethyl-1,4,7,10-tetraazacyclododecane-1,7-diacetate; M40401, manganese(II)dichlorido{2*S*,21*S*-dimethyl-(4*R*,9*R*,14*R*,19*R*)-3,10,13,20,26-pentaazatetracyclo[20.3.1.0^{4,9}0^{14,19}]hexacosa-1(26),22(23),24-triene}; M40403, manganese(II)dichlorido{(4*R*,9*R*,14*R*,19*R*)-3,10,13,20,26-pentaazatetracyclo[20.3.1.0^{4,9}0^{14,19}]hexacosa-1(26),-22(23),24-triene}; M40404, manganese(II)dichlorido{2*R*,21*R*-dimethyl-(4*R*,9*R*,14*R*,19*R*)-3,10,13,20,26-pentaazatetracyclo[20.3.1.0^{4,9}0^{14,19}]hexacosa-1(26),22(23),24-triene}; 4′MeIndH, 1,3-bis(4′-methyl-2′-pyridylimino)isoindoline; Me-PhimpH, 2-(1-(2-phenyl-2-(pyridine-2-yl)hydrazono)ethyl)phenol; Me$_2$EBC, 4,11-dimethyl-1,4,8,11-tetraazabicyclo[6.6.2]hexadecane; Me$_2$-Pyane, Me$_2$[15]pyridinaneN$_5$, *trans*-2,13-dimethyl-3,6,9,12,18-pentaazabicyclo [12.3.1]octadeca-1(18),14,16-triene; Me$_2$-Pyene, 2,13-dimethyl-3,6,9,12,18-pentaazabicyclo[12.3.1]-octadeca-1(18),2,12,14,16-pentaene; MPBMPA, methyl 3-[bis(2-pyridylmethyl)amino]propanoate; MnPD, 1,3-di[5-(*N*-methylene-pyridinium-4-yl)-10,15,20-triphenylporphynato manganese(III)]; M4PyP$_3$P, 5-(*N*-methylpyridinium-4-yl)-10,15,20-triphenyl porphyrin; N4py, *N*,*N*-bis(2-pyridylmethyl)-*N*-bis(2-pyridyl)methylamine; naphtophen, 1,2-bis((2-hydroxynaphthalen-1-yl)methyleneamino)benzene; naphpn, 1,3-bis((2-hydroxynaphthalen-1-yl)methyleneamino)propane; NBT, nitrobluetetrazolium; N-PhimpH, 2-((2-phenyl-2-(pyridin-2-yl)hydrazono)methyl)napthalen-1-ol; P^1, [Mn(III)-*meso*-tri(*N*-methylpyridinium-4-yl)mono(4-carboxyphenyl)porphyrin]; P^2, [Mn(III)-*meso*-tri(*N*-methylpyridinium-4-yl)mono(*N*-4-carboxybenzyl-4-pyridyl)porphyrin]; PBMPA, 3-[bis(2-pyridylmethyl)amino]propanoate; PEG, polyethyleneglycol; PhIH, 4-(2-salicylamino-ethyl)-imidazole; PhimpH, 2-((2-phenyl-2-(pyridin-2-yl)hydazono)methyl)phenol; Pi, inorganic phosphate; PI$^-$, 2-{[(1-methyl-2-imidazolyl)methyl]amino}phenolate; Pimp, pyridine-2,6-bis(carbaldehydeimine-2-hydroxyphenyl); Pyane, pyridine[15]aneN$_5$, 3,6,9,12,18-pentaazabicyclo[12.3.1]octadeca-1(18),14,16-triene; Py$_2$N$_2$, 2,11-diaza-[3,3](2,6)pyridinophane; S-1, (*1S*,*2S*)-*N*,*N*′-bis-[3-*tert*-butyl-5-chloromethyl-salicylidine]-1,2-cyclohexanediamine; S1m, chiral macrocyclic salen ligand; SalbutOH, 1,4-bis(salicylidenamino)butan-2-ol; Salen, 1,2-bis(salicylidenamino)ethane; Salophen, *N*,*N*′-bis(salicyliden)-1,2-phenylendiamine; Salpn, 1,3-bis(salicylidenamino)propane; SalpnOH, 1,3-bis(salicylidenamino)propan-2-ol; SL, aza-scorpiand like macrocycles; S$_2$Py$_3$, 2,6-bis[((2-pyridylmethyl)thio)methyl]pyridine; TBAP, 5,10,15,20-tetrakis(4-benzoate)porphyrin; TDMImP, 5,10,15,20-tetrakis-(1,3-dimethylimidazolium-2-yl)porphyrin; TE-2-PyP, 5,10,15,20-tetrakis(*N*-ethyl-2-pyridyl)porphyrin; TECP, 5,10,15,20-tetrakis-(ethoxycarbonyl)porphyrin; TM-2-PyP, 5,10,15,20-tetrakis(*N*-methyl-2-pyridyl)porphyrin; TM-3-PyP, 5,10,15,20-tetrakis(*N*-methyl-3-pyridyl)porphyrin; TM-4-PyP, 5,10,15,20-tetrakis-(*N*-methyl-4-pyridyl)porphyrin; TMIMA, tris[(1-methyl-2-imidazolyl)methyl]amine; TnBuOE-2-PyP, 5,10,15,20-tetrakis(*N*-(2′-n-butoxyethyl)pyridinium-2-yl)porphyrin; TnHex-3-PyP, 5,10,15,20-tetrakis(*N*-hexyl-3-pyridyl)porphyrin.

* Corresponding author.
E-mail address: signorella@iquir-conicet.gov.ar (S. Signorella).

https://doi.org/10.1016/j.ccr.2018.03.005
0010-8545/© 2018 Elsevier B.V. All rights reserved.

Keywords:
Manganese complexes
Catalase mimics
Superoxide dismutase mimics
Structure/activity

investigations have been directed to the design of low molecular-weight antioxidant catalysts (SOD- or CAT-mimics). To disproportionate superoxide and hydrogen peroxide efficiently, the reduction potential of MnSOD and MnCAT is fine-tuned to values much lower than that of the $Mn^{3+}(aq)/Mn^{2+}(aq)$ couple. In the artificial catalysts, the number and type of ligands, the local charge, the geometry around the metal, are among the factors that introduce a way of tuning the redox potential of Mn to face redox reactions. However structural and electronic factors affecting SOD activity do not parallel those controlling CAT activity. This review focus on synthetic mononuclear Mn complexes with SOD and/or CAT activity, stressing the role of ligand donor sites, endogenous acid/base groups, metal environment and second-sphere effects in the catalytic activity.

© 2018 Elsevier B.V. All rights reserved.

Contents

1. Introduction

Molecular oxygen is indispensable to the life on this planet and essential for efficient aerobic metabolism where the four electron reduction of O_2 to water constitutes the terminal reaction of the aerobic respiratory chain. However, during normal cellular metabolism, O_2 can be converted to the superoxide radical anion ($O_2^{\cdot-}$), a deleterious reduction intermediate species which is the primary source for other reactive oxygen species (ROS) such as hydrogen peroxide (H_2O_2) and hydroxyl radical ($HO^{\cdot}$). These powerful oxidants can attack tissues, membranes and their proteic environment, thereby turning into lethal agents against cell structure and functioning. *In vivo* protection occurs via suppression of the ROS cytotoxins through a cascade of dismutation processes. These reactions are mediated by two key classes of metalloenzymes: superoxide dismutases (SODs) and catalases (CATs). Dismutation of $O_2^{\cdot-}$ leads to O_2 and H_2O_2 either spontaneously or through the enzymatic processes catalyzed by SODs [1]. As a consequence, wherever $O_2^{\cdot-}$ is generated, H_2O_2 is also formed. H_2O_2 is stable at biological pH, easily crosses lipid membranes [2] and can readily react with reduced transition metal ions to generate the highly reactive $HO^{\cdot}$ by Fenton-like reactions [3]. Accordingly, full detoxification of $O_2^{\cdot-}$ may not be achieved by SOD alone, but only when it is coupled to CAT, the enzyme that catalyzes the disproportionation of H_2O_2 to molecular oxygen and water [4]. In a variety of pathological situations, ROS generation overwhelms the capacity of endogenous scavengers to neutralize them and tissues become vulnerable to damage. Exogenous SOD and CAT have been used as therapeutic agents to reduce oxidative stress damage [5], although with limited success [6]. The major limitations associated with the therapeutic applications of these enzymes are their large size, solution instability, short half-lives, antigenicity and high-manufacturing costs [7]. To overcome these limitations, investigations have been directed to the design of low molecular-weight antioxidant catalysts (SOD- or CAT-mimics) [8]. These catalytic ROS scavengers would be clinically superior to stoichiometric ones [9] and should have better bioavailability than exogenously administered antioxidant enzymes. Among them, manganese based mimics are the most widely investigated, mainly because of its low toxicity (Mn is not prone to generate $HO^{\cdot}$ in Fenton type reactions) compared, for instance, to iron or copper in the case that free metal is released from the catalyst [10]. Most of these manganese-based catalytic antioxidants have been tested as decomposition catalysts for $O_2^{\cdot-}$. However, since catalase activity would be a key attribute for synthetic ROS scavenging compounds, some efforts have focused on development of catalysts with dual SOD/CAT activity for possible therapeutic use. This review focus on advances on synthetic Mn complexes with SOD and/or CAT activity that can be used as artificial small molecule catalysts for ROS detoxification, with emphasis on the role of redox potentials, coordination geometry and ligands donor sites in the mimicking activity. Our purpose is to compare structural and electronic properties of manganese complexes with SOD, CAT or dual SOD/CAT activity and analyze how these features modulate their reactivity.

2. Manganese superoxide dismutases and catalases

2.1. Manganese superoxide dismutase (MnSOD)

In water, $O_2^{\bullet-}$ disproportionates into O_2 and H_2O_2 spontaneously with second order kinetics and strong dependence on pH. The maximum rate for $O_2^{\bullet-}$ self-disproportionation is observed at pH = pK_a = 4.8, where $k_{disp} = 9.7 \times 10^7\ M^{-1}\ s^{-1}$ [11]. The value of k_{disp} decreases to $8.3 \times 10^5\ M^{-1}\ s^{-1}$ at low pH, it is around $5 \times 10^5\ M^{-1}\ s^{-1}$ at pH 7, and no reaction occurs at high pH where deprotonated $O_2^{\bullet-}$ radicals repel each other and bare O_2^{2-} is unstable. In aqueous solutions, the potentials for the one electron $O_2^{\bullet-}$ reduction and oxidation are $E_{O_2^{\bullet-}/H_2O_2}^{H_2O} = 0.89$ V (vs NHE at pH 7) and $E_{O_2/O_2^{\bullet-}}^{-H_2O} = -0.16$ V (vs NHE at pH 7), respectively. An electron transfer to bare $O_2^{\bullet-}$ is almost impossible because the product of this reaction, peroxide dianion, is highly unstable. Therefore, the reduction of superoxide $O_2^{\bullet-}$ is either a proton-coupled process or metal-assisted reaction, where the latter requires coordination of $O_2^{\bullet-}$ and subsequent inner-sphere electron transfer. The above potentials correspond to outer-sphere reduction and oxidation of $O_2^{\bullet-}$ and differ from those of coordinated superoxide which depends on the nature of the ligand, charge density and electronic properties of the metal center. In particular the reduction potential of coordinated $O_2^{\bullet-}$ is expected to shift toward more positive values because peroxide, the reduction product, is significantly stabilized by coordination to a metal center [12].

SOD enzymes transform the second-order disproportionation of $O_2^{\bullet-}$ to a sequence of two first-order reactions in $[O_2^{\bullet-}]$ and proceed to near the diffusion controlled limit with very little variation over the physiologically relevant pH range [13]. At physiological pH the enzyme has an overall negative charge. A positively charged loop is present in all known SODs and contributes local electrostatic effects to guide $O_2^{\bullet-}$ from the protein exterior towards the metallic active site [1]. MnSOD enzymes catalyze $O_2^{\bullet-}$ disproportionation through a ping-pong mechanism with $O_2^{\bullet-}$ acting alternately to reduce the Mn(III) ion and oxidize Mn(II) ion. To disproportionate $O_2^{\bullet-}$ efficiently, the reduction potential of MnSOD is fine-tuned by the protein environment to 0.29 V [14] a value much lower than for the $Mn^{3+}_{(aq)}/Mn^{2+}_{(aq)}$ couple (1.54 V vs NHE).

The active site of MnSODs is invariant, with one manganese ion in a trigonal bipyramidal structure bound to two histidines and one aspartate in the equatorial plane, and a third histidine and one OH^- ion/H_2O molecule in axial positions [15] (Fig. 1). This site undergoes little change in geometry when the enzyme is oxidized or reduced. The manganese is occluded from the solvent and surrounded by a hydrogen-bonded network that extends from the bound water and comprises the side chains of several residues; among them a tyrosine and a glutamine (Tyr34 and Gln143, in human MnSOD), and an adjacent water molecule that sits at the opening of the cavity. The role of the hydrogen bonded network is presumably to facilitate proton transfer during reduction of $O_2^{\bullet-}$ to H_2O_2.

MnSODs have different cellular activities at high and low concentrations of superoxide, as a result of a phenomenon known as "gating" [16]. A proposed mechanism that can explain the kinetics involves two parallel pathways for reaction of the reduced MnSOD with superoxide (Scheme 1). In this mechanism, the $O_2^{\bullet-}$ is rapidly converted to H_2O_2 or binds to the manganese site, forming a Mn(II)superoxo or Mn(III)peroxo complex ($MnO_2^+(H_2O)$), which is known as "inhibited complex" and that after protonation releases H_2O_2.

The gating mechanism was attributed to a conformational change or a reversible isomerization where the bound peroxy moiety isomerizes from a *side-on* to an *end-on* configuration [1]. Modification of residues belonging to the hydrogen-bonding network

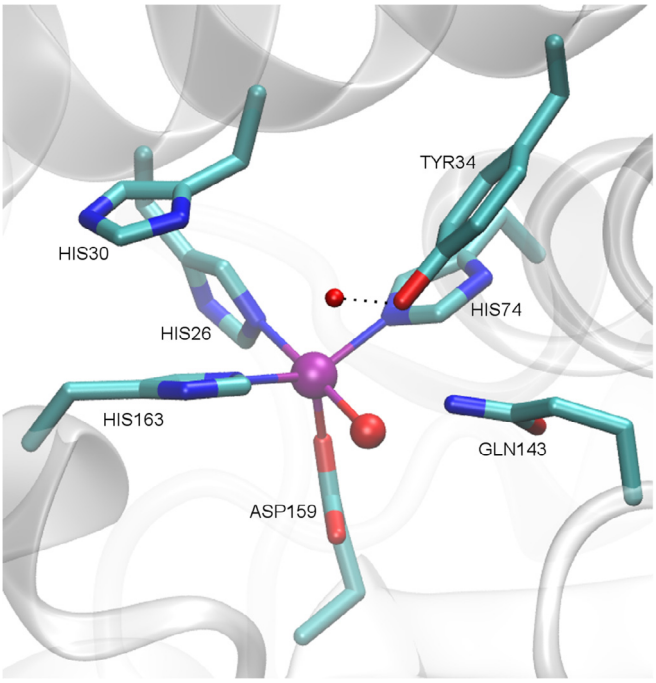

Fig. 1. Crystal structure of the manganese active site of wild type human MnSOD adapted from PDB code: 1LUV.

$$Mn^{3+}SOD(OH^-) + O_2^{\bullet-}(+H^+) \rightarrow Mn^{2+}SOD(H_2O) + O_2 \quad (1)$$

$$Mn^{2+}SOD(H_2O) + O_2^{\bullet-}(+H^+) \rightarrow Mn^{3+}SOD(OH^-) + H_2O_2 \quad (2)$$

$$Mn^{2+}SOD(H_2O) + O_2^{\bullet-} \rightarrow MnO_2^+SOD(H_2O) \quad (3)$$

$$MnO_2^+SOD(H_2O)(+H^+) \rightarrow Mn^{3+}SOD(OH^-) + H_2O_2 \quad (4)$$

Scheme 1. Proposed mechanism for $O_2^{\bullet-}$ disproportionation by MnSOD.

produced impressive changes in mechanism, as observed for Tyr34Phe [17], His30Asn [18] and Gln143Ala [19] mutants of human MnSOD; the last perturbation resulting in a dramatic loss of activity, thus evidencing its important role in catalysis. It was proposed that during catalysis, the metal alternates between five- and six-coordination [20] through inner-sphere electron transfer processes, with coordinated OH^-/H_2O acting as proton acceptor/donor to assist the redox reaction with minimal disturbance of the metal environment [1].

2.2. Manganese catalases (MnCAT)

The disproportionation of H_2O_2 is a thermodynamically favorable process ($\Delta G° = -233.56$ kJ mol^{-1}) but proceeds slowly in the absence of catalyst. The rapid and efficient removal of H_2O_2 is essential to all aerobically living prokaryotic and eukaryotic cells and nature has developed catalase enzymes to catalyze the redox disproportionation of hydrogen peroxide into dioxygen and water at reasonable rates [21]. Although the majority of known catalase enzymes are iron-heme-based enzymes, several organisms utilize non-heme manganese-containing enzymes to disproportionate hydrogen peroxide that are widespread among prokaryotes and have been isolated from bacteria, a hyperthermophilic archeon, and some cyanobacteria [21a,c]. All known MnCAT enzymes share an unusual bridged binuclear manganese cluster that serves as the active site to perform the efficient two-electron disproportionation

of H_2O_2, interconverting between reduced $Mn(II)_2$ and oxidized $Mn(III)_2$ states during turnover [22]. At pH 7, the electrochemical potentials for the two electron O_2/H_2O_2 and H_2O_2/H_2O redox couples are +0.28 and +1.35 V (vs NHE), respectively. To efficiently catalyze the H_2O_2 disproportionation, the protein environment controls the reduction potential of the dimanganese active site to a value much lower than that of the $Mn^{3+}_{(aq)}/Mn^{2+}_{(aq)}$ couple (1.54 V), and facilitates the two electron redox half-reactions through a "ping-pong" mechanism (Eqs. (5) and (6)), without formation of hydroxyl radicals [23].

$$Mn(III)_2CAT + H_2O_2 \rightarrow Mn(II)_2CAT(+2H^+) + O_2 \quad (5)$$

$$Mn(II)_2CAT(+2H^+) + H_2O_2 \rightarrow Mn(III)_2CAT + 2H_2O \quad (6)$$

In the active site of these enzymes the two Mn ions are each coordinated in the equatorial plane to one His residue and one Glu residue as terminal ligands (Fig. 2), and are triply bridged by a $\mu_{1,3}$-carboxylate ligand from a Glu residue and two solvent-derived μ-oxygen bridges (either aqua, hydroxo, or oxo ligands). Also, a solvent-derived ligand is bound to one of the Mn ions in the sixth position. Substrate binding to the $Mn(III)_2$ form of the enzyme is presumed to occur by displacing this terminally bound solvent molecule coupled to proton transfer to the μ-oxo bridge, followed by reduction of the dimanganese center and release of O_2 [4,24]. A second H_2O_2 molecule is proposed to bind to the $Mn(II)_2$ form of the enzyme as a bridging $\mu_{1,1}$-hydroperoxo, that after protonation undergoes heterolytic O—O bond cleavage coupled to reoxidation of the diMn centre with loss of water, to complete the catalytic cycle.

Terminal and bridging peroxide binding to the $Mn(III)_2$ and $Mn(II)_2$ forms of the enzyme, respectively, are supported by X-ray studies of the azide and halide inhibited enzyme [4,22b,24]. Besides, hyperfine parameters obtained from 2D ^1H and ^{14}N HYSCORE spectroscopy on the superoxidized Mn(III)Mn(IV) form of the enzyme provided direct evidence that the water molecule is coordinated to one of the Mn ions of MnCAT and is replaced by the N_3^- ion in the azide-treated enzyme [25]. A comparison of experimental and broken symmetry density functional theory calculated ^{14}N, ^{17}O, and ^1H hyperfine couplings showed that in the superoxidized enzyme water is coordinated to the Mn(IV) ion [26]. The presence of donor/acceptor residues near the active site (e.g., Glu178 in MnCAT from *Lactobacillus plantarum*, Fig. 2) facilitates proton transfer between nonadjacent atoms in the complex and is central for efficient catalysis.

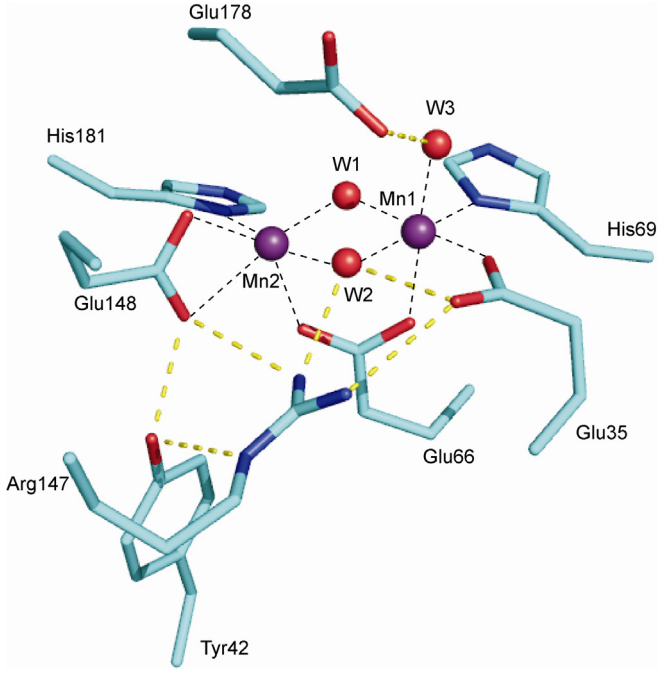

Fig. 2. Crystal structure of the dimanganese active site of native MnCAT from *L. plantarum* adapted from PDB ID 1JKU.

3. Synthetic catalytic antioxidants

Manganese is a particularly useful catalytic center due to its unrivaled repertoire of redox chemistry. Inspired by the Mn active site of MnSOD and MnCAT, a number of catalytic systems in which manganese can interact with $O_2^{\cdot-}$ or H_2O_2 have been tested. The number and type of ligands, the local charge, the geometry around the metal, are among the factors that introduce a way of tuning the redox potential of Mn to face redox reactions. Synthetic advances have led to the isolation and characterization of a number of Mn model complexes, and activity studies in conjunction with spectroscopy and theory have helped to understand some structural and electronic properties of the metal centres that modulate their reactivities.

A relevant catalytic antioxidant should have the ability to decompose $O_2^{\cdot-}$ and H_2O_2 efficiently and without being irreversibly modified by these reactive species, and should be stable towards metal dissociation in aqueous media. Due to the structure of the active site of MnSOD and MnCAT, a variety of mononuclear manganese complexes have been reported as SOD mimics [8a-c] and dinuclear manganese ones as CAT mimics [8d,e], although only a few were evaluated for dual SOD/CAT activity. In all cases where dual SOD/CAT activity was reported, the catalysts were mononuclear Mn complexes. Therefore, we will do an overview of the major classes of mononuclear Mn complexes that have been examined as MnSOD and/or MnCAT mimics, with emphasis on structure/activity relationships, and we will describe those cases where dual SOD/CAT activity has been observed.

3.1. Mn-Schiff base complexes

3.1.1. Mn-Schiff base complexes with antioxidant activity

Mn-Schiffbase complexes have proven to be efficient ROS scavengers and to protect cells from oxidative damage in several animal models [27]. *In vitro* and *in vivo* results demonstrated that Mn(III)-salen complexes are effective as mito-protecting agents [28], suppressing brain mitochondrial oxidative injury and alleviating neurological impairments in animal models for neurodegeneration and age-associated decline [29]. Several complexes of this series have been patented by Eukarion, Inc. (i.e., **EUK-8**, **EUK-108**, **EUK-113**, **EUK-134**, **EUK-172**, **EUK-207**, shown in Chart 1). Doctrow et al. reported that complexes of the salen series exhibit combined CAT and SOD activity with varying CAT and cytoprotective activities, but no differences in SOD activity [30]. For all complexes of the salen family, the $k_{McCF}(O_2^{\cdot-})$ [31a,b], the catalytic constants for $O_2^{\cdot-}$ scavenging calculated from IC_{50} values determined through the NBT [31c,d] or cytochrom c [31e,f] indirect assays, are around $0.6 \times 10^6\ M^{-1}\ s^{-1}$ [30]. Later, Friedel et al. re-evaluated the SOD activity of **EUK-113** ([Mn(**3-OMe-salen**)OAc]) by a direct stopped-flow method and the obtained $k_{cat}(O_2^{\cdot-})$ was $1.23 \times 10^6\ M^{-1}\ s^{-1}$ in HEPES buffer of pH 8.1, and $1.18 \times 10^6\ M^{-1}\ s^{-1}$ in phosphate buffer of pH 7.8, twice the value calculated from indirect methods [32]. In this work, it was shown that the activity of **EUK-113** is close to that of $MnCl_2$ in phosphate buffer, but it has even higher activity in HEPES buffer, a medium where $MnCl_2$ does not exhibit SOD activity (Table 1, entries 1 and 2). Besides, the SOD activity of **EUK-113** did not change significantly

by varying ionic strength, meaning that these SOD mimics with an overall 1+ charge are not very affected by ionic strength and endogenous anions. These observations support that the measured SOD activity of **EUK-113** does not result from free manganese species potentially present in the solution.

Because H_2O_2 is produced *in vivo* during $O_2^{\cdot-}$ disproportionation, the ability to consume H_2O_2 has been regarded as an advantageous property of the Mn-salen complexes. The CAT activity of complexes of this series was increased by the introduction of alkoxy substituents on the salen rings and by aromatic bridges between the imino groups replacing the CH_2CH_2 fragment. These changes affected the CAT activity but had no effect on SOD activity. Doctrow et al. demonstrated that the best complexes for CAT activity within this series were **EUK-134** and **EUK-113** that were able to disproportionate H_2O_2 with first order kinetics on catalyst and rates of 243 and 260 μM O_2/min, respectively, although with a maximal amount of 8 mol O_2 produced per mol of complex [30]. Besides, addition of a six-membered aromatic bridge increased the CAT activity of the complexes. Therefore, the best catalyst of this series possesses two 3-OMe ring substituents and an aromatic bridge (**EUK-172**) and disproportionates H_2O_2 with rate of 1073 μM H_2O_2/min.

Coordination of imidazole at the axial position of **EUK-134** showed little effect on the reduction potential and CAT activity

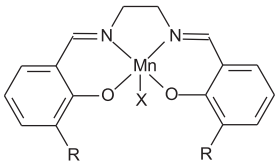

EUK-8: R=H, X=Cl
EUK-108: R=H, X=OAc
EUK-113: R=OMe, X=OAc
EUK-134: R=OMe, X=Cl
EUK-189: R=OEt, X=OAc

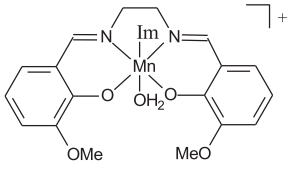

[Mn(**3-OMe-salen**)(Im)(H_2O)]$^+$

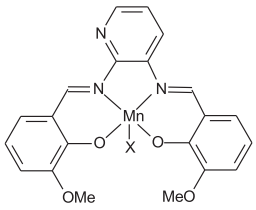

EUK-172, X = OAc

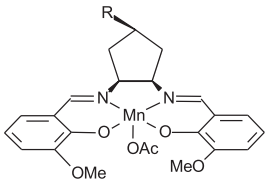

[Mn(**3-OMe-salenR**)(OAc)]
R = Ureido, acid-base auxiliary

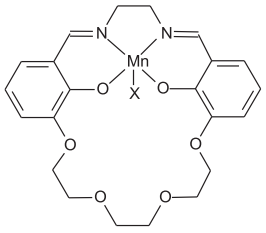

EUK-207, X = OAc

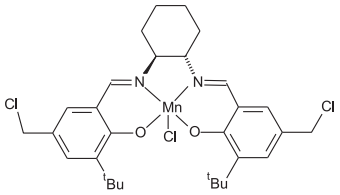

[Mn(**S-1**)Cl]

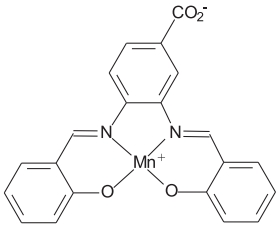

[Mn(**Csalophen**)]

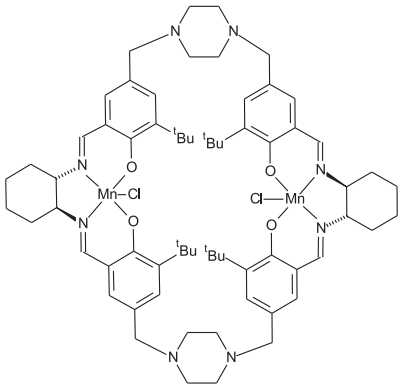

[Mn_2(**S1m**)Cl_2]

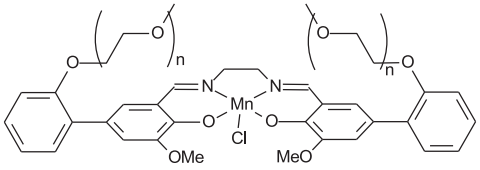

[Mn(III)(**salenPEG**)Cl]; n = 1-8

Chart 1. Structure of Mn-Schiff base complexes.

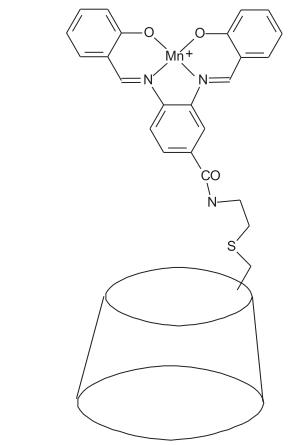

Mn-**CDL**

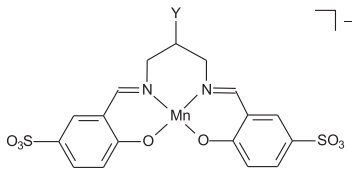

[Mn(**5-SO$_3$-salpnY**)]$^-$
Y = H, OH

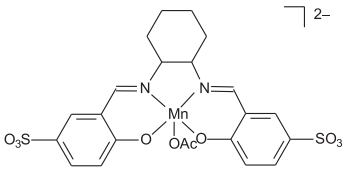

[Mn(OAc)(**CySalenSO$_3$**)]$^{2-}$

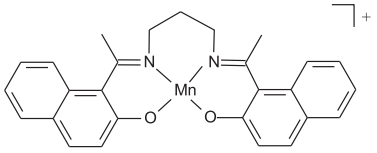

[Mn(**naphpn**)]$^+$

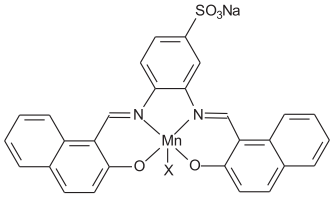

[Mn(**naphtophenSO$_3$**)X]

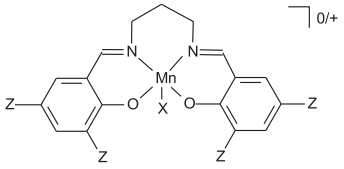

[Mn(**Z$_2$salpn**)X]$^{0/+}$
X= OAc, H$_2$O

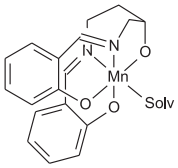

[Mn(**salbutO**)(solv)]

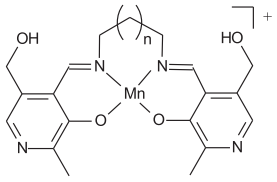

[Mn(**pyr$_2$en/pn**)]$^+$

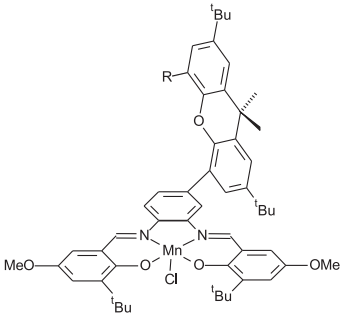

[Mn(**HSX-salophOMe**)(Cl)]
R = PhCO$_2$H

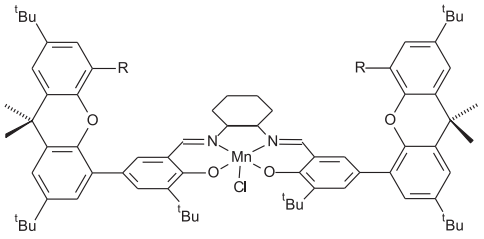

[Mn(**HSX,^{t}Bu-Cysalen**)(Cl)]
R=CO$_2$H, PhCO$_2$H

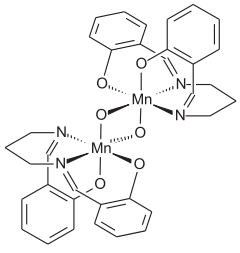

[Mn(μ-O)(**salpn**)]$_2$

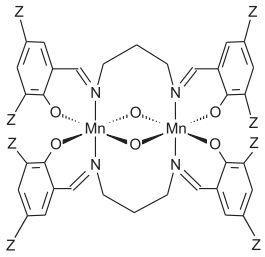

[Mn(μ-O)(**Z$_2$salpn**)]$_2$

Chart 1 (*continued*)

[33]. Thus, the rate of H_2O_2 disproportionation catalyzed by [Mn(III)(**3-OMe-salen**)$(H_2O)_2]^+$ and [Mn(III)(**3-OMe-salen**)(Im)$(H_2O)]^+$ in aqueous medium only increased 30% for the imidazole derivative (Table 1, entry 3). Dissociation of imidazole from the complex during reaction was disregarded on the basis of HPLC analysis of the reaction mixtures.

Noritake et al. designed a series of Mn-salen derivatives by arranging an acid-base auxiliary proximal to the Mn atom with the intention of increasing the CAT activity of this type of complexes [34]. This molecular design was inspired by the structure and reaction mechanism of Fe (hemo) catalase that cycle between [Fe(IV)=O]$^{\cdot+}$ and Fe(III) [21b]. In this way, the acid–base auxiliary

Table 1
Mn complexes with CAT and/or SOD activity.

	Complex	CAT activity		SOD activity		*E* (II/III) (V, NHE)	Refs.
		r_i ([H_2O_2] min^{-1} [Cat]$^{-1}$)[a]	Conditions	10^6 k_{McCF} or k_{cat} (M^{-1} s^{-1})[b]	Method		
1	[Mn(**3-OMe-salen**)OAc]	26	pH 7–8 (phosphate)	0.6 1.23	A, pH 7.8 (phosphate) SF, pH 8.1 (HEPES)	−0.13 (water) −0.45 (DMSO)	[30,32, 34,107a]
2	$MnCl_2$	–		6.9–2.7 inactive	SF, pH 7 to 7.8 (phosphate) SF, pH 7.1 and 8.1 (HEPES)	1.54	[32]
3	[Mn(**3-OMe-salen**)(Im)(H_2O)]$^+$	33	H_2O	–	–	0.04 (MeOH)	[33]
4	[Mn(**3-OMe-salenR**)(OAc)]	8–53	pH 7.4 (phosphate)	0.4–1.4	A, pH 7.4 (phosphate)	−0.40 to −0.45 (DMSO)	[34,35]
5	[Mn_2(**S1m**)Cl_2]	ND	–	2.8	B, pH 7, (phosphate)		[37]
6	[Mn(**Z_2-salpn**)]$^+$	1–15	DMF + 10 eq TBAOH	0.77–0.92	B, pH 7.8, (phosphate)	0.22–0.27 (DMSO)	[41]
7	[Mn(**Y-salpn**)]$^+$	17–25 (TON)	MeOH	–	–	−0.164–0.315 V (DMF)	[40a,b]
8	[Mn(**naphpn**)]$^+$	0.5	MeCN	–	–		[42]
9	[Mn(**5-SO_3-salen**)]$^-$	ND	–	1.2	B, pH 7.8, (phosphate)	0.443 (H_2O)	[43]
10	[Mn(**5-SO_3-salpn**)]$^-$	25.2	pH 8 (borate)	2.4	B, pH 7.8, (phosphate)	0.196 (MeOH)	[43]
11	[Mn(**5-SO_3-salpnOH**)]$^-$	178	pH 8 (borate)	3.6	B, pH 7.8, (phosphate)	0.166 (MeOH)	[43]
12	[Mn(**Csalophen**)]	ND		12	C, pH 7.4, (phosphate)	–	[46]
13	[Mn(OAc)(*R,R*-**CySalenSO_3**)]$^{2-}$	ND		5.49	C, pH 7.4, (phosphate)	–	[47]
14	[Mn(OAc)(*S,S*-**CySalenSO_3**)]$^{2-}$	ND		10.9	C, pH 7.4, (phosphate)	–	[47]
15	[Mn(**naphthophenSO_3**)]	ND		3.11	C, pH 7.4, (phosphate)	–	[48]
16	[Mn(**salbutO**)N_3]	3.4	DMF	1.91	B, pH 7.8, (phosphate)	0.60 (DMF, Mn(III)/Mn (IV))	[50]
17	[Mn(**pyr_2en**)]$^+$	ND		1.05	B, pH 7.8, (phosphate)	–	[51]
18	[Mn(**pyr_2pn**)]$^+$	ND		1.84	B, pH 7.8, (phosphate)	–	[51]
19	[$Mn_2(O)_2$(**salpn**)$_2$]	575	CH_2Cl_2/MeCN	ND		0.07 (irrev)	[59]
20	[Mn(**BMPG**)(H_2O)]$^+$	–		4.8	A, pH 7.8, (phosphate)	0.684 (E_{pa}, pH 7.5)	[31a]
21	[Mn(**TMIMA**)$_2$]$^{2+}$	–		3.6	A, pH 7.8, (phosphate)	0.884 (E_{pa}, pH 7.5)	[31a]
22	[Mn(**BIG**)(H_2O)$_2$]$^+$	–		1.5	A, pH 7.8, (phosphate)	1.00 (E_{pa}, pH 7.5)	[31a]
23	[Mn(**IPG**)(MeOH)]$^+$	–		1.9	A, pH 7.8, (phosphate)	1.00 (E_{pa}, pH 7.5)	[31a]
24	[Mn(**PI**)$_2$]$^+$	–		6.6	A, pH 7.8, (phosphate)	−0.021 (E_{pc}, MeCN) 0.584 (E_{pa}, pH 7.5)	[31a,65]
25	[Mn(**PhI**)$_2$]$^+$	–		3.4	C, pH 7.8, (phosphate)	−0.086 (E_{pc}, MeCN)	[65]
26	[Mn(**PBMPA**)Cl]	0.28	pH 11 (phosphate)	4.9	A/C, pH 7.6, (HEPES)	0.71 (MeCN)	[66]
27	[Mn(**MPBMPA**)Cl_2]	0.37	pH 11 (phosphate)	4.7	A/C, pH 7.6, (HEPES)	0.70 (MeCN)	[66]
28	[Mn(**baba**)Cl_2]	–		2.3	B, pH 7.8, (phosphate)	Inactive (DMF)	[68]
29	[Mn(**PCINOL**)Cl_2]	16.9	pH 7 (TRIS)	9.4	C (pH 7.8, phosphate)	1.05 (DMF)	[72]
30	[Mn(**L2**)]$_4^{4+}$	1.86 (V_{max})	MeCN	–		1.5 (MeCN)	[73]
31	[Mn(**L3**)Cl_2]	251 (V_{max})	MeCN	–		0.98 (MeCN)	[73]
32	[Mn(**L4**)]$^+$	6.9	pH 7.4	7.0 5.0	C, pH 7.8, (phosphate) SF, H_2O, pH 7.4	0.44 (pH 7.5)	[76,77,78]
33	[Mn(**L4**-Arg_{n-1})]$^{n+}$	–		5.0–6.6	SF, H_2O, pH 7.4	0.51–0.54 (pH 7.5)	[78]
34	[Mn(**ptp1**$^-$)(OH_2)]$^+$	–		3.6	SF, pH 7.4 (HEPES)	0.688 (pH 6.5)	[86]
35	[Mn(**L6**)]	13.2	MeCN	1.7	B, pH 7.8, (phosphate)	0.774 (MeCN, Mn(IV)/ Mn(III))	[88]
36	[Mn(**[15]aneN$_5$**)Cl_2]	–		41	SF, pH 7.4 (HEPES)	0.76 (MeOH)	[93]
37	**M40403**	–		16.4 49.1 1.9 12.4	SF, pH 7.4 SF, pH 7.4 (HEPES) SF, pH 7.4 (phosphate) SF, pH 8.1 (HEPES)	0.94 (DMSO) 0.84 (MeOH)	[32,95c, 106]
38	**M40401** (*2S,21S*-Me_2)	–		1600	SF, pH 7.4	0.87 (MeCN)	[95c,97]
39	**M40404** (*2R,21R*-Me_2)	–		Inactive	PR, pH 7.4 (phosphate)	0.88 (MeCN)	[97]
40	[Mn(**Me_2-pyane**)]$^{2+}$	–		27.3 8.4 12.1 5.3 5.4	SF, pH 7.4 (HEPES) SF, pH 7.4 (phosphate) SF, pH 8.1 (HEPES) SF, DMSO/water pH 10	0.87 (DMSO) 0.95 (MeOH) 1.14 (E_{pa}, pH 7)	[32,101, 104,106]
41	[Mn(**Me_2-Pyene**)]$^{2+}$	–		Inactive	SF, pH 7.4 (HEPES)	0.88 (E_{pa}, pH 7)	[104]
42	[Mn(**H_2dapsox**)]$^{2+}$	–		12	SF, DMSO/water	0.65 (DMSO)	[101]
43	[Mn(**Dcphp**)(H_2O)$_2$]	–		6.1	SF, DMSO/water	0.372 (DMSO)	[102]
44	[Mn(**Pimp**)Cl_2]	2.5 mL O_2 /s	MeOH, Et_3N	1.67	C, pH 7.8	–	[103]

(*continued on next page*)

Table 1 (*continued*)

	Complex	CAT activity		SOD activity		*E* (II/III) (V, NHE)	Refs.
		r_i ([H_2O_2] min^{-1} [Cat]$^{-1}$)[a]	Conditions	10^6 k_{McCF} or k_{cat} (M^{-1} s^{-1})[b]	Method		
45	[Mn_2(**bi-Me$_2$-pyane**)Cl_4]	–		47.0 10.2 23.0 19.0	SF, pH 7.4 (HEPES) SF, pH 7.4 (phosphate) SF, pH = 8.1 (HEPES) SF, pH 10	1.15 (E_{pa}, pH 7)	[104,108]
46	[Mn_2(**bi-Me$_2$-pyene**)Cl_4]	–		Inactive	SF, pH 7.4 (HEPES)	1.12 (pH 7)	[104]
47	[Mn(**L8-10**)Cl_2]	–		14.1–15.1 1.4–5.9 12.1–12.3	SF, pH 7.4 (HEPES) SF, pH 7.4 (phosphate) SF, pH 8.1 (HEPES)	0.83–0.90 (DMSO) 0.97–0.98 (MeOH)	[106]
48	[Mn(**Py$_2$N$_2$Me$_2$**)(H_2O)$_2$]$^{2+}$	0.108	H_2O	–		0.74 (MeCN)	[111]
49	[Mn(**Imtacn**)Cl_2]	6.3	MeOH/H2O	0.33	B, pH 7.8 (phosphate)	0.392 (MeOH)	[61]
50	[Mn(**Bimtacn**)Cl]ClO_4	2.3	MeOH/H2O	0.51	B, pH 7.8 (phosphate)	0.769 (MeOH)	[61]
51	[Mn(N_5-**SL**)]$^{2+}$	Inactive		3.6–15	C, pH 7.4 (phosphate)	0.66–0.75 (pH 7)	[113]
52	[Mn(N_6-**SL**)]$^{2+}$	Inactive		0.97–5.2	C, pH 7.4 (phosphate)	0.55–0.85 (pH 7)	[113]
53	[Mn(**TM-2-PyP**)]$^{5+}$	54	pH 7.8 (phosphate)	61.6	A, pH 7.8 (phosphate)	0.22 (pH 7.8)	[120,126]
54	[Mn(**TM-3-PyP**)]$^{5+}$	–		4.1	A, pH 7.8 (phosphate)	0.052 (pH 7.8)	[120]
55	[Mn(**TM-4-PyP**)]$^{5+}$	12	pH 7.8 (phosphate)	3.8	A, pH 7.8 (phosphate)	0.060 (pH 7.8)	[120,122]
56	[Mn(**TBAP**)]$^{3-}$	3.5	pH 7.8 (TRIS)	0.00145	A, pH 7.8 (phosphate)	−0.194 (pH 7.8)	[118]
57	[Mn(**TE-2-PyP**)]$^{5+}$	38 24	pH 7.8 (TRIS) pH 7.8 (phosphate)	57.5	A, pH 7.8 (phosphate)	0.228 (pH 7.8)	[118,120] [126]
58	[Mn(**TE-4-PyP**)]$^{5+}$	31.2	pH 7.8 (TRIS)	7.2	A, pH 7.8 (phosphate)	0.070 (pH 7.8)	[118]
59	[Mn(**TECP**)]$^{+}$	19	pH 7.8 (phosphate)	9 (U/mg)	A, pH 7.8 (phosphate)	–	[126]
60	**EUK-418**	0.47 (μM H_2O_2/min)	pH 7.4 (TRIS)	0.34	C, pH 7.8 (phosphate)	–	[127]
61	**EUK-423**	0.45 (μM H_2O_2/min)	pH 7.4 (TRIS)	0.093	C, pH 7.8 (phosphate)-	–	[127]
62	**EUK-425**	0.57 (μM H_2O_2/min)	pH 7.4 (TRIS)	0.047	C, pH 7.8 (phosphate)	–	[127]
63	**EUK-451**	0.64 (μM H_2O_2/min)	pH 7.4 (TRIS)	0.18	C, pH 7.8 (phosphate)	–	[127]
64	**EUK-452**	0.54 (μM H_2O_2/min)	pH 7.4 (TRIS)	0.051	C, pH 7.8 (phosphate)	–	[127]
65	**EUK-453**	0.50 (μM H_2O_2/min)	pH 7.4 (TRIS)	0.099	C, pH 7.8 (phosphate)	–	[127]
66	**MnPD**	198	pH 7.4 (phosphate)	4.7 (per Mn ion)	SF, pH 8.1 (HEPES)	–	[132]
67	[Mn(**TM-4-PyP**)]$^{5+}$/**CM-PVIm**	90	pH 7 (phosphate)	ND	–	–	[133]
68	**HSJ-0017**	104	pH 7 (phosphate)	27	C, pH 7.8 (phosphate)	–	[134]
69	[Mn(**TnBuOE-2-PyP**)]$^{5+}$	53.1	pH 7.8 (TRIS)	68	A, pH 7.8 (phosphate)	0.277 (pH 7.8)	[118]
70	[Mn(**TnHex-2-PyP**)]$^{5+}$	17.0	pH 7.8 (TRIS)	30	A, pH 7.8 (phosphate)	0.314 (pH 7.8)	[118]
71	[Mn(**TnHex-3-PyP**)]$^{5+}$	27.72	pH 7.8 (TRIS)	4.4	A, pH 7.8 (phosphate)	0.066 (pH 7.8)	[118]
72	[Mn(**TnHex-4-PyP**)]$^{5+}$	35.43	pH 7.8 (TRIS)	5.6	A, pH 7.8 (phosphate)	0.068 (pH 7.8)	[118]
73	[Mn(**TnOct-2-PyP**)]$^{5+}$	16.57	pH 7.8 (TRIS)	51	A, pH 7.8 (phosphate)	0.340 (pH 7.8)	[118]
74	[Mn(**TnOct-3-PyP**)]$^{5+}$	40.46	pH 7.8 (TRIS)	3.4	A, pH 7.8 (phosphate)	0.074 (pH 7.8)	[118]
75	[Mn_2(**L12**)$_2$**P^1**]$^{5+}$	ND		4.4	A, pH 7.8 (phosphate)	0.515 (pH 7.8)	[137]
76	[Mn_2(**L12**)$_2$**P^2**]$^{6+}$	1134	pH = 7.8 (BBS)	11	A, pH 7.8 (phosphate)	0.515 (pH 7.8)	[137]
77	**1-Mn**	3.36	pH = 9.5	0.48	A, pH 7.8 (phosphate)	1.075 (III/IV) pH = 7.4	[145,147]
78	**3-Mn**	–		0.87	A, pH 7.8 (phosphate)	1.145 (III/IV) pH 7.4	[145]
79	**4-Mn**	–		2.2	A, pH 7.8 (phosphate)	1.115 (III/IV) pH 7.4	[145]
80	**5-Mn**	–		1.8	A, pH 7.8 (phosphate)	0.995 (III/IV) pH 7.4	[145]
81	[Mn(bis(**R′-Ind**)$_2$]	1.2–1.7	DMF	0.83–3.28	A/C, pH 7.6 (HEPES)	0.646–0.826 (DMF)	[149,150]
82	[Mn(**IndH**)Cl_2]	47 0.9	pH 9.5 (carbonate) MeCN, ImH	–		–	[151]
83	[Mn(**Etobb**)Cl_2]	–		1.2	B, pH 7.8 (phosphate)	–	[153]
84	[Mn(**Etobb**)$_2$]$^{2+}$	–		1.9	B, pH 7.8 (phosphate)	–	[153]
85	[Mn(**Phimp**)$_2$]$^{+}$	–		30	C, pH 7.8 (phosphate)	0.515 (MeCN)	[154]
86	[Mn(**L13**)$_2$]	–		0.95	NADH/PMS/NBT	–	[155]

Table 1 (*continued*)

	Complex	CAT activity		SOD activity		*E* (II/III) (V, NHE)	Refs.
		r_i ([H_2O_2] min^{-1} [Cat]$^{-1}$)[a]	Conditions	10^6 k_{McCF} or k_{cat} (M^{-1} s^{-1})[b]	Method		
87	[Mn(**S_2Py_3**)(OTf)$_2$]	1.6	MeCN + NaOH	8	C, pH 7.4 (phosphate)	ND[c]	[157]
88	Human MnSOD	–		800	SF, pH 9.6	0.29	[13c,14]
89	MnCAT	$1.4–8.4 \times 10^6$		–		–	[21]

A = Xanthine-xanthine oxidase-cytochrome c assay.
B = Riboflavin–methionine–NBT assay.
C = Xantine/xantine oxidase/NBT assay.
SF = stopped-flow.
PR = pulse radiolysis.
Z = Cl, F. Y = OEt, Cl, Br. R = cyclopentane-fused with ureido or acid–base catalyst auxiliary. R′ = 2′-benzimidazolyl, 2′-*N*-methylbenzimidazolyl, 2′-thiazolyl, 2′-pyridyl, 3′-methyl-2′-pyridyl, 4′-methyl-2′-pyridyl.
TON = mmol H_2O_2/mmol catalyst.

[a] r_i values calculated from reported data or kinetic parameters, for [H_2O_2] = 10 mM.

[b] k_{cat} is the catalytic constant directly measured by pulsed radiolysis or stopped-flow techniques and k_{McCF} is the calculated rate constant from the IC_{50} (50% inhibition concentration value) using the McCord–Fridovich cytochrome c assay (A) [31e,f] and modified NBT (B, C) [31c,d] assays. $k_{cyt\ c} = 2.6 \times 10^5$ M^{-1} s^{-1} [31g] and $k_{NBT} = 5.94 \times 10^4$ M^{-1} s^{-1} [31b].

[c] Featureless between −1.5 V and +1.5 V (vs. Ag/$AgNO_3$).

was thought to assist both a high-valent intermediate formation and H_2O_2 oxidation. One imidazolyl or pyridyl moiety was attached to a cyclopentane ring bridging the imino-*N* donor sites, affording the *cis-syn* form of the complex and a highly planar Mn(salen) moiety ([Mn(**3-OMe-salenR**)(OAc)] in Chart 1). However, the activity of the imidazolyl-substituted complex was lower than the parent **EUK-113**, and although pyridyl improved CAT activity (r_i was three-times higher than **EUK-113** under the same conditions), introduction of electron-donating-group into the pyridyl ring resulted in activities lower than with the unsubstituted pyridyl group. These complexes were also evaluated as SOD mimics showing similar or better activity than the parent **EUK-113** (Table 1, entry 4); however, the most active of this series was the phenyl-substituted derivative. The same authors had proved that introduction of an ureido auxiliary enhanced the CAT activity three times compared to **EUK-113** (under the same reaction conditions), and this was attributed to the ability of urea to recognize H_2O_2 [35].

Khan et al. evaluated the antioxidant activity of several *1S,2S* and *1R,2R*-chiral Mn(III)-Cysalen complexes with different substituents at 5,5′-position [36]. In all cases, the *S*-enantiomers of the complexes were more active than their respective *R*-enantiomers to react with both $O_2^{\cdot-}$ and H_2O_2, and showed stronger DNA binding ability. The different reactivity of the enantiomeric Mn(III)-Cysalen complexes should arise from the interaction with the chiral agents used. Among the studied chiral Mn(III)-Cysalen complexes, complex [Mn(**S-1**)Cl] (Chart 1) showed the highest DNA binding affinity as well as antioxidant activities. The $O_2^{\cdot-}$ scavenging was improved by using chiral macrocycle Mn(III)-Cysalen complexes [37]. Also in this case, the *S*-enantiomers exhibited higher antioxidant activity than the *R* ones, and the Mn(III) complexes formed with **S1m** ([Mn_2(**S1m**)Cl_2] in Chart 1) showed the best SOD activity (Table 1, entry 5) and exhibited strong DNA interaction with a binding constant value of 1.20×10^6 M^{-1}.

With the aim to increase the stability through the macrocyclic effect, the Mn(III) complex of a cyclic salen-crown ether (**EUK-207**, Chart 1) was prepared. This complex exhibited similar CAT activity and higher lipophilicity, biological stability and neuroprotective activity than **EUK-134** [38]. In other approach, Park et al. attached oligo(ethyleneglycol) chains at the *para* positions of **EUK-134** to protect the metal center [39]. The resulting [Mn(III)(**salenPEG**)Cl] complexes (Chart 1) had better SOD activity than the parent complex, but decreased catalase rate. However, the PEG conjugates with longer chains (n = 6, 8) displayed higher turnover numbers and improved stability under conditions of the catalase assay.

Mn complexes of Schiff-base ligands with different spacers between the imine groups and various substituents on the phenyl rings were evaluated as SOD and CAT mimics [40,41]. Complexes of the salpn series reacted with $O_2^{\cdot-}$ faster than the Mn-salen counterparts [41] but disproportionated H_2O_2 slower than Mn-salen complexes [40] although with higher turnover numbers (up to 115 mmol H_2O_2/mmol catalyst) in basic medium [41] (Table 1, entries 6 and 7). The faster H_2O_2 disproportionation rate by Mn-salen complexes was interpreted in terms of the higher elongation of the labile axial position in the Mn-salen series compared to Mn-salpn analogues [40]. Replacing the phenolate by the naphtolate moiety (where electrons are delocalized over two fused aromatic rings, i.e., [Mn(III)(**naphpn**)]$^+$ in Chart 1) depleted CAT activity (Table 1, entry 8) [42].

Owing to the slight water solubility of the tested salen/salpn Mn complexes, sulphonate groups were introduced into the ligand to improve their solubility in aqueous medium. Moreno et al. tested three water soluble complexes [Mn(III)(**5-SO_3-salpnOH**)]$^-$, [Mn(III)(**5-SO_3-salpn**)]$^-$ and [Mn(III)(**5-SO_3-salen**)]$^-$ as SOD mimics [43]. In these compounds, Mn(III) is in a tetragonal environment with the two axial positions occupied by solvent molecules. Rate constants for $O_2^{\cdot-}$ dismutation by the water soluble complexes were higher than for the water insoluble counterparts (Table 1, entries 9–11) and Mn-SO_3-salpn(OH) resulted better SOD mimics than Mn-SO_3-salen. Electrochemical/kinetics correlations suggested these compounds employ the Mn(II)/Mn(III) redox cycle for catalysis and that oxidation of the metal centre (concurrent to $O_2^{\cdot-}$ reduction) takes place in the slow step. [Mn(III)(**5-SO_3-salpnOH**)]$^-$ and [Mn(III)(**5-SO_3-salpn**)]$^-$ were also evaluated as CAT mimics (Table 1, entries 10 and 11). They were able to disproportionate H_2O_2 in aqueous medium, at pH 8 (borate buffer), with turnover numbers several times larger than for complexes of the salen family [43]. To explain the faster initial rate of H_2O_2 dismutation by [Mn(III)(**5-SO_3-salpnOH**)]$^-$, it was suggested that the presence of the OH^- group on C2 of the propane backbone probably facilitates the formation of the dimer required for CAT acitivity.

The glycoconjugation of Mn(III)salen mimics also improved their water solubility. Mn(III) complexes of β-cyclodextrin (CD) conjugates with salen-type ligands (Mn-**CDL** in Chart 1), showed SOD activity about ten times higher than the corresponding simple salen complexes (**EUK-108** and **EUK-113**) [44]. However, in the case of the salophen derivative, the functionalization gave rise to a slightly increased SOD activity of the system *in vitro* compared to **EUK-172** [45]. Furthermore these systems also showed CAT

activity higher (**EUK-108** and **EUK-113**) than or similar (**EUK-172**) to the simple salen systems.

In a similar way to the cyclodextrin cavity, Oliveri et al. took advantage of the non-covalent binding of Mn(III)-salen type complexes to bovine serum albumin (BSA) to generate a microenvironment around the complex more hydrophobic than that of water [46]. In the tested cases, the protein environment exerted a positive effect on the SOD activity of the complex and the complex-BSA adduct showed a significantly increased SOD activity. [Mn(III)(**Csalophen**)] (Chart 1) and the non-covalent conjugate BSA-[Mn(III)(**Csalophen**)] were evaluated to scavenge $O_2^{\cdot-}$. The rate constant for the reaction of $O_2^{\cdot-}$ with the complex was 1.2×10^7 M^{-1} s^{-1}, while in presence of albumin, the $k_{McCF}(O_2^{\cdot-})$ for the complex-BSA adduct was 7.7×10^7 M^{-1} s^{-1}, a significantly higher value resulting from the positive effect of albumin [46]. The same non-covalent approach was employed to prepare adducts between BSA and two chiral sulphonato-Schiff base Mn(III) complexes [Mn(OAc)(***R,R*-CySalenSO$_3$**)]$^{2-}$ and [Mn(OAc)(***S,S*-CySalenSO$_3$**)]$^{2-}$ [47]. BSA showed one binding site for the two complexes ($n = 1$), and binding constants determined by fluorescence spectroscopy were $K_b = 0.95 \times 10^5$ M^{-1} and 0.23×10^5 M^{-1}, for the *R,R*- and *S,S*-isomer, respectively. The two complexes catalyzed the $O_2^{\cdot-}$ dismutation with rate constants (Table 1, entries 13 and 14) higher than other Mn(III) compounds of lipophylic salen ligands, and the binding with BSA promoted the SOD activity of [Mn(OAc)(***R,R*-CySalenSO$_3$**)]$^{2-}$. The calculated $k_{McCF}(O_2^{\cdot-})$ for the adduct was 11.05×10^6 M^{-1} s^{-1}, twice greater than the complex without BSA. For the *S,S*-isomer, a modest improvement was observed when BSA was added. Similarly, BSA binding improved the SOD activity of a sulphonate derivative of a Schiff-base ligand with two naphtolate rings, [Mn(III)(**naphthophenSO$_3$**)] (Chart 1) [48]. For this complex, conjugation to BSA resulted in 17-fold faster reaction with $O_2^{\cdot-}$ compared to the complex alone (Table 1, entry 15).

Aimed at improving the complex stability, Yu et al. prepared a system based on immobilization of [Mn(**salophen**)]$^+$ into an insoluble hydrophilic rigid matrix by introduction of a carboxylate group into the salophen ligand to give [Mn(**Csalophen**)], followed by covalent linking on the surface of highly ordered hollow silica microspheres (HSM) through the esterification of the carboxylate with silanol [49]. The rigid metallosalen modified HSM showed $O_2^{\cdot-}$ scavenging activity 4.5-times higher than [Mn(**Csalophen**)].

Daier et al. tested a Mn(III) complex of a Schiff-base ligand with a four C linker between the imino-*N* donor sites and an alkoxo group on C2, [Mn(III)(**salbutO**)] (Chart 1), as SOD and CAT mimic [50]. In this complex, the longer ligand is less constrained to lie in the equatorial plane of the metal ion and folds around the Mn ion leaving one vacant coordination site occupied by a labile solvent molecule. [Mn(III)(**salbutO**)] showed combined SOD/CAT activity (Table 1, entry 16), with SOD activity similar to Mn-salen complexes and turnover numbers for H_2O_2 dismutation (1200 mmol H_2O_2/mmol catalyst) significantly higher than Mn-salen series, although measured in DMF. The last was attributed to the high proportion of the [Mn(III)(**salbutO**)]$_2$ dimer in the starting solution, favored by the ligand folding that leaves the phenolate well-disposed to bind a Mn ion of a neighbor molecule. The ligand folding around Mn and the additional alkoxido donor site also shift the metal centered redox potentials to values lower than those in [Mn(**salen**)]$^+$ or [Mn(**salpn**)]$^+$ and this explained the involvement of a Mn(III)/Mn(IV) cycle during SOD catalysis.

The role played by the length of the alkyl spacer in the diimino fragment on the SOD activity of Schiff-base Mn(III) complexes was also analyzed by comparing the structure and activity of catalysts obtained with Schiff-base ligands derived from pyridoxal: [Mn(**pyr$_2$en**)(H$_2$O)$_2$]Cl and [Mn(**pyr$_2$pn**)(H$_2$O)$_2$]ClO$_4$ (Chart 1) [51]. Under the same reaction conditions, [Mn(**pyr$_2$pn**)(H$_2$O)$_2$]$^+$ was twice as active as [Mn(**pyr$_2$en**)(H$_2$O)$_2$]$^+$. Instead of the planar disposition of pyr$_2$en in the equatorial plane, pyr$_2$pn^{2-} resulted in a complex with 25° deviation from planarity in a dome-shaped octahedral geometry, with one of the axial water molecules very weakly coordinated. The bending of the tetradentate ligand leads to a weakly coordinated exchangeable axial solvent molecule which facilitates substrate binding resulting in higher rate for $O_2^{\cdot-}$ scavenging (Table 1, entries 17 and 18). The same increment of activity had been observed when SOD activities of Mn-salpn and Mn-salen were compared [41,42].

3.1.2. Mechanism of CAT activity for Mn-salen and Mn-salpn complexes

Even when a number of studies have been reported on the CAT activity of mononuclear Mn-Schiff base complexes, their mode of action remains poorly understood. The Mn-salen complexes have been proposed to react with H_2O_2 through a mechanism involving mononuclear Mn(III)(H$_2$O)/Mn(V)=O species [52]. This proposal was supported by theoretical predictions for the Mn-salen model [53], and spectroscopic evidence for the formation of Mn(V)=O species upon O-O bond heterolysis of a peroxo species was reported for a Mn-salophen complex in which one carboxylic group was placed over the metal center via a rigid xanthene scaffold, [Mn(**HSX-salophOMe**)(Cl)] (Chart 1) [54]. Salen ligands incorporating two functionalized xanthene scaffolds and a chiral cyclohexanediamine backbone functionalized with *tert*-butyl groups in the *3* and *3′* positions of the phenol rings (**HSX,^{t}Bu-Cysalen**, Chart 1) led to a significant increase in CAT activity and turnover numbers up to 5328 mmol H_2O_2/mmol catalyst, in a biphasic CH_2Cl_2/MeOH mixture [55]. It was proposed that H bonding with the carboxylic group favors the *end-on* approach of the H_2O_2 and that the bulky *tert*-butyl substituents further promote the *end-on* assembly by blocking the *side-on* approach. These two concerted effects were thought to prevent the deactivation of the catalyst.

Mundlapati et al. employed the ^{17}O NMR line broadening technique to investigate the kinetics of water exchange in *trans*-[Mn(III)(**salen**)(H$_2$O)$_2$]$^+$ using $^{17}OH_2$ enriched aqueous medium [56]. The water exchange reaction was found to occur through an associative interchange mechanism (I_a) with a rate constant $k_{ex}^{298}/[H_2O] = 0.7 \times 10^5$ M^{-1} s^{-1}. At pH 10, the hydroxo complex [(OH$_2$)Mn(III)(**salen**)(OH)] formed and water exchange occurred concurrently with dimerization to the hydroxo-bridged [(OH$_2$)Mn(III)(**salen**)(μ-OH)Mn(III)(**salen**)(OH)] complex; so, at this pH, calculated kinetic parameters were not so precise but pointed to a dissociative interchange (I_d) mechanism with $k_{ex}^{298}/[H_2O] = 6.3 \times 10^5$ M^{-1} s^{-1}, reflecting the *trans*-labilizing effect of the hydroxo group. These second order $k_{ex}/[H_2O]$ values are much higher than $k_{cat}(H_2O_2) = 8.3$ M^{-1} s^{-1} reported for CAT activity of **EUK-8** at pH 7 [57]. Therefore, exchange of coordinate water by H_2O_2 should not be rate limiting in the CAT activity of Mn(III)-salen. The same authors determined the dimerization rate constant for [(OH$_2$)Mn(III)(**salen**)(OH)] is $k_{dim} = 1.7$ M^{-1} s^{-1} (pH 10) [57]. Thus, in basic medium the dimerization can compete with reaction with H_2O_2, except a large excess of H_2O_2 is used.

Recently, on the basis of paramagnetic ^1H NMR, FTIR and ESI-MS studies, Kurahashi proposed a mechanism for the aerobic dimerization of [Mn(III)(**^{t}Bu-salen**)Cl] in basic medium to yield [Mn(IV)(**^{t}Bu-salen**)(μ-O)]$_2$ (the "*reverse catalase reaction*") [58]. According to spectroscopic evidences, Cl^-/OH^- substitution on the metal followed by deprotonation generated [Mn(III)(**^{t}Bu-salen**)O]$^-$(Eq. 7, Scheme 2). Because of its strong reducing ability, [Mn(III)(**^{t}Bu-salen**)O]$^-$ was postulated to reduce [Mn(III)(**^{t}Bu-salen**)Cl] yielding [Mn(IV)(**^{t}Bu-salen**)=O] + [Mn(II)(**^{t}Bu-salen**)] (Eq. 8). In the proposed mechanism, the reduced Mn(II) complex reacts with O_2 to yield the dimer (Eq. 9), while the remaining Mn

$$[Mn(III)(\ ^{t}Bu\text{-}salen)Cl] + 2OH^{-} \rightarrow [Mn(III)(\ ^{t}Bu\text{-}salen)O]^{-} \quad (7)$$

$$[Mn(III)(\ ^{t}Bu\text{-}salen)O]^{-} + [Mn(III)(\ ^{t}Bu\text{-}salen)Cl] \Leftrightarrow [Mn(IV)(\ ^{t}Bu\text{-}salen)O] + [Mn(II)(\ ^{t}Bu\text{-}salen)] \quad (8)$$

$$2[Mn(II)(\ ^{t}Bu\text{-}salen)] + O_2 \rightarrow [(\ ^{t}Bu\text{-}salen)Mn(IV)(O_2)Mn(IV)(\ ^{t}Bu\text{-}salen)]$$

$$\rightarrow [Mn(IV)(\ ^{t}Bu\text{-}salen)(\mu\text{-}O)]_2 \quad (9)$$

$$2[Mn(IV)(\ ^{t}Bu\text{-}salen)=O] \rightarrow [(\ ^{t}Bu\text{-}salen)Mn(IV)(O_2)Mn(IV)(\ ^{t}Bu\text{-}salen)]$$

$$\rightarrow [Mn(IV)(\ ^{t}Bu\text{-}salen)(\mu\text{-}O)]_2 \quad (10)$$

Scheme 2. Proposed mechanism for the reverse catalase reaction of [Mn(III)(**^{t}Bu-salen**)Cl].

(IV)-oxo species also dimerizes to the same final bis-oxo-bridged complex (Eq. 10). These $[Mn(IV)_2(O_2)L_2]$ dimers formed in basic medium could react with H_2O_2 in a similar way as proposed for the bis-oxo diMn(IV) dimers of salpn.

Based on kinetics, spectroscopy and mass spectrometry studies, the CAT activity of several complexes of the Mn-salen and/or Mn-salpn families in basic medium was related to their ability to form dimers [40,59], through a mechanism involving dimeric Mn_2 species as do the enzyme and other mononuclear Mn complexes of flexible amino or polyamino ligands with a vacant or labile site in the Mn coordination sphere [60,61].

It is well known that Mn(III)-X-salpn complexes react with O_2 (or stoichiometric amount of H_2O_2) in basic medium or in donor solvents to afford oxo-bridged Mn(IV) dimers [(**X-salpn**)Mn(IV)$(O)_2$Mn(IV)(**X-salpn**)] [62]. These dimers are among the most efficient catalysts for decomposing H_2O_2 known up to date, although at a rate that is still far behind the native enzyme (Table 1, entry 19) [59]. This efficient CAT activity was exhibited in anhydrous Cl_2CH_2, where hydrolytic inactivation processes are not competitive with catalysis and high turnover numbers (>1000 mmol H_2O_2/mmol catalyst) can be achieved. Based on spectroscopic and kinetic evidence, Larson et al. postulated a mechanism for the CAT reaction of these oxo-bridged dimers, involving the exchange of the bridging oxo groups, where both oxygen atoms originate from the same peroxide molecule [63]. The proposed catalytic cycle shuttles between the [(**X-salpn**)$_2$Mn(IV)$_2$(O)$_2$] and [(**X-salpn**)Mn(III)(O_2H)] + [(**X-salpn**)Mn(III)OH] species, probably through a [(**X-salpn**)$_2$Mn(III)$_2$$(O_2)$] peroxo-dimer.

In a recent work, Palopoli et al. showed that [Mn(III)(**F_2salpn**)]$^+$ and [Mn(III)(**Cl_2salpn**)(OAc)] disproportionate H_2O_2 in basic medium with second-order kinetics, involving Mn(III) and Mn(IV) oxidation states during catalysis [41]. Interestingly, without addition of base, the reaction rates were extremely slow, indicating that the starting Mn(III)-**X_2salpn** compounds do not possess good CAT activity "per se", in spite of having correct reduction potentials for H_2O_2 disproportionation (Table 1, entry 6). However, in basic medium, these complexes behaved catalytically, with turnover numbers of 58–115 mmol H_2O_2/mmol complex. It was postulated that in basic medium, the complex is rapidly converted into the hydroxo complex, [Mn(III)(OH)(**X_2salpn**)], followed by hydroxo/hydroperoxo exchange (Eq. 11, Scheme 3) and reaction with a second hydroxo-Mn(III) complex to generate the oxidized dimer (Eq. 12) which enters into the catalytic cycle for H_2O_2 dismutation (Eq. 13).

3.2. Mn-amine and diamine complexes

It is well known that an *O*-rich environment and/or a distorted geometry decrease the potential of the Mn(III)/Mn(II) couple. In a detailed work, Durot et al. studied the dismutation of $O_2^{\cdot-}$ by a series of Mn complexes with tertiary (**TMIMA**) and secondary (**BMPG**, **IPG**, **BIG**, **PI**) amine ligands (Chart 2), and demonstrated that the catalytic rate constants for the dismutation of $O_2^{\cdot-}$ are related to the metal-centered reduction potential of the Mn(III)/Mn(II) couple, which in turn can be modulated by varying the ratio of *N/O* donor sites around the metal and geometry of the Mn coordination sphere [31a,64]. The oxidation potentials of complexes of this series are linearly correlated to $\log(k_{cat})$ for $O_2^{\cdot-}$ dismutation. Thus, [Mn(II)(**PI**)$_2$], with Mn in a N_4O_2 environment, was the easiest to oxidize and the most active (Table 1, entries 20–24); followed by [Mn(II)(**BMPG**)$(H_2O)]^+$ and [Mn(II)(**TMIMA**)$_2]^{2+}$, where steric crowding of the ligands generated a distorted environment that favored the conversion to Mn(III).

The fact that the complex that was easier to oxidize reacted faster was taken as evidence for the oxidation of Mn(II) to Mn(III) to occur in the rate-limiting step of the catalytic cycle. Interestingly, [Mn(III)(**PhI**)$_2]^+$, with a longer linker between the amine and the imidazole moiety and an even more negative potential for the Mn(III)/Mn(II) couple compared to [Mn(III)(**PI**)$_2]^+$ (Table 1, entries 24 and 25), showed a poorer activity [65] because in this case the reduction potential of [Mn(III)(**PhI**)$_2]^+$ was too negative to account for efficient redox cycling of $O_2^{\cdot-}$. Complexes [Mn(II)(**PBMPA**)(H_2O)Cl] and [Mn(II)(**MPBMPA**)Cl_2] (Chart 2), formed with the tripodal bis(2-picolyl)β-alanylamine and its methyl ester, can be added to this series [66]. The two complexes have very close oxidation potentials (around 0.7 V vs NHE), similar to [Mn(II)

$$[Mn(III)(OH)(\mathbf{X_2salpn})] + H_2O_2 \rightarrow [Mn(III)(O_2H)(\mathbf{X_2salpn})] + H_2O \quad (11)$$

$$[Mn(III)(O_2H)(\mathbf{X_2salpn})] + [Mn(III)(OH)(\mathbf{X_2salpn})] \rightarrow [Mn(IV)(O)(\mathbf{X_2salpn})]_2 + H_2O \quad (12)$$

$$[Mn(IV)(O)(\mathbf{X_2salpn})]_2 \underset{2H_2O}{\overset{H_2O_2}{\rightleftharpoons}} 2\,[Mn(III)(OH)(\mathbf{X_2salpn})] \quad (13)$$

Scheme 3. Proposed mechanism for the reaction of [Mn(III)(OH)(**X_2salpn**)] with H_2O_2.

(**BMPG**)$(H_2O)]^+$, and reacted with $O_2^{\cdot-}$ at similar rates in buffer HEPES of pH 7.6 (Table 1, entries 26 and 27)). Milaeva et al. introduced a pendant 2,6-di-*tert*-butylphenol – an organic radical scavenger that reacts with $O_2^{\cdot-}$ very poorly-, into bis(2-picolyl)amine to obtain complexes [Mn(II)(**L1**)X_2] (X = Cl, OAc) (Chart 2) that act as polytopic agents combining the organic antioxidant phenol groups and the metal center for electron transfer [67]. The presence of Mn (II) improved the antioxidant activity of the ligand in the *in vitro* biological experiments and contributed to SOD activity, affording rate constants of 0.8×10^6 (Cl) and 3.0×10^6 (OAc) $M^{-1}\,s^{-1}$ for $O_2^{\cdot-}$ disproportionation. Wu et al. employed **baba**, another N_3-tridentate amine ligand with alkylbenzimidazole instead of pycoline arms, to prepare a pentacoordinate Mn(II) complex [Mn(II)(**baba**)Cl_2] (Chart 2), which contains Mn(II) in a trigonal bipyramidal geometry with two *N*-donor atoms from benzimidazole groups and one Cl^- ion in the equatorial plane [68]. This complex resulted electrochemically inactive in the range −1.0 to +1.0 V, in DMF; however, it scavenged $O_2^{\cdot-}$ with *a* rate constant value higher than [Mn(**IPG**)(MeOH)]$^+$ (Table 1, entry 28).

Several Mn(II) complexes of polydentate amino ligands were tested as catalysts for H_2O_2 disproportionation. In all cases where spectroscopic data were provided, the starting complexes

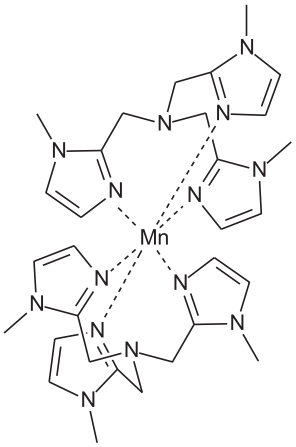

[Mn(II)(**TMIMA**)$_2$]$^{2+}$

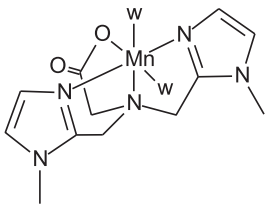

[Mn(**BIG**)$(H_2O)_2]^+$

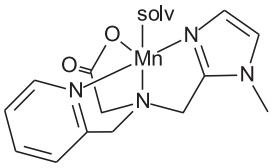

[Mn(**IPG**)(MeOH)]$^+$

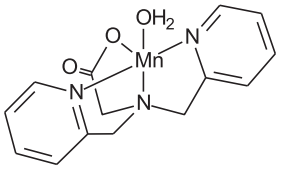

[Mn(II)(**BMPG**)$(H_2O)]^+$

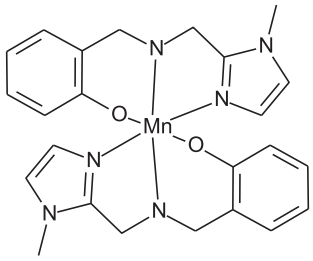

[Mn(II)(**PI**)$_2$]

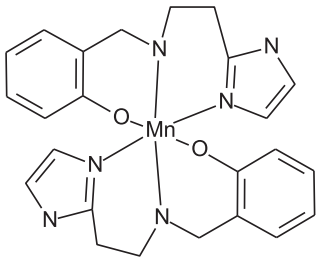

[Mn(II)(**PhI**)$_2$]

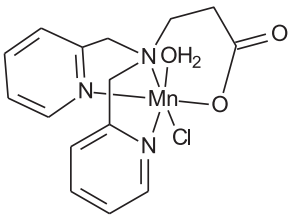

[Mn(II)(**PBMPA**)Cl$(H_2O)]$

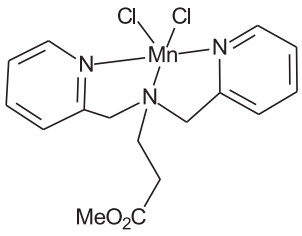

[Mn(II)(**MPBMPA**)$Cl_2]$

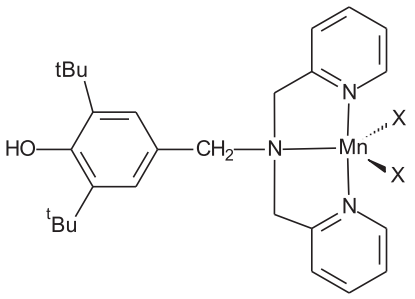

[Mn(II)(**L1**)$X_2]$

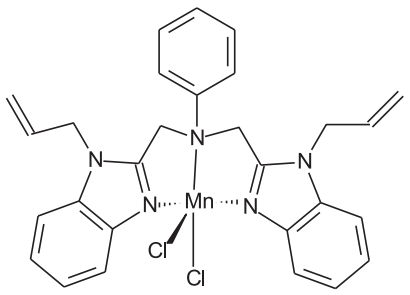

[Mn(II)(**baba**)$Cl_2]$

Chart 2. Structure of Mn-amine and diamine complexes.

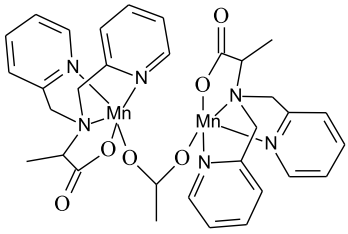

[Mn(II)$_2$(**Adpa**)$_2$(OAc)]$^+$

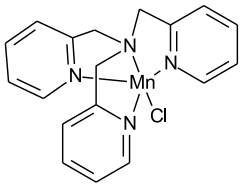

[Mn(II)(**TPA**)Cl]$^+$

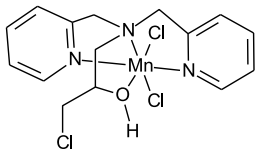

[Mn(II)(**PCINOL**)Cl$_2$]

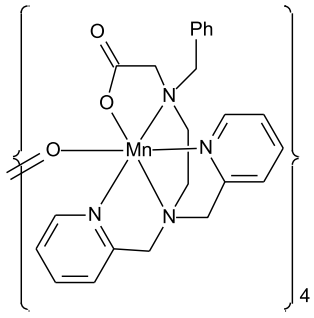

[Mn(II)(**L2**)]$_4^{4+}$

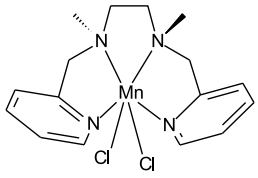

[Mn(II)(**L3**)Cl$_2$]

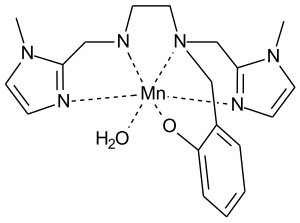

[Mn(II)(**L4**)(H$_2$O)]$^+$

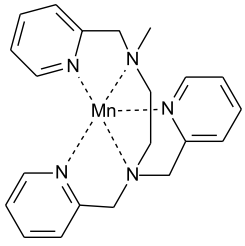

[Mn(II)(**L5**)]$^{2+}$

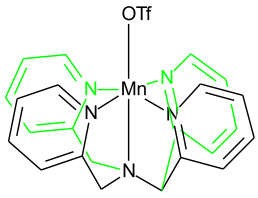

[Mn(II)(**N4py**)(OTf)]$^+$

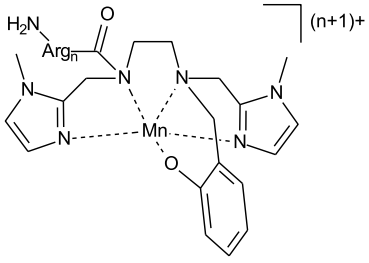

[Mn(II)(**L4-Arg$_n$**)]$^{(n+1)+}$

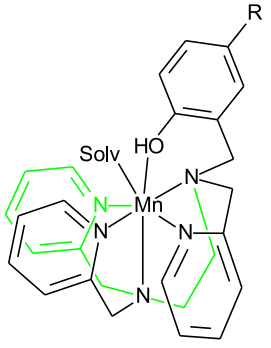

R = Me: [Mn(II)(**Hptp1**)(solv)]$^{2+}$
R = OH: [Mn(II)(**H$_2$qtp1**)(solv)]$^{2+}$

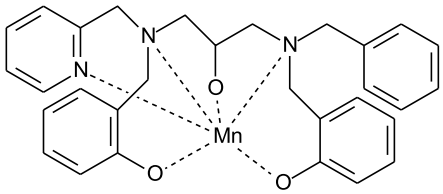

[Mn(III)(**L6**)]

Chart 2 (*continued*)

converted into high valent oxo-bridged dimers that were probably responsible for catalysis. It must be mentioned that dioxo-bridged Mn(III)Mn(IV) and Mn(III)$_2$ complexes of **TPA** (tris(2-pycolyl) amine) and the related tripodal ligands obtained by replacement of pyridyl by carboxylate groups, bis(2-picolyl)glycylamine (**Hbpg**) and 2-picolyldiglycylamine (**H$_2$pda**), exhibited CAT activity in MeCN [69]. EPR monitoring of the reaction showed that these complexes cycled between Mn(III)Mn(IV)/Mn(II)Mn(III) and Mn(III)$_2$/Mn(II)$_2$ oxidation states, respectively, during catalysis. In both series of hetero- and homovalent complexes, the substitution of

pyridine by carboxylate led to a strong increase of the reaction rate which was attributed to the ability of carboxylate ligands to act as internal bases. Pap et al. evaluated the CAT activity of two monuclear Mn(II) complexes formed with bis(2-picolyl)β-alanylamine and its methyl ester, [Mn(II)(**PBMPA**)Cl] and [Mn(II)(**MPBMPA**)Cl_2], in aqueous medium, in the pH range 7–11. These compounds showed maximal rates for H_2O_2 disproportionation at pH = 11 [66], where [Mn(II)(**MPBMPA**)Cl] reacted 30% faster than the complex with the non-methylated ligand (Table 1, entries 26 and 27). Therefore, the aqueous medium seems to level the effect of the internal carboxylate on the CAT activity. Zhou et al. employed the related N_3O-ligand **Adpa** to prepare a carboxylate bridged diMn(II) complex, [(**Adpa**)Mn(II)(μ-OAc)Mn(II)(**Adpa**)]$^+$ (Chart 2), that was considered a good model for the carboxylato-bridged diMn site of MnCAT [70]. This complex exhibited a first reversible oxidation potential at 0.39 V followed by an irreversible peak at E_{pa} 1.01 V (NHE) in MeCN. In aqueous solution of pH 7 [(**Adpa**)Mn(II)(μ-OAc)Mn(II)(**Adpa**)]$^+$ was able to disproportionate H_2O_2 after a lag period, with k_{cat} 593 min^{-1} (calculated from fitting to the Hill equation in TRIS buffer) and at least 363 turnover numbers, employing a high valent oxo-bridged dimer for catalysis [70].

Shin et al. reported that the mononuclear complex [Mn(II)(**TPA**)Cl]$^+$ (Chart 2), formed with the tetradentate N_4-donor tris(2-picolyl)amine, does not show CAT activity in aqueous medium, probably because water inhibits the substrate binding to the metal centre [71]. However, the authors demonstrated that this mononuclear complex was formed as a precursor of an active Mn(III)Mn(IV) species in the reaction of [(**TPA**)Mn(II)Cl_2Mn(II)(**TPA**)]$^{2+}$ with an excess of H_2O_2, in anhydrous MeCN [71]. [(**TPA**)Mn(II)Cl]$^+$ was also found to react with excess of anhydrous H_2O_2 (MeCN) and convert into the mixed valence [(**TPA**)Mn(III)(μ-O)$_2$(Mn(IV)(**TPA**)]$^+$. Based on spectroscopic studies, it was proposed that H_2O_2 disproportionation involves the cycling between Mn(III)Mn(IV) and Mn(III)Mn(II) oxidation states, to yield O_2 and H_2O with k_{cat} = 107 s^{-1} and K_M = 3.1 M (obtained from fitting to the Hill equation). At the end of the reaction, the inactive [Mn(**TPA**)$_2$]$^{2+}$ complex was isolated.

The Mn(II) complex of the N_3O-tetradentate bis(2-picolyl)amin o-3-chloropropan-2-ol, [Mn(II)(**PCINOL**)Cl_2], showed both high SOD and CAT activities in spite of the high oxidation potential of 1.05 V (NHE) of the Mn(II)/Mn(III) couple [60,72]. For the reaction with $O_2^{\cdot-}$, the measured rate constant (Table 1, entry 29) was higher than for other Mn(II) complexes of ligands with N_3O-donor sites. Second-order kinetics on [catalyst] was determined for the CAT activity of this compound in aqueous medium at pH 7, with $k_{cat}(H_2O_2)$ = 1690 M^{-2} s^{-1}, which implies the involvement of two complex molecules or a dimer in the slow step of the catalytic cycle. Additionally, the *in vitro* SOD and CAT activities of [Mn(II)(**PCINOL**)Cl_2] were much higher than for the Fe(II) analogue, and even if both compounds exhibited a remarkable protection of yeast strains against severe oxidative stress, the Mn(II) complex was much less effective than the Fe(II) counterpart [72]. The difference was attributed to changes in the coordination environment of the complexes inside cells and showed that *in vitro* SOD and CAT activities of the compounds may not be directly related to their *in vivo* activities.

Berggren et al. evaluated the CAT activity of two complexes, [Mn(II)(**L2**)]$_4^{4+}$ and [Mn(II)(**L3**)Cl_2] (Chart 2), formed with N_4-tetradentate and N_4O-pentadentate ligands derived from ethylenediamine. In this case, the additional carboxylate donor in the ligand resulted in a drop of H_2O_2 disproportionation activity (Table 1, entries 30 and 31) as a consequence of the higher denticity [73]. In [Mn(II)(**L3**)Cl_2] the ligand adopts the *cis*-α conformation with two labile Cl^- ions to exchange with the substrate [74]. **L2** forms tetrameric [Mn(II)(**L2**)]$_4^{4+}$ where the Mn(II) ions are surrounded by the N_4O-donor sites of the ligand and the sixth position is occupied by a carboxylate from a neighboring molecule resulting in a N_4O_2 coordination sphere around each Mn ion [75]. The longer lag phase and lower rate of H_2O_2 dismutation catalyzed by [Mn(II)(**L2**)]$_4^{4+}$ compared to [Mn(II)(**L3**)Cl_2] were interpreted in terms of the requirement for larger structural rearrangement to convert into the active catalyst [73]. The same behavior was observed for other two complexes of related compartmental dinucleating ligands with two chambers each providing with N_4- or N_4O-environment around the Mn ions [73].

Bernard et al. prepared the complex [Mn(II)(**L4**)(H_2O)]$^+$ (Chart 2) with another N_4O-pentadentate ligand derived from ethylenediamine, which reproduces the coordination sphere of the metal center of MnSOD, with one phenol mimicking the monodentate carboxylate bound to Mn at the active site and two 1-methylimidazole groups mimicking the histidine side-chains. This complex proved to be an efficient SOD mimic *in vitro* by cycling between the Mn(III)/Mn(II) redox states [76] and showed CAT activity (table 1, entry 32) [77]. Further, [Mn(II)(**L4**)(H_2O)]$^+$ was shown to reduce efficiently the superoxide flow in activated murine macrophages [77], exert an intracellular anti-inflammatory activity *in vivo* and complement mitochondrial MnSOD [78]. To get insights into the intermediates involved in the reaction of [Mn(II)(**L4**)]$^+$ with $O_2^{\cdot-}$ and the reactivity of these intermediates, Ching et al. studied the oxidative addition of electrochemically generated $O_2^{\cdot-}$ to [Mn(II)(**L4**)]$^+$ [79]. The reaction yielded a *side-on* peroxo [Mn(III)(**L4**)(O_2)] species. Spectroelectrochemical studies showed that strong acids favored Mn—O bond breakage resulting in the release of H_2O_2, while in the presence of H_2O (weak acid), [Mn(III)(**L4**)(O_2)] was reduced through a two electron process with O—O bond cleavage. A peroxoMn(III) species had also been observed in the reaction of [Mn(II)(**L5**)]$^{2+}$ (Chart 2) with KO_2 in anhydrous DMSO at −25 °C [80], and as an intermediate in a mixture of [Mn(II)(**N4py**)(OTf)]$^+$ (Chart 2) with $O_2^{\cdot-}$ in MeCN at −40 °C [81]. In the last case, reaction of the formed [(**N4py**)Mn(III)(OO)]$^+$ with [(**N4py**)Mn(II)(OTf)]$^+$ generated an heterovalent oxo-bridged Mn(III,IV) dimer [82]. Overall, these results support an inner-sphere mechanism for reaction of superoxide with this kind of Mn(II) complexes.

To emulate the electrostatic channel of the enzyme, Ching et al. functionalized [Mn(II)(**L4**)]$^+$ with cationic polyarginine peptides [83]. The functionalized complexes, [Mn(II)(**L4**-Arg$_n$)]$^{(n+1)+}$ (Chart 2), retained the association constants and ligand coordination to Mn(II) with slight increasing of the Mn(III)/Mn(II) redox potential, which remained at an appropriate value for $O_2^{\cdot-}$ dismutation. It was shown that the alkylation of the secondary amine of [Mn(II)(**L4**)]$^+$, with retention of the same overall charge, led to a lower k_{cat} for $O_2^{\cdot-}$ dismutation (i.e., $k_{cat}(O_2^{\cdot-})$ = 4.2 × 10^6 M^{-1} s^{-1} for [Mn(II)(**L4**-Gly1)]$^+$ *vs* $k_{cat}(O_2^{\cdot-})$ = 5.0 × 10^6 M^{-1} s^{-1} for [Mn(II)(**L4**)]$^+$, measured by stopped flow). However, under the same conditions, [Mn(II)(**L4**-Arg$_n$)]$^{(n+1)+}$ conjugates reacted at rates similar to [Mn(II)(**L4**)]$^+$ (Table 1, entries 32 and 33) indicating that the cationic residue compensated for the loss in activity [83]. Analysis of the effect of ionic strength on $k_{cat}(O_2^{\cdot-})$ suggested that only the charges closest to the SOD active metal centre exerted an electrostatic favorable influence.

Yu et al. demonstrated that the reaction of [Mn(II)(**Hptp1**)(MeCN)]$^{2+}$ (Chart 2) with H_2O_2 in either MeCN or water caused the complex to oxidatively couple to itself through a bimolecular reaction involving the phenol groups of two **Hptp1** ligands to yield the binuclear complex [(**Hptp1**-**ptp1**$^-$)Mn(II)$_2$(solv)$_2$]$^{3+}$ [84]. In a related complex, [Mn(II)(**H$_2$qtp1**)(MeCN)]$^{2+}$, with a *p*-quinol instead of *p*-cresol group, Mn was reported to catalyze the reversible oxidation of the quinol group of the ligand upon reaction with H_2O_2, thus serving as a turn-on sensor of H_2O_2 [85]. In this complex the reversible quinol/quinone redox process occurs at 0.31 V (NHE), while Mn(II) is oxidized at 0.88 V (NHE). Both, [Mn(II)

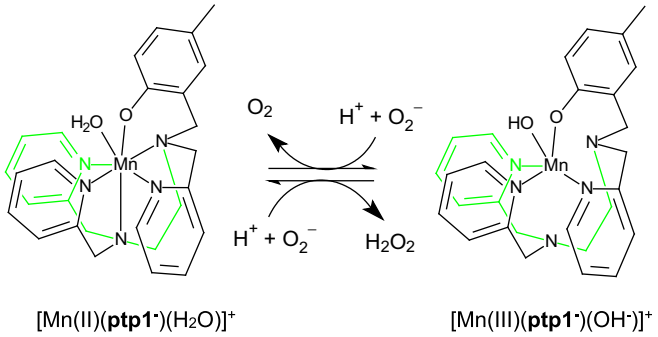

Scheme 4. Proposed species involved in $O_2^{\cdot-}$ dismutation by [Mn(II)(**ptp1**)$(H_2O)]^{2+}$.

(**H_2qtp1**)$]^{2+}$ and [Mn(II)(**Hptp1**)$]^{2+}$ showed to be effective at degrading $O_2^{\cdot-}$, with IC_{50} values of 11.3 nM (**H_2qtp1**) and 7.7 nM (**Hptp1**). Kenkel et al. studied the aqueous chemistry of [Mn(II)(**Hptp1**)$(H_2O)]^{2+}$ and determined the impact of the bound water molecule on the rate and mechanism of SOD catalysis [86]. It was shown that at pH > 6 the phenol group of the ligand was deprotonated and the monocationic [Mn(II)(**ptp1**$^-$)$(H_2O)]^+$ complex oxidized at E_{pa} 0.768 V (NHE) followed by deprotonation of the bound water molecule to yield [Mn(III)(**ptp1**$^-$)$(OH^-)]^+$. At lower pH, the Mn(II) could not be oxidized because the phenol group and the aqua ligand cannot stabilize a Mn(III) species. It was proposed that coordinated water facilitated proton-coupled-electron-transfer (PCET) lowering the oxidation potential of [Mn(II)(**ptp1**$^-$)$(H_2O)]^+$. The SOD activity of [Mn(II)(**ptp1**)$(H_2O)]^{2+}$ was evaluated at pH 7.4 and $k_{cat}(O_2^{\cdot-})$ was measured by stopped-flow in excess of $O_2^{\cdot-}$ (Table 1, entry 34) [86]. Based on solution studies and computational calculations the authors proposed that SOD catalysis displayed by this compound is achieved through a mechanism that involves heptacoordinate [Mn(II)(**ptp1**$^-$)$(H_2O)]^+$ and pentacoordinate [Mn(III)(**ptp1**$^-$)$(OH^-)]^+$ (Scheme 4) where the metal-bound water molecule facilitates the PCET lowering the Mn(III)/Mn(II) redox potential enough to allow efficient outer-sphere SOD catalysis.

The measured $k_{cat}(O_2^{\cdot-})$ for [Mn(II)(**ptp1**)$(H_2O)]^{2+}$ is much lower than for Mn(II)-pentaazamacrocycles (Section 3.3.), even when the last exhibit much more positive redox potentials that disfavor $O_2^{\cdot-}$ dismutation [86]. This different activity was explained taking into account that [Mn(II)(**ptp1**)$(H_2O)]^{2+}$ dismutates $O_2^{\cdot-}$ through an outer-sphere mechanism, while Mn(II)-pentaazamacrocycles react through an inner-sphere mechanism that compensate their unfavorable redox potential.

Ledesma et al. studied the antioxidant activity of Mn complexes of a compartmental N_3O_3-hexadentate diamine with two chemically different adjacent coordination chambers, **L6**$^{3-}$ [87]. **L6**$^{3-}$ is a versatile ligand that can afford complexes of different nuclearity depending on the reaction conditions [88,89]. The mononuclear Mn(III) complex of this asymmetric ligand, [Mn(III)**L6**] (Chart 2), possesses a coordination sphere saturated by the ligand. However, it was able to catalyze the disproportionation of both H_2O_2 and $O_2^{\cdot-}$ [88], with activity in the same range as other mononuclear Mn complexes with one or two labile coordination positions on the metal ion (Table 1, entry 35) and high turnover numbers (>300 mmol H_2O_2/mmol catalyst) for H_2O_2 disproportionation. Based on the low anodic potential of the Mn(III)/Mn(IV) couple of [Mn(III)**L6**], it was suggested that this complex decomposes either $O_2^{\cdot-}$ or H_2O_2 employing a high-valent catalytic cycle. Due to the lack of vacant or labile sites around the metal, the initial binding to the substrate was proposed to occur through ligand shift with the ligand acting as internal base to assist substrate deprotonation coupled to the redox reaction. Disproportionation of H_2O_2 by [Mn(III)**L6**] occurred with second-order kinetics on catalyst, thus evidencing the requirement of two molecules of catalyst in the slow redox half-reaction, as observed for other complexes that employ a high-valent catalytic cycle [60,71].

3.3. Mn(II) azamacrocyclic complexes

Mn(II) complexes of macrocyclic ligands derived from 1,4,7,10,13-pentaazacyclopentadecane (**[15]aneN$_5$**) [90] are the most active synthetic catalysts for superoxide disproportionation known to date and were the first to enter clinical trials [5]. [Mn(**[15]aneN$_5$**)Cl_2] (Chart 3) is an excellent catalyst for the dismutation of $O_2^{\cdot-}$ to O_2 and H_2O_2 (Table 1, entry 36), with a catalytic activity about 20% of the native human MnSOD enzyme [91]. The complex possesses seven-coordinate geometry, with a planar macrocyclic ligand conformation and two apical chlorides [92].

C-substituted pentaazamacrocyclic ligands afford high-spin d^5 Mn(II) *trans*-dichloro complexes with $E_{1/2}$ (NHE) in the range of +0.74–0.78 V and increased thermodynamic and kinetic stabilities upon increasing the number of C-substituents [93]. Riley and collaborators showed that stereochemistry has a remarkable effect on catalytic rates [92]. So, [Mn(*2R,3R,8R,9R*-**Cy[15]aneN$_5$**)Cl_2] (Chart 3), was able to dismutate $O_2^{\cdot-}$ with $k_{cat}(O_2^{\cdot-}) = 1.2 \times 10^8$ $M^{-1}\,s^{-1}$ at pH 7.4, and displayed high thermodynamic ($\log(K) = 13.3$) and kinetic stability (at any pH). In contrast, the isomeric complex [Mn(*2R,3R,8S,9S*-**Cy[15]aneN$_5$**)Cl_2], exhibited a similar stability profile but had no catalytic SOD activity. The basicity of the ligand was also found critical for kinetic stability. Thus, [Mn(**pyane**)Cl_2] (Chart 3) showed an improved stability profile compared to the parent [15]aneN$_5$ complex, while retained the SOD catalytic rate constant [94]. Among Mn(pyane)Cl_2 derivatives, the complexes with the bis(cyclohexyl)pyridine moiety, such as **M40403** (Chart 3, Table 1, entry 37), proved to be efficient in animal models of inflammation and reperfusion injury protecting against tissue damage [95]. **M40403** was employed in clinical trials to evaluate analgesic activity in subjects with pain due to cancer, and its enantiomer has entered phase 2 trials as a drug candidate for protection against radiation and chemotherapy-induced oral mucositis [96]. The *2S,21S*-dimethyl substituted **M40401** (Chart 3) derivative showed a catalytic rate for $O_2^{\cdot-}$ dismutation at pH 7.4 exceeding that of native mitochondrial MnSOD, while the *2R,21R*-dimethyl isomer **M40404** was inactive (Table 1, entries 38 and 39) [95c]. The X-Ray diffraction structure of **M40401** displayed two crystallographically-independent Mn(II) complexes [95b]: one complex molecule with the usual *trans*-dichloro seven-coordinate geometry and a second complex cation with a folded six-coordinate geometry in which one of the secondary amino groups occupies an axial site *trans* to one chloride in a pseudo-octahedral geometry and the second chloride is a counteranion. The ability of the complex to adopt such a folded conformation was thought as a reason for the high catalytic activity of **M40401** [90].

Maroz et al. performed kinetic and spectroscopic studies to show that the ability of a pentazamacrocycle ligand to accommodate Mn(III) pseudo-octahedral coordination influences the reactivity of a peroxoMn(III) intermediate formed in the catalytic process [97]. By applying stopped-flow techniques, a $MnLO_2^+$ intermediate could be detected and a mechanism was proposed where the catalytic activity is governed by the geometry of this intermediate and its reactivity with a second $O_2^{\cdot-}$. In this mechanism (Scheme 5) the first fast step corresponds to the activation of the Mn(II) complex by reaction with $O_2^{\cdot-}$ (Eq. 14). Reduction of the activated intermediate complex by a second superoxide was proposed to occur in the slow step (Eq. 15), with retention of the pseudo-octahedral geometry. In the third step (Eq. 16), proton assisted release of H_2O_2 takes place with conformational relaxation of the

Mn(II) complex to the starting complex with pentagonal-bipyramidal coordination sphere.

Dees et al. evaluated the water exchange process in seven-coordinate Mn(II) complexes of **[15]aneN$_5$** derivatives with the macrocyclic ligand in the equatorial plane and two water molecules in the axial positions [98]. This study supported a dissociative interchange (I_d) mechanism with $k_{ex}/[H_2O]$ (where k_{ex} is the first-order water exchange rate constant) values independent of pH but significantly lower than the second-order rate constants for the $O_2^{\bullet-}$ catalytic dismutation, suggesting that water release cannot be a rate determining step in the catalytic dismutation of $O_2^{\bullet-}$. An inner-sphere SOD catalytic pathway was proposed in terms of an interchange mechanism for the substitution of the water molecule on pentagonal-bipyramidal Mn(II) complexes, with $O_2^{\bullet-}$ acting as entering nucleophile. Ivanović-Burmazović et al. suggested that $O_2^{\bullet-}$, a nucleophile stronger than water, can react through an associative interchange (I_a) substitution mechanism [99]. Such an interchange mechanism requires an eight-coordinate transition state. An inner-sphere electron transfer within the SOD mechanism was supported by the lack of SOD activity of an eight-coordinate Mn(II) complex with reduction potential of 0.78 V (vs NHE) similar to [Mn(**[15]aneN$_5$**)] SOD mimics [12]. Based on these results the authors concluded that the redox potential is not the only important requirement for SOD activity, especially in the case of complexes with a relatively high redox potential, where coordination of superoxide seems to be crucial for its efficient reduction.

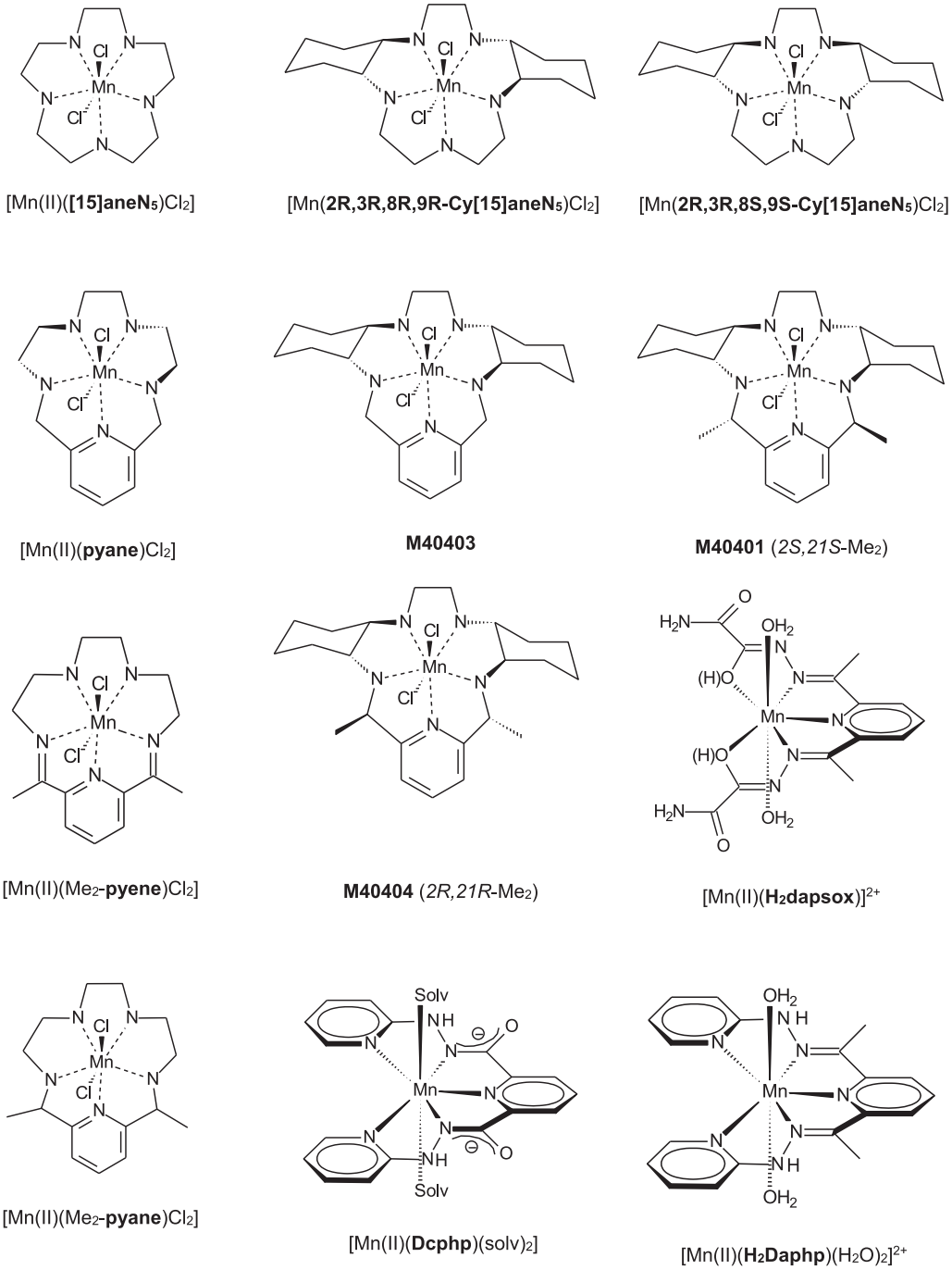

Chart 3. Structure of Mn-azamacrocyclic complexes.

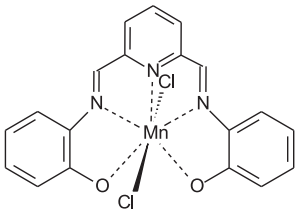

[Mn(II)(**Pimp**)Cl_2]

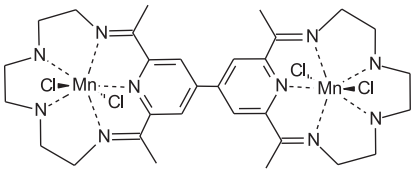

[$Mn(II)_2$(**bi-Me_2-pyene**)Cl_4]

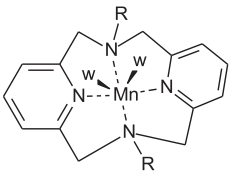

[Mn(II)(**$Py_2N_2R_2$**)$(H_2O)_2]^{2+}$
R = H, Me, ^{t}Bu

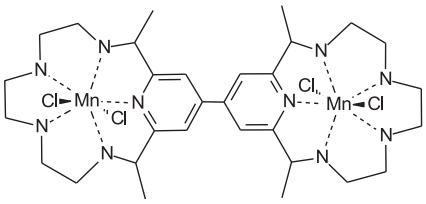

[$Mn(II)_2$(**bi-Me_2-pyane**)Cl_4]

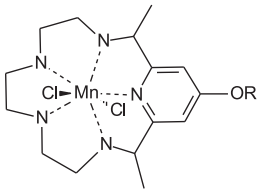

[Mn(II)(**L8-10**)Cl_2]
R = $C_{12}H_{25}$ (**L8**); $C_{16}H_{33}$ (**L9**);
$C_{22}H_{45}$ (**L10**)

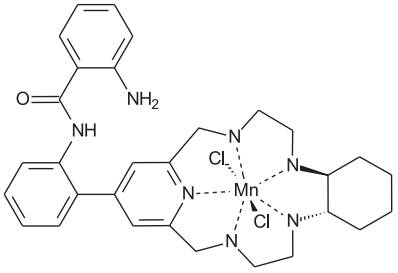

[Mn(II)(**L7**)Cl_2]

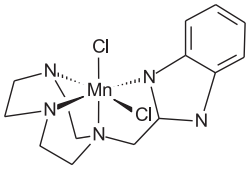

[Mn(II)(**Imtacn**)Cl_2]

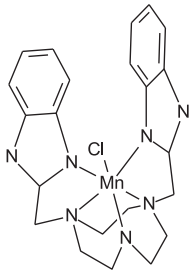

[Mn(II)(**Bimtacn**)Cl]$^+$

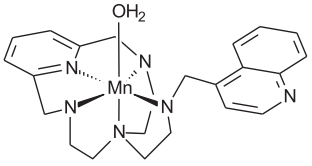

[$Mn(N_5$-**SL**$)(H_2O)]^{2+}$

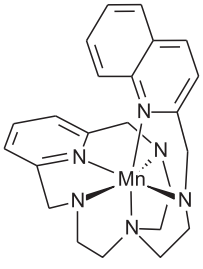

[$Mn(N_6$-**SL**$)]^{2+}$

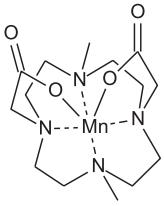

[Mn(II)(**L11**)]

Chart 3 (*continued*)

Complex [Mn(**Me_2-pyene**)Cl_2] (Chart 3), where the amino groups were replaced by imino groups, was SOD inactive. This lack of activity was first attributed to the rigidity of the macrocycle [90]. However, it was then observed that these imine complexes were stable in a quite narrow pH range due to acid/base hydrolytic processes and this could be the reason for the lack of SOD activity

$$Mn(II)L^{2+} + O_2^{\bullet-} \rightarrow Mn(III)LO_2^{+} \text{ (fast)} \quad (14)$$

$$Mn(III)LO_2^{+} + O_2^{\bullet-} \rightarrow Mn(II)LO_2 + O_2 \text{ (rate determining)} \quad (15)$$

$$Mn(II)LO_2 + 2H^{+} \rightarrow Mn(II)L^{2+} + H_2O_2 \text{ (fast)} \quad (16)$$

Scheme 5. Proposed mechanism for superoxide dismutation by Mn(II) azamacrocycles.

[100]. In particular, [Mn(**Me$_2$-pyene**)$(H_2O)_2$]$^{2+}$ is only stable at pH 6.1 [100]. Liu et al. studied the seven-coordinate Mn(II) complex of the rigid H_2dapsox ligand ([Mn(II)(**H$_2$dapsox**)]$^{2+}$, Chart 3), which is stable in the pH range of 6–10.5 and exhibits an $E_{1/2}$ = 0.65 V (vs NHE) in DMSO similar to Mn(II) complexes of **[15]aneN$_5$** derivatives. This compound reacted with $O_2^{\bullet-}$ even faster than the complex with the flexible macrocyclic [Mn(II)(**Me$_2$-pyane**)]$^{2+}$ (Chart 3) under the same reaction conditions (Table 1, entries 40–42) [101]. The fact that a seven-coordinate Mn complex of an acyclic rigid ligand showed ability for catalytic decomposition of $O_2^{\bullet-}$ supported that conformational flexibility of the ligand is not the key factor assisting SOD activity and that acyclic and rigid ligand systems can also be considered as structural motifs for the design of SOD mimics. Liu et al. also evaluated the redox potentials and SOD activity of two Mn(II) pentagonal bipyramidal sevencoordinate complexes formed with acyclic N_5-pentadentate ligands, [Mn(II)(**Dcphp**)$(CH_3OH)_2$] and [Mn(II)(**H$_2$Daphp**)$(H_2O)_2$]$^{2+}$ (Chart 3) [102]. These authors found that replacement of two imine-*N* by two hydrazido-*N* (amido-*N*) atoms decreased the Mn(III)/Mn(II) redox potential by at least 0.8 V, stabilizing the Mn(III) form of the complex, without changing the donor atom set and coordination geometry. Thus, neutral [Mn(II)(**Dcphp**)$(CH_3OH)_2$] exhibited a quasi-reversible Mn(III)/Mn(II) couple at 0.372 V in DMSO and reacted with $O_2^{\bullet-}$ with rate similar to [Mn(II)(**Me$_2$-pyane**)]$^{2+}$ (Table 1, entry 43), while [Mn(II)(**H$_2$Daphp**)$(H_2O)_2$]$^{2+}$ was electrochemically silent in the scan range from −1 to 1.2 V and was inactive. More recently, Kose et al. evaluated the SOD and CAT activities of another seven-coordinate Mn(II) complex of an acyclic rigid Schiff-base ligand, [Mn(II)(**Pimp**)Cl_2] (Chart 3) (Table 1, entry 44). In this complex the Mn(II) ion possesses a pentagonal bipyramidal geometry with the ligand lying in the equatorial plane and two chloride ions at the axial positions [103]. This complex was able to catalyze the dismutation of $O_2^{\bullet-}$, although with low SOD activity, probably as a result of the compound instability in the conditions of the SOD assay. [Mn(II)(**Pimp**)Cl_2] showed CAT activity in methanol only after addition of Et_3N, with a rate of 2.5 mL O_2 s^{-1} and 997 mmol H_2O_2 decomposed per mmol of complex per min [103]. Presumably, addition of base increased the complex stability and lengthened its half-life to achieve high TONs.

Lieb et al. examined the *trans*-effect of the hydroxo group on water exchange and catalytic SOD activity of dinuclear seven-coordinate Mn(II) complexes [104] obtained with pentaazamacrocyclic ligand scaffolds in combination with a 2,2′,6,6′- tetraa cetyl-4,4′-bipyridine building block ([Mn$_2$(**bi-Me$_2$-pyene**)Cl_4] and [Mn$_2$(**bi-Me$_2$-pyane**)Cl_4], Chart 3). Magnetic, potentiometric, electrochemical, and water exchange measurements showed that the two manganese(II) centers of [Mn$_2$(**bi-Me$_2$-pyane**)Cl_4] and [Mn$_2$(**bi-Me$_2$-pyene**)Cl_4] behave independently from each other. However, the dinuclear amine complex possessed increased stability and acidity of the coordinated water molecules (pK_{a1} = 8.92 for deprotonation of the first aqua ligand in [Mn$_2$(**bi-Me$_2$-pyane**)$(H_2O)_4$]$^{4+}$) compared to the corresponding mononuclear analogue allowing the detection of a stable *trans*-aqua-hydroxo-Mn(II) species in aqueous solution. The *trans*-effect of the hydroxo ligand on $O_2^{\bullet-}$ dismutation was evidenced comparing the SOD activity (per Mn) of [Mn$_2$(**bi-Me$_2$-pyane**)Cl_4] and [Mn(**Me$_2$-Pyane**)Cl_2], at pH 10. The $k_{cat}(O_2^{\bullet-})$ measured for the *trans*-aqua-hydroxo complex [Mn$_2$(**bi-Me$_2$-pyane**)$(OH)_2(H_2O)_2$]$^{2+}$, at pH 10, resulted about 1.8-fold higher than the corresponding mononuclear complex [Mn(**Me$_2$-Pyane**)]$^{2+}$ that is not able to form stable hydroxo species (Table 1, entries 40 and 45).

Mn complexes of aminophenyl substituted pyridine pentaazamacrocyclic ligands bearing amino or carboxy auxiliary placed near the axial position of the metal showed similar or better activity than **M40403**, measured by indirect methods under the same conditions [105]. Among this series, the *o*-aminobenzoyl derivative [Mn(II)(**L7**)Cl_2] (Chart 3), was the most potent with seven fold higher SOD activity than **M40403**. The introduction of the acid-base auxiliary proximal to the Mn center was proposed to assist proton transfer coupled to $O_2^{\bullet-}$ reduction. The same effect had been observed for Mn complexes with a pyridyl auxiliary derived from **EUK-113** (see Section 3.1) [34].

Lieb et al. introduced a long linear aliphatic chain into the ligand framework of the manganese pentaazamacrocyclic SOD mimics to afford compounds with increased lipophilicity [106]. These authors obtained amphiphilic analogues of [Mn(**Me$_2$-Pyane**)Cl_2] with linear aliphatic chains linked to the macrocyclic core by an ether functionality ([Mn(**L8-10**)Cl_2]), (Chart 3) which form supramolecular aggregates that exist as defined micellar assemblies and show thermodynamic stability dependent on the hydrocarbon chain [106]. These compounds exhibited the same redox properties (in MeOH and DMSO) and SOD activity at pH 8.1 (HEPES buffer) as the nonsubstituted [Mn(**Me$_2$-Pyane**)Cl_2] analogue, although lower at pH 7.4, in particular in the presence of phosphate (Table 1, entries 40 and 47). Cell culture studies of SOD activity in the cytosol and mitochondria indicated that increased lipophilicity enhanced the beneficial effect of these compounds at low concentration, probably as a result of the improved diffusion through the lipid bilayer of the cell membranes. However, at concentrations higher than 10 μM, toxic effects have been observed that became more prominent with elongation of the aliphatic chain [106].

In phosphate buffer the SOD activity of macrocyclic polyamine Mn(II) complexes was lower than in HEPES buffer of the same pH (shown for **M40403** and [Mn(**Me$_2$-Pyane**)Cl_2] in Table 1, entries 37 and 40). It was demonstrated that phosphate does not contribute to metal dissociation [32], so the decrease in SOD activity should not be related to complex instability in phosphate buffer but to phosphate-specific interactions (electrostatic or through coordination) with the metal centre that hampers $O_2^{\bullet-}$ binding. This was especially evidenced for **M40403** due to its tendency to adopt six-coordinate geometry with only one free coordination site for anion binding [90]. Friedel et al. suggested that [Mn(**Me$_2$-Pyane**)Cl_2] was not strongly affected by phosphate because in this complex the ligand prefers a planar disposition and there is still one labile water molecule *trans* to phosphate in the sevencoordinate environment, which can be easily replaced by superoxide [32]. Another important point is that $MnCl_2$ has shown activity in phosphate buffer, but not in HEPES (Table 1, entry 2) [32,107]. Thus, even a SOD inactive complex could convert into an active catalyst *in vivo*, through metal dissociation into the phosphate containing physiological environment. Recently, Weekley et al. demonstrated that phosphate binding is related to the transformation of Mn pentaazamacrocycles into MnPi in cells, which, depending on the extent of the complex–phosphate interactions, can level their SOD activity in cellular environments to that of MnPi [108]. This was evidenced in cells treated with [Mn$_2$(**bi-Me$_2$-pyane**)Cl_4], with high phosphate binding constants, $K_1(HPO_4^{2-})$ = 13300 M^{-1} and K_2-(HPO_4^{2-}) = 440 M^{-1}, where 75–85% of the Mn(II) of the complex transformed into MnPi, even when this complex possesses high thermodynamic stability. By contrast, [Mn(**Me$_2$-Pyane**)Cl_2], with weak phosphate binding ($K_1(HPO_4^{2-})$ = 90 M^{-1}), remained largely

intact in cells and exhibited *in vitro* SOD activity higher than [Mn_2(**bi-Me_2-pyane**)Cl_4] in the presence of phosphate (Table 1, entries 40 and 45).

Although during some time, Mn(II) pentaazamacrocycles were considered selective toward superoxide, it was shown that [Mn(II)(**Me_2-pyane**)Cl_2] also disproportionates nitric oxide *in vitro* and in cells [109]. However, they fail almost completely in terms of their CAT activity. A different reactivity with H_2O_2 was observed for Mn(II) complexes of the tetraazamacrocycle pyridinophane (**$Py_2N_2R_2$**) ligands. These pyridine containing tetraazamacrocycle binds Mn(II) to give monomeric complexes with the tetradentate ligand folded around the metal centre leaving two *cis* positions occupied by labile water molecules (Chart 3). Lee et al. have shown that the *N*-substituent (R = H, Me, ^{t}Bu) can tune steric properties to favor or prevent dimer formation [110]. Thus, the Mn(II) complex with two small *N*-Me substituents [(**$Py_2N_2Me_2$**)$Mn(H_2O)_2]^{2+}$ was found to disproportionate H_2O_2 in aqueous solution over a wide pH range (pH = 2–8.5) achieving turnover numbers as high as 58,000 in water, although with moderate rate (Table 1, entry 48) [111a]. The reaction started after an induction period that was attributed to the slow formation of [Mn(**$Py_2N_2Me_2$**)$(H_2O)(O_2H)]^+$ in the first reaction step. At high complex concentrations catalyst self-inhibition occurred probably by the formation of a catalytically inactive dimer, while in diluted solutions the starting complex was recovered. Similarly, [Mn(**Py_2N_2**)$(H_2O)_2]^{2+}$ (R = H) disproportionated H_2O_2 with high initial rates but much lower turnover numbers (830 mol H_2O_2/mol catalyst) in water. In contrast, complex [Mn(**$Py_2N_2{}^tBu_2$**)$(H_2O)_2]^{2+}$ with the bulkiest ^{t}Bu substituent, showed no evidence for H_2O_2 disproportionation, probably due to the increased hindrance of the amine substituent [110]. Interestingly, the authors showed that the ^{t}Bu-derivative became active for aqueous electrocatalytic H_2O oxidation and this was related to the oxidation potential ($E_{pa} \approx 1.0$ V) lower than the unsubstituted or Me-substituted derivatives ($E_a \approx 1.2$ V). More recently, Xu et al. investigated two other derivatives [Mn(**$Py_2N_2R_2$**)Cl_2] (R = Cy, ^{i}Pr) toward H_2O_2 disproportionation and compared them to pyridinophane complexes with R = Me and ^{t}Bu, aimed at better delineate the effect of pyridinophane substitution on the catalytic reaction [111b]. In this work, the authors confirmed that the donor strength of the ligand is the key factor that affects the stability of the Mn(III) oxidation state while the ligand bulkiness is critical to the rate of catalysis. The last was supported by the linear relationship between log(k_{cat}) and the steric parameter (*A* value) for the substituents.

Li et al. obtained two Mn(II) complexes of a triazamacrocycle bearing one or two pending imidazol groups, [Mn(II)(**Imtacn**)Cl_2] and [Mn(**Bimtacn**)Cl]ClO_4 (Chart 3), which differ in their half-wave potentials by about 0.4 V. The two compounds showed combined SOD (modest) and CAT activities, the last in the presence of base with turnover numbers as high as 600 mmol H_2O_2/mmol catalyst (Table 1, entries 49 and 50)) [61]. These complexes showed high stability over pH with a percentage of free Mn^{2+} less than 0.07–0.08%, and a predominant $[MnL(OH)]^+$ species at physiological or higher pH. This was taken as evidence of suitability of the vacant site at the Mn(II) atom for the coordination of hydroxyl ion and, in consequence, small anions. The higher SOD activity of [Mn(**Bimtacn**)Cl]ClO_4, with two benzimidazole groups, than [Mn(II)(**Imtacn**)Cl_2] was attributed to the benzimidazole groups surrounding the metal ion to form a hydrophobic channel which favors the attack of $O_2^{\cdot-}$. By contrast, the higher CAT activity of $[Mn(II)(\textbf{Imtacn})OH]^+$ was associated to the enhanced ability of this complex to form a dinuclear Mn active species required for H_2O_2 dismutation, hampered in $[Mn(II)(\textbf{Bimtacn})OH]^+$ due to the steric hindrance of the two benzimidazole groups. The involvement of dinuclear species during CAT activity of $[Mn(II)(\textbf{Imtacn})OH]^+$ was confirmed by ESI-MS, which showed peaks corresponding to oxygen-bridged or hydroxyl-bridged binuclear complex cations.

Clares et al. obtained highly stable Mn(II) complexes with a family of aza-scorpiand like tetraazamacrocycles (**SL**) functionalized with a side chain containing quinoline [112], pyridine, naphthalene or propylamine groups in the tail, that exhibit $E_{1/2}$ in the range 0.55–0.85 V (vs NHE) at pH 7.0 [113]. Coordination of the heteroaromatic group to the Mn ion depended on its substitution position, affording $[Mn(N_6\text{-}\textbf{SL})]^{2+}$ with propylamine-, 2- pyridine- or 2-quinoline-**SL** derivatives acting as hexadentate ligands, and $[Mn(N_5\text{-}\textbf{SL})(H_2O)]^{2+}$ with 3-pyridine- or 4-quinoline-**SL** derivatives acting as pentadentate ligands (Chart 3). The reaction of these compounds with $O_2^{\cdot-}$ was evaluated at pH 7.4 (Table 1, entries 51 and 52). Complexes $[Mn(N_5\text{-}\textbf{SL})(H_2O)]^{2+}$, with the sixth coordination position occupied by a water molecule, showed higher SOD activity than $[Mn(N_6\text{-}\textbf{SL})]^{2+}$. The lower rates for $O_2^{\cdot-}$ dismutation by $[Mn(N_6\text{-}\textbf{SL})]^{2+}$ was attributed to the protection of the Mn ion exerted by the hydrocarbon chains of the macrocyclic core and the pyridine/quinoline ring, reducing the accessibility of the substrate to the active site. The complex containing the 4-quinoline group in the side arm showed the highest SOD efficiency both *in vitro* ($k_{McCF}(O_2^{\cdot-}) = 1.5 \times 10^7\ M^{-1}\ s^{-1}$) and *in vivo* in prokaryotic (bacteria) and eukaryotic (yeast and fish embryo) organisms. The high SOD activity of this compound was explained in terms of the easier accessibility of the substrate, the presence of one bound water molecule (as in the active site of MnSOD) and the quinoline in the tail to assist proton transfer during catalysis. Interestingly, none of these mononuclear complexes showed any CAT activity in the performed assays.

Other tetraazamacrocyle ligand bearing two *N*-substituted carboxylate groups **L11**, forms a very stable Mn(II) complex, [Mn(II)(**L11**)] (Chart 3), with an irreversible oxidation peak at 1.39 V (NHE) at pH 7 [114]. In spite of the high potential and irreversibility of the oxidation process, [Mn(II)(**L11**)] was effective to scavenge $O_2^{\cdot-}$ and exhibited very low toxicity in biological systems.

3.4. Manganese porphyrins (MnPs) and corroles

3.4.1. MnPs as antioxidant agents

Metalloporphyrins are among the first synthetic catalytic antioxidants employed to eliminate $O_2^{\cdot-}$. An Fe porphyrin, [Fe(**TM-4-PyP**)]$^{5+}$, with a rate constant of $3 \times 10^7\ M^{-1}\ s^{-1}$ for $O_2^{\cdot-}$ dismutation, was the first introduced as a SOD mimic [115]. The citotoxicity of Fe porphyrins and the similar SOD activity and higher stability of the Mn analogues, led research towards MnPs as catalytic antioxidants [116]. MnPs employ the Mn(III)/Mn(II) redox couple for $O_2^{\cdot-}$ dismutation and the SOD activity of these compounds increases as their Mn(III)/Mn(II) potentials shift anodically. This fact suggests that the reduction of Mn(III) to Mn(II) occurs in the rate-limiting step of the catalytic cycle, through a predominantly outer-sphere mechanism which does not involve $O_2^{\cdot-}$ binding to the Mn site [117]. In a detailed work, Miriyala et al. described MnPs that behave as successful mitochondria-targeted MnSOD mimics [118]. The impact of electrostatics on the $O_2^{\cdot-}$ dismutation catalyzed by MnP was clearly addressed, resulting that electron-withdrawing cationic groups close to the Mn site constitute the most important feature for the catalysis of $O_2^{\cdot-}$ [118]. This positive charge converts the Mn(III) center in an electron-defficient site, preparing it to admit electrons from superoxide in the first stage of the dismutation reaction. Besides, the closeness and distribution of the positive charge around the metal center "electro statically" guides $O_2^{\cdot-}$ to the active metal site enhancing the SOD activity [119]. This is well exemplified by three Mn(III) complexes of porphyrin substituted with positively charged methylpyridinium groups on the *meso* positions, [Mn(**TM-4-PyP**)]$^{5+}$,

[Mn(**TM-3-PyP**)]$^{5+}$ and [Mn(**TM-2-PyP**)]$^{5+}$ (Chart 4). While [Mn(**TM-3-PyP**)]$^{5+}$ displayed SOD activity comparable to that of [Mn(**TM-4-PyP**)]$^{5+}$, the rate constant measured for [Mn(**TM-2-PyP**)]$^{5+}$ was 10-fold higher (Table 1, entries 53–55) [120]. The increased activity of [Mn(**TM-2-PyP**)]$^{5+}$ was attributed to the close proximity of the positive charges to the metal center (*ortho* effect), a feature that affects the Mn(III)/Mn(II) redox potential and facilitates the reaction with the negatively charged $O_2^{\bullet-}$ [121]. It was stated that cationic Mn *N*-substituted pyridyl- and *N,N′*-disubstituted imidazolylporphyrins combine in their structure critical features to mimic both the action and the site of mitochondrial MnSOD: (1) redox active Mn site, (2) multiple cationic charge and (3) (the possibility of) four alkyl chains. The longer the alkyl chains, the higher the Mn porphyrin accumulation in mitochondria [118].

Given that the ability to remove H_2O_2 generated during $O_2^{\bullet-}$ dismutation can be regarded as an advantageous property, several MnPs that are efficient SOD mimics were evaluated as CAT mimics. Day et al. tested two Mn(III) porphyrins [Mn(**TM-4-PyP**)]$^{5+}$ and [Mn(**TBAP**)]$^{3-}$ (Chart 4) for H_2O_2 disproportionation [122]. These authors found that [Mn(**TBAP**)]$^{3-}$ and [Mn(**TM-4-PyP**)]$^{5+}$ possess CAT activity in addition to the previously reported SOD activity, in the presence of EDTA, and determined their ability to protect endothelial cells against H_2O_2-mediated injury. Trova and colleagues synthesized a series of analogues of the [Mn(**TBAP**)]$^{3-}$,

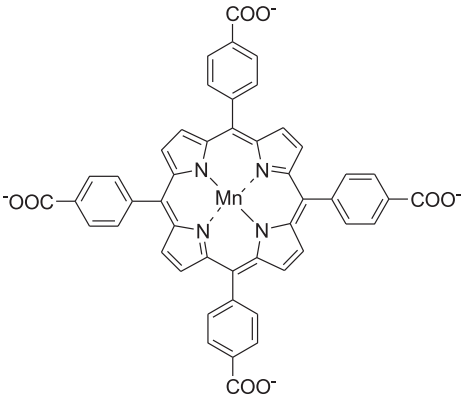

[Mn(**TBAP**)]$^{3-}$

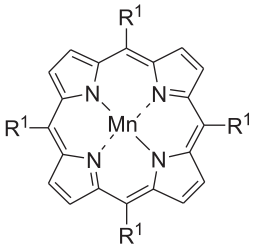

R^1 = *N*-Me-4-py$^+$: [Mn(**TM-4-PyP**)]$^{5+}$
R^1 = *N*-Me-3-py$^+$: [Mn(**TM-3-PyP**)]$^{5+}$
R^1 =*N*-Me-2-Py$^+$: [Mn(**TM-2-PyP**)]$^{5+}$
R^1 = *N*-Et-2-Py$^+$: [Mn(**TE-2-PyP**)]$^{5+}$
R^1 = -CO_2Et: [Mn(**TECP**)]$^+$

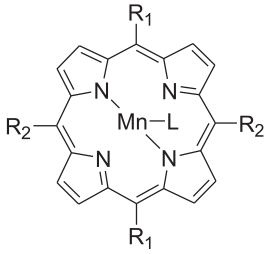

EUK-	L	R_1	R_2
418	OAc	cyclopropyl	H
423	OAc	phenyl	H
425	OAc	ethyl	ethyl
450	OAc	3,4-methoxy-phenyl	H
451	Cl	4-tetra-hydropyrano	H
452	Cl	cyclohexyl	H
453	Cl	propyl	H

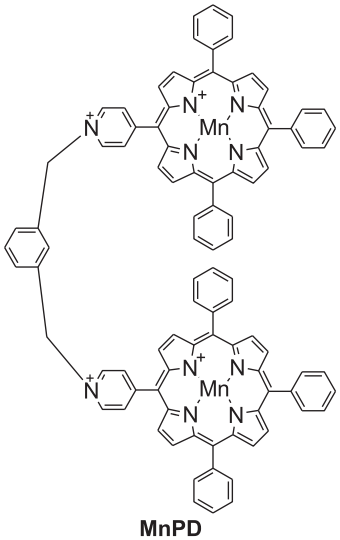

MnPD

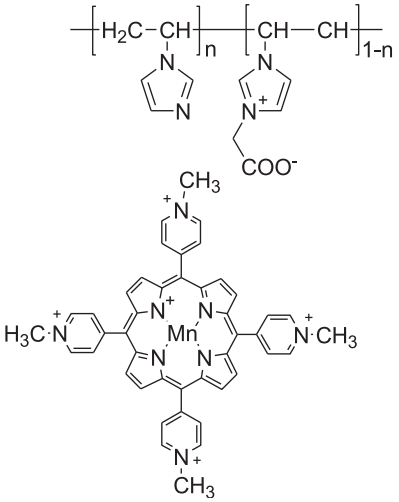

[Mn(**TM-4-PyP**)]$^{5+}$ **CM-PVIm**

Chart 4. Structure of Mn-porphyrins and corroles.

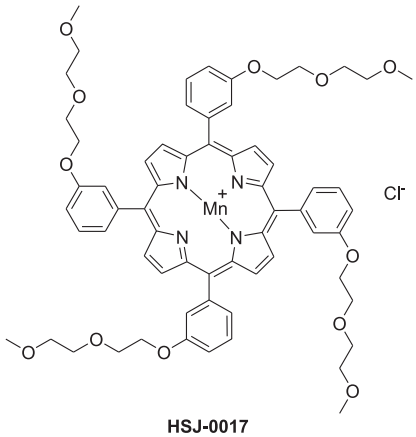

HSJ-0017

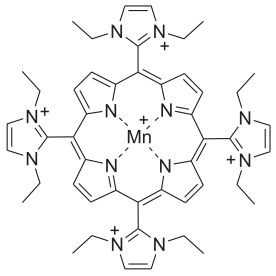

[Mn(**TDE-2-ImP**)]$^{5+}$

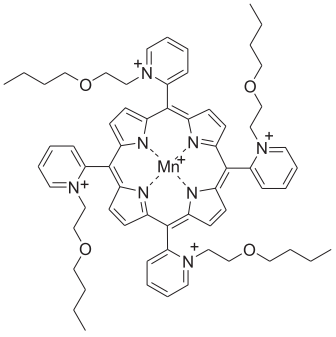

[Mn(**TnBuOE-2-PyP**)]$^{5+}$

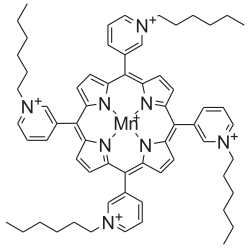

[Mn(**TnHex-3-PyP**)]$^{5+}$

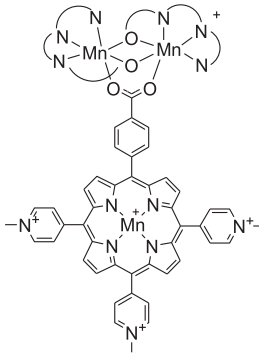

[Mn$_2$(**L12**)$_2$**P1**]$^{5+}$

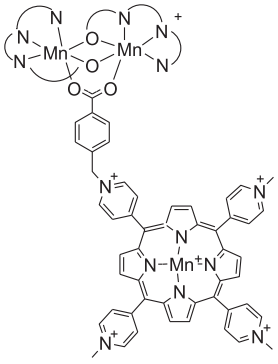

[Mn$_2$(**L12**)$_2$**P2**]$^{6+}$

Chart 4 (*continued*)

with glyoxylate- and glyoxamide-derivatives [123]. Complexes of this series exhibited similar or enhanced SOD activity compared to [Mn(**TBAP**)]$^{3-}$ [124] but most of them displayed better CAT activity than the [Mn(**TBAP**)]$^{3-}$ analogue. This work demonstrated that the direct attachment of carboxylate group to the *meso* positions of the porphyrin ring (instead of benzoate groups), enhances the CAT activity with a slight improvement of SOD activity. Besides, the porphyrins bearing two unsubstituted *meso* positions showed higher CAT activity than mono-substituted and tetra *meso*-substituted compounds. It was demonstrated later that commercial samples of [Mn(**TBAP**)]$^{3-}$ contained Mn impurities (oxo/hydroxo/acetate Mn clusters) which were responsible for the measured SOD activity and that pure [Mn(**TBAP**)]$^{3-}$ does not show any detectable SOD activity in aqueous medium [125] (Table 1, entry 56).

Parks and co-workers evaluated cationic porphyrins with alkylpyridinium and ethylester groups in *meso* position, [Mn(**TE-2-PyP**)]$^{5+}$, [Mn(**TM-2-PyP**)]$^{5+}$ and [Mn(**TECP**)]$^{+}$ (shown in Chart 4) with known SOD and CAT activities, to reduce the effects of liver injury in isolated perfused rat livers [126]. In this series, the highest SOD activity was observed for [Mn(**TE-2-PyP**)]$^{5+}$ and [Mn(**TM-2-PyP**)]$^{5+}$, while [Mn(**TM-2-PyP**)]$^{5+}$ showed two times higher CAT activity than [Mn(**TE-2-PyP**)]$^{5+}$ or [Mn(**TECP**)]$^{+}$ (Table 1, entries 53, 57, 59). The MnPs with the highest SOD activity ([Mn(**TE-2-PyP**)]$^{5+}$ and [Mn(**TM-2-PyP**)]$^{5+}$), were the most effective at attenuating ischemia reperfusion injury, while [Mn(**TECP**)]$^{+}$, with minimal SOD activity but catalase similar to [Mn(**TE-2-PyP**)]$^{5+}$, was markedly less effective at attenuating liver injury. The three MnPs also exhibited inhibition of lipid peroxidation, with comparable IC_{50} values (1.1–1.5 μM), indicating these compounds are more potent than CuZnSOD.

In the search of orally active therapeutics agents, Rosenthal et al. informed the study of **EUK-418** and new analogues of Mn (III) 5,15-disubstituted porphyrins (called **EUK-400** series, Chart 4) [127]. Although some of the studied compounds were synthetized previously [128], the strength of this work was the complete

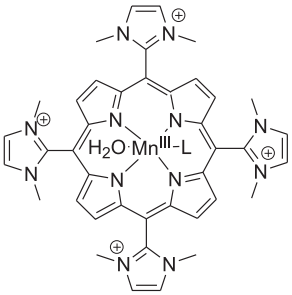

[Mn(**TDMImP**)]$^{5+}$

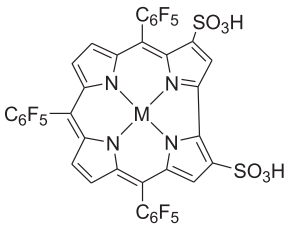

1-Fe: M = Fe
1-Mn: M = Mn

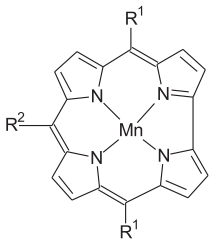

R^1 = R^2 = N-Me-2-Py$^+$: **3-Mn**
R^1 = N-Me-2-py$^+$, R^2 = C_6F_5: **4-Mn**
R^1 = N-Me-4-py$^+$, R^2 = C_6F_5: **5-Mn**
R^1 = N-Me-4-py$^+$, R^2 = C_6FH_4: **6-Mn**
R^1 = N-Me-4-py$^+$, R^2 = C_6H_5: **7-Mn**
R^1 = N-Me-4-py$^+$, R^2 = anysil: **8-Mn**
R^1 = N-Me-4-py$^+$, R^2 = 4-morpholinophenyl: **9-Mn**

Chart 4 (*continued*)

characterization of the new **EUK-400** series compounds and the evaluation of their antioxidant activity and bioavailability. All the **EUK-400** compounds exhibited SOD, CAT and peroxidase activity, although lower than Mn-salen complexes **EUK-189** and **EUK-207** (Chart 1). Complexes of the **EUK-400** series have similar catalase and peroxidase activities, but their SOD activities vary about tenfold from the most active (**EUK-418**) to the least active (**EUK-425**) (Table 1, entries 60–65). This behaviour is in contrast to Mn-salen complexes, which have similar SOD activities, but wide ranging catalase and peroxidase activities depending on the substituent (See Section 3.1). Even though their catalytic activities are lower, MnPs of the **EUK-400** series protect cells at lower concentrations than the Mn-salen complexes **EUK-189** and **EUK-207**, possess greater intracellular stability and oral availability.

Later, the same research group investigated the ability of MnPs of the **EUK-400** series and Mn-salen complexes **EUK-189** and **EUK-207** to prevent apoptosis of endothelial cells [129]. Agents that scavenge reactive oxygen species, such as SOD, glutathione peroxidase and catalase, are able to reduce radiation-induced apoptosis and necrosis when administered previous to irradiation [130] or within few minutes after exposition to radiation [131]. It was demonstrated that all **EUK-400** compounds resist intracellular degradation and are mitigating agents that reduce radiation injury. Among this class of MnPs, **EUK-451** was identified as the lead compound, which exhibited low toxicity and eliminated at least one form of radiation injury, by mitigating radiation induced apoptosis.

In a recent work, Kubota et al. reported the syntheses of **MnPD** (Chart 4), a novel dinuclear manganese porphyrin complex with multiple antioxidant activities, under nearly physiological conditions [132]. The **MnPD** complex contains two cationic Mn-porphyrins ([Mn(**M4PyP$_3$P**)]$^{2+}$) cross-linked by *m*-xylene, with the purpose of keeping the two manganese ions separated at the appropriate distance to favor catalase activity (Table 1, entry 66). The rate constants for $O_2^{\cdot-}$ dismutation and peroxynitrite ($ONOO^-$) reduction measured for **MnPD** were the same as found for the mononuclear [Mn(**M4PyP$_3$P**)]$^{2+}$, indicating that the SOD and peroxinitrite reducing activities of the mononuclear Mn-porphyrin are not affected by formation of the dimer. By contrast, there was a remarkable difference in CAT activity between the dinuclear **MnPD** and mononuclear [Mn(**M4PyP$_3$P**)]$^{2+}$, with $k_{cat}(H_2O_2)$ = 330 M^{-1} s^{-1} for the dimer much higher than $k_{cat}(H_2O_2)$ = 11 M^{-1} s^{-1} for the mononuclear Mn-porphyrin. The CAT activity of **MnPD** was ascribed to synergism of the two Mn active sites, where hydroxo-Mn(IV) was detected as an intermediate. The antioxidant activity of **MnPD** was examined *in vivo*, as a preliminary study, with the "running test" in SOD deficient mice. The intraperitoneal administration of **MnPD** restored notably the running time (after 8 and 24 hs) converting this compound in a potential therapeutic antioxidant.

The same research group took advantage of an artificial polymer as a support for metal complex incorporation. The designed complex contains the cationic manganese porphyrin ([Mn(**TM-4-PyP**)]$^{5+}$) and carboxymethylpoly(1-vinylimidazole), **CM-PVIm**. [Mn(**TM-4-PyP**)]$^{5+}$ binds **CM-PVIm** through multivalent binding between carboxyl groups of **CM-PVIm** and the pyridinium cations of [Mn(**TM-4-PyP**)]$^{5+}$, leading to a complex surrounded by the imidazole groups of the polymer (Chart 4) [133]. Incorporation of **CM-PVIm** enhanced CAT activity, with $k_{cat}(H_2O_2)$ value of 150 M^{-1} s^{-1}, which was measured using a Clark-type oxygen electrode. The electron-withdrawing porphyrin structure and the chain length of the **CM-PVIm** polymer affect the CAT activity of the complex. By modulating the polymer chain length from 10,000 to 3000, the catalase activity of the complex increased. This report was the first example of a water-soluble CAT mimic based on a polymer-bound Mn-porphyrin, active at physiological pH.

In 2014, Li et al. investigated the SOD and CAT activity and the therapeutic potential of a lipophilic Mn(III) porphyrin, **HSJ-0017** (Chart 4, Table 1, entry 68), in free radical-related diseases [134]. This novel agent was designed with four diethyleneglycolmonoethyl

ether chains on the *meso*-phenyl rings in order to promote its distribution within tissues [135] and attenuate the toxicity. **HSJ-0017** showed SOD activity, although was nearly 20-fold less active than bovine Cu/ZnSOD. The CAT activity of **HSJ-0017** was determined spectrophotometrically according to the method described by Beers and Sizer [136]. No significant H_2O_2 scavenging activity was detected with concentration of **HSJ-0017** smaller than 0.01 μmol/L, whereas higher concentration of **HSJ-0017** (from 0.1 to 10 μmol/L) quickly scavenged H_2O_2. Besides dual SOD/CAT activity, **HSJ-0017** showed antioxidant, antitumor, anti-inflammatory, radioprotective, chemoprotective and hepatoprotective effects.

Tovmasyan et al. performed a comprehensive evaluation of the CAT activity of different compounds, including MnPs and other SOD mimics [117]. The CAT activity of 12 Mn(III) *N*-substituted (alkyl and alkoxyalkyl) pyridylporphyrin-based and Mn(III) *N,N′*-dialkylimidazolium porphyrin, [Mn(**TDE-2-ImP**)]$^{5+}$ (Chart 4) was evaluated and rate constants were compared to the enzyme ($k_{cat}(H_2O_2) = 1.5 \times 10^6\ M^{-1}\ s^{-1}$) under the same experimental conditions. The lowest value of $k_{cat}(H_2O_2) = 5.8\ M^{-1}\ s^{-1}$ was determined for the anionic and SOD inactive [Mn(**TBAP**)]$^{3-}$ while for all the other tested MnPs $k_{cat}(H_2O_2)$ ranged from 23 to 88 $M^{-1}\ s^{-1}$ (rates given in Table 1, entries 69–74), with the highest value found for the cationic [Mn(**TnBuOE-2-PyP**)]$^{5+}$ (Chart 4). In all cases, low values of TONs were measured, ranging from 3.94 ([Mn(**TnHex-3-PyP**)]$^{5+}$ (Chart 4) to 12.49 ([Mn(**TBAP**)]$^{3-}$) mol O_2/mol catalyst, which resulted from either the instability of MnPs towards oxidative degradation and/or their low ability to catalyze H_2O_2 dismutation. A detailed analysis of the impact of electron density at the metal center of MnPs on the catalysis of H_2O_2 dismutation concluded that high electron deficiency of the Mn site supports high $k_{cat}(H_2O_2)$ values. Besides, $\log[k_{cat}(H_2O_2)]$ correlates with the $\log[k_{cat}(O_2^{\bullet-})]$ linearly, indicating that the best SOD mimics also dismutate H_2O_2 faster. However, even the most efficient SOD mimics do not present enough CAT activity; the most active MnP has only 0.0004% of the enzyme activity. In the same work, MnPs (as well as other redox-active compounds) were evaluated in an *Escherichia coli* model of H_2O_2-induced damage. Protection against H_2O_2 was only observed when *E. coli* was incubated simultaneously with high concentrations of MnP and H_2O_2. In view of these results, the authors concluded that elimination of H_2O_2 with MnPs in a CAT-like fashion seems to be biologically irrelevant [117].

In a very recent and motivating work, Squarcina et al. have informed the design of a novel dual synthetic enzyme (di-zyme) with the aim of bringing together SOD and CAT artificial mimics in one synthetic architecture [137]. In their design, a Mn(III) single site is coupled to a dinuclear [Mn_2(II)(**L12**)$_2$] unit, in an attempt to combine effectively the dismutation of $O_2^{\bullet-}$ into O_2 and H_2O_2 with the subsequent conversion of H_2O_2 into H_2O and O_2. In particular, a polycationic Mn-porphyrin with one pendant terminal carboxylate linker was designed to bind the Mn_2**L12**$_2$ core. The assembly of porphyrins **P^1** and **P^2** to the Mn_2(**L12**)$_2$ core led to [Mn_2(**L12**)$_2$-**P^1**]$^{5+}$ and [Mn_2(**L12**)$_2$**P^2**]$^{6+}$ (Chart 4). Conjugation with the polycationic heme produced a remarkable increase of the complex solubility in water and resulted in enhanced bioavailability of the di-zyme. The catalytic SOD and CAT activities of the di-zymes were determined by evaluating the $O_2^{\bullet-}$ scavenging rate and the H_2O_2 decomposition kinetics, respectively (Table 1, entries 75 and 76). The high rates of $O_2^{\bullet-}$ and H_2O_2 decomposition show that the conjugation of Mn-based SOD/CAT mimics leads to efficient difunctional antioxidants. The order found for SOD activity: [Mn_2(**L12**)$_2$**P^2**]$^{6+}$ > [Mn_2(**L12**)$_2$**P^1**]$^{5+}$ > [Mn(**TM-4-PyP**)]$^{5+}$ ≫ [Mn_2(**L12**)$_2$(OAc)]$^+$, indicates the dominant role of the Mn-heme unit implemented by an additional contribution of the Mn_2-core in $O_2^{\bullet-}$ scavenging, while the Mn_2-core dictates the CAT activity since similar H_2O_2 dismutation rates were observed for the three systems. The remarkable high CAT activity of [Mn_2(**L12**)$_2$**P^2**]$^{6+}$ indicates that this di-zyme is one of the best artificial catalases under physiological conditions. Besides, given that the weak point of heme-based functional systems is associated to the porphyrin fragility when exposed to oxidative risk, the authors explored the self-protection of [Mn_2(**L12**)$_2$**P^2**]$^{6+}$ when exposed to H_2O_2, simulating oxidative stress. The coupling of the porphyrin with the Mn_2-core stops the oxidative degradation process after a few seconds, with a porphyrin recovery of 75–85% (in H_2O_2 200 μM) based on the residual Soret absorption. Authors also tested its activity *in vivo* by means of quantification of H_2O_2 accumulated in *Chlamydomonas reinhardtii* when this photosynthetic alga was exposed to high illumination conditions. The results indicated that the presence of [Mn_2(**L12**)$_2$**P^2**]$^{6+}$ (0.1 μM) reduces H_2O_2 accumulation up to 60%. These di-zymes conjugate key features to enhance photoprotection of photosynthetic cells under oxidative stress.

3.4.2. Anti- and pro-oxidant activities of MnPs

The reaction of dismutation of H_2O_2 catalyzed by MnPs in aqueous system has been suggested to take place *via* the Mn(III)P/$(O)_2$Mn(V)P redox pair [117], involving the two-electron transfer steps depicted in Eqs. (17) and (18).

$$(H_2O)_2Mn(III)P^{5+} + H_2O_2 \Longleftrightarrow (O)_2Mn(V)P^{3+} + 2H_2O + 2H^+ \quad (17)$$

$$(O)_2Mn(V)P^{3+} + H_2O_2 + 2H^+ \Longleftrightarrow (H_2O)_2Mn(III)P^{5+} + O_2 \quad (18)$$

$(O)_2Mn(V)P^{3+}$ was proposed on the basis of several reports informing the isolation of a dioxoMn(V) product from heterolytic cleavage of H_2O_2 by MnP [138,139]; i.e., the relatively stable *trans*-dioxoMn(V) generated by reaction of H_2O_2 and the water-soluble [Mn(**TDMImP**)]$^{5+}$ (Chart 4). This reaction occurs through a Mn(III)(OH)(OOH)-**TDMImP** intermediate, which converts into the dioxoMn(V) species through a concerted mechanism in which the O—O bond heterolysis is coupled to the deprotonation of the trans OH^- ligand, mimicking the "push–pull" mechanism found in heme enzymes.

Due to the presence of cellular reductants (as ascorbate, simple thiols or thiols from proteins), it has been proposed that *in vivo* Mn(III)P would reduce rapidly to Mn(II)P [140], so that the dismutation of H_2O_2 would involve the Mn(II)P/(O)Mn(IV)P redox pair (Eqs. (19) and (20)).

$$(H_2O)Mn(II)P^{4+} + H_2O_2 \Longleftrightarrow (H_2O)(O)Mn(IV)P^{4+} + H_2O \quad (19)$$

$$(H_2O)(O)Mn(IV)P^{4+} + H_2O_2 \Longleftrightarrow (H_2O)Mn(II)P^{4+} + O_2 + H_2O \quad (20)$$

In a scenario of high concentration of cellular reductants and low concentration of H_2O_2 (*in vivo* conditions) MnP can be oxidized by H_2O_2, (Eqs. (17) and (19)) behaving as H_2O_2 reductase, and the high-valent oxo-Mn complexes can rapidly be back reduced by cellular reductants, instead of using H_2O_2 (Eqs. (18) and (20)) [117]. A similar behavior has been suggested for $O_2^{\bullet-}$ dismutation reaction: in place of oxidizing and reducing $O_2^{\bullet-}$, MnPs could perform a superoxide reductase action, closing the catalytic cycle with cellular reductants [141].

In view of the high levels of cellular reductants and as it has been established that CAT activity of MnPs is no relevant *in vivo* due to their low $k_{cat}(H_2O_2)$, it is more probable that in biological systems MnPs do associate with H_2O_2 in a pro-oxidative and catalytic mode [141]. This is supported by a number of works where MnPs have been employed as pro-oxidant catalysts for oxidation of organic substrates by H_2O_2, where high-valent oxo-Mn porphyrins are the active species [142].

Since MnPs are able to produce H_2O_2 (as result of dismutation of $O_2^{\bullet-}$ and through reaction with cellular reductants followed by reduction of $O_2^{\bullet-}$) [140,143] and the formed H_2O_2 could oxidize a

number of biological molecules (ascorbate oxidation; thiol oxidation; thiol peroxidation; lipid oxidation; lipid peroxidation; NAD oxidation; NADP oxidation), it was proposed that MnPs rather than removing H_2O_2 can take advantage of its generation for therapeutic treatments [141]. This proposal considers that the mechanism of action of MnPs with H_2O_2 is more likely a peroxidase- or thiol-oxidase- rather than a catalase-type [8b,140,141].

3.4.3. Manganese(III) corroles

Metallocorroles have also been explored as catalysts for $O_2^{\bullet-}$ and H_2O_2 dismutation [144]. Gross' group published the first report on the SOD activity of two classes of water-soluble manganocorroles, one with two sulfonic acid head groups on the 3,17-pyrrole carbon atoms (**1-Mn**) and the other with either *ortho*- or *para*-pyridinium ring in the *meso* positions (**3-Mn** – **5-Mn**) (Chart 4) [145]. These Mn(III) corroles cannot achieve the Mn(II) oxidation state within the electrochemical window in aqueous solution but can be oxidized to Mn(IV) at potentials shown in Table 1, entries 77–80. On this basis, authors proposed that Mn(III) corroles shuttle between the Mn(III)/Mn(IV) oxidation states during the catalytic dismutation of $O_2^{\bullet-}$. Accordingly, and unlike porphyrins, a negative shift of redox potentials results in an increase in SOD activity of corroles (Table 1, entries 77–80), while the close proximity of positive charges to the metal center still enhances catalytic rates (**4-Mn** > **5-Mn**). This series was expanded by examining positively charged Mn(III) corroles that differ from **5-Mn** in the C10 *meso* substituent (**6-Mn**–**9-Mn** in Chart 4) [146]. These Mn(III) corroles are oxidized to Mn(IV) at potentials ranging from 0.75 V for the complex with the most electron-withdrawing substituent (**6-Mn**) to 0.65 V (vs NHE) for the most electron-donor substituent (**9-Mn**). A significant decrease in IC_{50} values calculated from the cytochrome *c* assay was observed as a function of the C10 aryl substituent: from 181 and 160 nM for the electron-poor **5-Mn** and **6-Mn** to 20 ± 3 nM for the more electron rich **7-Mn**, **8-Mn** and **9-Mn**. This behavior led the authors to propose that the reduction of $O_2^{\bullet-}$ by Mn(III) is the rate-limiting step for the disproportionation of $O_2^{\bullet-}$ by Mn(III) corroles. The same group reported that at neutral pH, **1-Mn** does not catalyze H_2O_2 disproportionation, but it starts to display catalytic activity at pH 9.5, with $k_{cat}(H_2O_2)$ of 5.6 M^{-1} s^{-1} [147]. Additionally, the efficiency of **1-Mn** to decompose H_2O_2 could be improved by the presence of proteins. HSA- and BSA-conjugated **1-Mn** release O_2 even at pH 7.4, albeit in rather slow processes of 2.2 ppm s^{-1} [147] and 14 μM s^{-1} [148], respectively. It must be noted that the Fe(III) analogue, **1-Fe** (Chart 4), reacts with H_2O_2 much faster ($k_{cat}(H_2O_2)$ of 6400 M^{-1} s^{-1}) and much more efficiently than **1-Mn** [147].

3.5. Other Mn complexes of acyclic ligands

Besides the four major classes of SOD/CAT mimics described above, a few other mononuclear complexes have been evaluated for $O_2^{\bullet-}$ and/or H_2O_2 decomposition and some of them will be briefly described in this section.

Kaizer' group reported a series of neutral octahedral Mn(II) complexes of iminoisoindoline derivatives, [Mn(II)(**R′-Ind**)$_2$], with Mn(II) bound to the six *N*-donor sites of two ligands [149]. Compounds of this family reacted with $O_2^{\bullet-}$ at similar rates (Table 1, entry 81) without observable dependence on the *E*(Mn(III)/Mn(II)) potentials spanned in the range of 0.646 to 0.826 V (vs NHE). Based on their redox behavior, an inner-sphere mechanism was suggested for the disproportionation of $O_2^{\bullet-}$ by these complexes, where the peripheral N—H functions of the (R′-imino)isoindoline ligands might assist in proton-channeling associated with the electron-transfer steps. Among complexes of this series, [Mn(II)(**Ind**)$_2$] and [Mn(II)(**4′Me-Ind**)$_2$] (Chart 5) were evaluated as CAT mimics, in DMF (Table 1, entry 81) [150]. [Mn(II)(**4′Me-Ind**)$_2$], with lower redox potential (0.662 V vs NHE) and a more electron-donating-

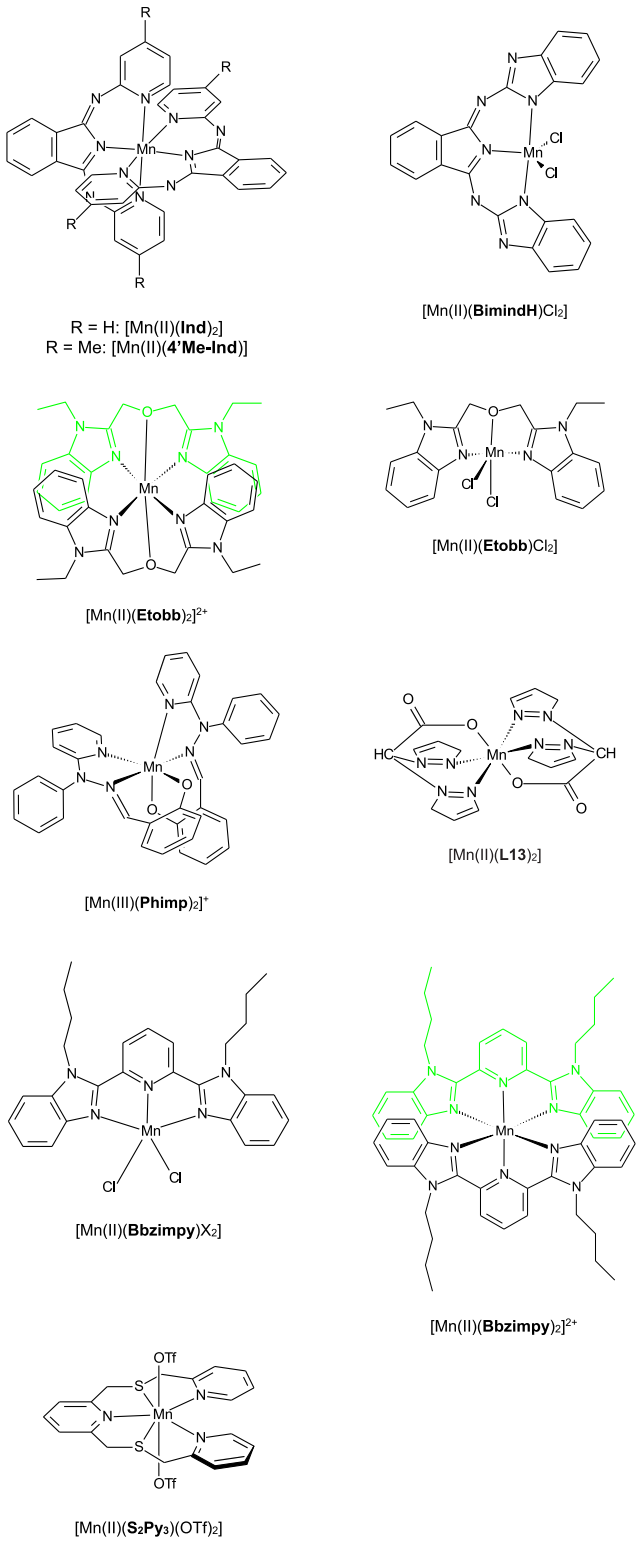

Chart 5. Structure of other Mn complexes of acyclic ligands.

methyl substituted pyridyl ring, reacted faster than [Mn(II)(**Ind**)$_2$] (0.759 V vs NHE), but showed lower affinity for the substrate. R′-iminoisoindoline ligands also afforded 1:1 Mn(II) complexes that showed CAT activity [151]. The pentacoordinate [Mn(II)(**IndH**)Cl_2] complex (Table 1, entry 82), while inactive without addition of an external base, disproportionated H_2O_2 in MeCN, in the presence of nitrogenous bases with second order kinetics ($k_{cat}(H_2O_2)$ = 1.5 M^{-1} s^{-1}). In aqueous buffer of pH = 9.5, this complex decomposed

H_2O_2 with saturation kinetics, with relatively high $k_{cat}(H_2O_2)$ = 38 s^{-1} but poor affinity for H_2O_2 (K_M = 489 mM; the larger the Michaelis-Mentem constant, K_M, the lower the affinity for the substrate) [151]. The related complex [Mn(II)(**BimindH**)Cl_2] (Chart 5) disproportionated H_2O_2 in EtCN, with second order kinetics ($k_{cat}(H_2O_2)$ = 4.12 M^{-1} s^{-1}) without addition of exogenous base [152]. The rate dependence on the basicity of the ligand suggested that the catalytic activity of these Mn(II) complexes can be controlled by the modification of electron donor properties of the ligand.

The N_2O-tridentate V-shaped bis-benzimidazole ligand, **Etobb**, formed with Mn(II) two kind of complexes, with one or two ligands per Mn(II) ion: [Mn(II)(**Etobb**)Cl_2] and [Mn(**Etobb**)$_2$]$^{2+}$ (Chart 5). In the former, Mn(II) is surrounded by N_2OCl_2 in trigonal bipyramidal geometry and in the second, Mn(II) is in a distorted octahedral N_4O_2 environment [153]. Although both complexes reacted with $O_2^{\cdot-}$, the octahedral complex reacted faster than [Mn(II)(**Etobb**)Cl_2] (Table 1, entries 83 and 84).

Ghosh et al. reported a Mn(III) complex formed with a tridentate N_2O hydrazone ligand containing phenolate, pyridine and imine donors, [Mn(III)(**Phimp**)$_2$]$^+$ (Chart 5), where the six coordination positions are occupied by the N_4O_2 donor sites of two ligands in a distorted octahedral geometry [154]. This complex was found to react with $O_2^{\cdot-}$ at a rate one order of magnitude higher than any other hexacoordinate Mn complex evaluated up to date (Table 1, entry 85). Replacement of phenolate by naphtolate in [Mn(III)(**N-Phimp**)$_2$]$^+$ or introduction of a Me residue on the C-imine in [Mn(III)(**Me-Phimp**)$_2$]$^+$, resulted in decreased activity with $k_{McCF}(O_2^{\cdot-})$ = 1 × 10^7 M^{-1} s^{-1} and 1.5 × 10^7 M^{-1} s^{-1} [154], respectively, although still one order of magnitude higher than other complexes with N_4O_2 coordination sphere. Reduction potentials for the Mn(III)/Mn(II) couples of these complexes were 0.37 (**N-Phimp**) and 0.64 (**Me-Phimp**) V vs NHE in MeCN, compared to 0.515 V for [Mn(III)(**Phimp**)$_2$]$^+$, so the activity was not directly related to the reduction potentials. Another Mn(II) complex with N_4O_2 coordination environment, [Mn(II)(**L13**)$_2$] (Chart 5), obtained with a pyrazolyl-based ligand **L13**$^-$, exhibited $O_2^{\cdot-}$ scavenging [155], with much lower rate constant (Table 1, entry 86) than [Mn(III)(**Phimp**)$_2$]$^+$, and even lower than [Mn(**Etobb**)$_2$]$^{2+}$ and amino-Mn(II) complexes with Mn bound to a N_4O_2 donor set [64,65], and did not react with H_2O_2.

Kose et al. tested the CAT activity of 1:1 and 1:2 Mn(II):**Bbzimpy** complexes, in which the N_3-tridentate ligand was disposed in a planar arrangement affording pentacoordinate [Mn(II)(**Bbzimpy**)X_2] (X = Cl^-, SCN^-) and hexacoordinate [Mn(II)(**Bbzimpy**)$_2$](ClO_4)$_2$ [156] (Chart 5). The two types of compounds showed CAT activity in methanol in the presence of base, after an induction period, and reacted at similar initial rates, in the range of 53–68 mmol O_2 per mol of complex per second, after a lag period. The hexacoordinate [Mn(II)(**Bbzimpy**)$_2$]$^{2+}$ showed longer induction period than [Mn(II)(**Bbzimpy**)]$^{2+}$, suggesting that ligand rearrangement or partial dissociation had to take place in the hexacoordinate complexes before HO_2^- binding to the metal centre to start the catalytic cycle.

Grau et al. found that seven-coordinate Mn(II) complexes (Chart 5) containing linear pentadentate ligands with an alternating NXNXN binding motif (X = N, O, S) disposed in the equatorial plane, were active single-site catalysts for the dismutation of $O_2^{\cdot-}$ and H_2O_2 in acetonitrile/water mixtures [157]. In particular the sulfur-containing complex, [Mn(II)(**S_2Py_3**)($OTf)_2$], was the best catalyst of this series for both SOD and CAT activities (Table 1, entry 87). The complex showed excellent stability during catalysis in the presence of added base, and this was attributed to the strong binding of the sulfur donors to the metal ion. The high stability of the catalyst was reflected in the high turnover numbers of 275 mmol H_2O_2 / mmol catalyst measured in the CAT assay.

Zienkiewicz et al. tested the CAT activity of Mn(II) complexes of simple *N,O*-bidentate pyridylalcohol ligands, [Mn(**2-$(CH_2)_2$OHpy**)$_2$($NCS)_2$] [158] and [Mn(**2-CH_2OHpy**)(SO_4)($H_2O)_2$] [159], in neutral aqueous solution. The authors claimed the complexes behaved as true catalysts since they reverted to their original form after depleting all the H_2O_2, although reacted with slow rates of 1.1–2.8 mmol H_2O_2 per mmol of catalyst per minute.

Joshi employed pulse radiolysis to study the reaction of $O_2^{\cdot-}$ with Mn(II) complexes generated *in situ* in the presence of small natural organic ligands, at pH 7 [160]. Rate constants in the range 0.27–1.52 × 10^8 M^{-1} s^{-1} were determined in phosphate buffer, with the highest values obtained in the presence of catechol and tetrahydroquinone ($k_{cat}(O_2^{\cdot-})$ 1.5 and 1.52 × 10^8 M^{-1} s^{-1}, respectively). It must be noted that the $O_2^{\cdot-}$ scavenging rate constant by Mn^{2+} ions, determined by the authors by pulse radiolysis under the same conditions, was 1.1 × 10^8 M^{-1} s^{-1}. Based on transient absorption traces it was proposed that reaction with $O_2^{\cdot-}$ takes place through intermediacy of $LMnO_2^+$ (formed in a fast step) followed by reaction with a second $O_2^{\cdot-}$ to yield O_2 and H_2O_2 and restore the starting Mn(II) complex.

4. Conclusions

The efficient conjugation of the two-electrons H_2O_2 dismutation with the one-electron $O_2^{\cdot-}$ disproportionation at a single Mn centre is still an unresolved question. Precissely, the best artificial catalyst with dual CAT/SOD activity is a compound combining a mononuclear cationic Mn(II) porphyrinic centre with a dinuclear $Mn(II)_2$ site [137], thus suggesting that bringing together these two key structural features into one molecule is the best option for efficient mimics that reproduce the activity of the two enzymes. However, some reflexions can be extracted from the plethora of mononuclear Mn complexes that have been studied.

MnSOD employs a mononuclear Mn site for the efficient $O_2^{\cdot-}$ removal, while MnCAT possesses a dinuclear Mn site for H_2O_2 dismutation. However, FeCAT decomposes H_2O_2 at a single heme site, and this feature inspired chemists to intend reproducing the same kind of chemistry with Mn complexes.

Most mononuclear Mn-based SOD mimics employ Mn(II)/Mn(III) cycles for $O_2^{\cdot-}$ dismutation –just the same as the enzyme-, although when the redox potential of the Mn(III)/Mn(IV) couple is low enough, a higher redox cycle is used. Therefore, to disproportionate $O_2^{\cdot-}$ these systems shuttle between oxidation states with the best adapted redox potential. Besides, complexes that are electrochemically inactive in a wide potential window or with oxidation potentials even higher than the $O_2^{\cdot-}/H_2O_2$ reduction potential, can dismutate $O_2^{\cdot-}$ through an inner-sphere mechanism. It is now known that the ligand flexibility is not a requirement for SOD activity, and that a positive charge near the metal centre can be an important factor favoring $O_2^{\cdot-}$ dismutation, which is especially evident in those complexes reacting through an outer-sphere mechanism (i.e., porphyrins). However, the last is not observed in other cases, i.e., sulphonate derivatives of Mn-Schiff-base complexes with enhanced SOD activity compared to the unsubstituted complexes. An even more important observation is that complexes with almost the same *in vitro* SOD activity differentiate in their *in vivo* protecting activity. This is well exemplified by comparing **EUK-134** and **M40403**. The two compounds have similar effectiveness for $O_2^{\cdot-}$ removal *in vitro*, but when mice deleted of mitochondrial MnSOD were treated with **EUK-134** an increased survival and "mito-protective" effect was observed, whereas **M40403** was ineffective [29,7].

Ligand donor sites, endogenous acid/base groups, the metal environment and second-sphere effects are effective to modulate

redox potentials of the metal centre, and in some cases the resulting potentials correlate well with the activity of the compound toward $O_2^{\cdot-}$; however, steric factors prevail over electronic ones for H_2O_2 dismutation, an observation in line with the need for dimer formation. This is particularly evident when comparing the CAT activity of Mn complexes of ligands with varied basicity and steric requirements. While the donor strength of the ligand controls the redox potentials (modulated by the electron withdrawing/donor effect of substituents in the ligand) the CAT activity shows a well defined linear correlation with steric parameters. The flexibility of the ligand is another important feature for the formation of the dimer required for catalytic removal of H_2O_2. Thus, those complexes with highly crowded faces or low ligand flexibility to fold around the metal ion, are poorer for H_2O_2 dismutation. Overall, there are several common features affecting the CAT activity of mononuclear Mn complexes: in all cases where mechanistic and/or spectroscopic studies were performed, dimer formation was observed, the reaction involved a high valent catalytic cycle – unlike the enzyme that employs $Mn(II)_2/Mn(III)_2$ oxidation states for H_2O_2 removal- and proceeded through an inner-sphere mechanism.

Ligand features modulate the stability of the Mn complexes toward dissociation in aqueous media and their substitution reactions rates, which are crucial for the long survival of the compounds, especially in biological systems. However, even when a number of Mn compounds have shown higher stability (longer half-lives) than the Fe counterparts – which are rapidely degraded by H_2O_2-, the total catalytic turnover numbers for H_2O_2 disproportionation in most cases are still low. Conjugation of simple Mn complexes to synthetic polymers or proteins has been a useful strategy to remove H_2O_2 and $O_2^{\cdot-}$ with improved TONs.

Acknowledgments

We are grateful for the financial support from the National University of Rosario (Grant number BIO401), CONICET (Grant number 337) and the Agency for Science, Technology and Innovation of Santa Fe (Grant number 2010-164-16).

References

[1] Y. Sheng, I.A. Abreu, D.E. Cabelli, M.J. Maroney, A.-F. Miller, M. Teixeira, J.S. Valentine, Chem. Rev. 114 (2014) 3854–3918.
[2] S.G. Rhee, T.-S. Chang, W. Jeong, D. Kang, Mol. Cells 29 (2010) 539–549.
[3] J.P. Kehrer, Toxicology 149 (2000) 43–50.
[4] J.W. Whittaker, Arch. Biochem. Biophys. 525 (2012) 111–120.
[5] S. Cuzzocrea, D.P. Riley, A.P. Caputi, D. Salvemini, Pharmacol. Rev. 53 (2001) 135–159.
[6] D. Salvemini, C. Muscoli, D.P. Riley, S. Cuzzocrea, Pulm. Pharmacol. Ther. 15 (2002) 439–447.
[7] D.P. Riley, Chem. Rev. 99 (1999) 2573–2588.
[8] (a) O. Iranzo, Bioorg. Chem. 39 (2011) 73–87;
(b) I. Batinic-Haberle, A. Tovmasyan, E.R. Roberts, Z. Vujaskovic, K.W. Leong, I. Spasojevic, Antioxid. Redox Signaling 20 (2014) 2372–2415;
(c) C. Policar, in: J.S. Reboucas, I. Batinic-Haberle, I. Spasojevic, D.S. Warner, D. St., Clair (Eds.), Redox Active Therapeutics, Springer, Berlin, 2016, pp. 125–164;
(d) S. Signorella, C. Hureau, Coord. Chem. Rev. 256 (2012) 1229–1245;
(e) A.J. Wu, J.E. Penner-Hahn, V.L. Pecoraro, Chem. Rev. 104 (2004) 903–938.
[9] V.L. Kinnula, J.D. Crapo, Am. J. Respir. Crit. Care Med. 167 (2003) 1600–1619.
[10] (a) B. Halliwell, J.M.C. Gutteridge, Free Radicals in Biology and Medicine, fourth ed., Oxford University Press, New York, 2007;
(b) J.G. Charrier, C. Anastasio, Atmos. Environ. 45 (2011) 7555–7562.
[11] B.H. Bielski, D.E. Cabelli, R.L. Arudi, A.B. Ross, J. Phys. Chem. Ref. Data 14 (1985) 1041–1106.
[12] I. Ivanović-Burmazović, M.R. Filipović, Adv. Inorg. Chem. Book Series 64 (2012) 53–95.
[13] (a) S. Goldstein, I. Fridovich, G. Czapski, Free Radical Biol. Med. 41 (2006) 937–941;
(b) L.M. Ellerby, D.E. Cabelli, J.A. Graden, J.S. Valentine, J. Am. Chem. Soc. 118 (1996) 6556–6561;
(c) C.A. Ramilo, V. Laveque, Y. Guan, J.R. Lepock, J.A. Tainer, H.S. Nick, D.N. Silverman, J. Biol. Chem. 274 (1999) 27711–27740.
[14] A.F. Miller, in: A. Messerschmidt, R. Huber, K. Wieghardt, T. Paulos (Eds.), Handbook of Metalloproteins, Wiley & Sons, Chichester, U.K., 2001, pp. 668–682.
[15] (a) G.E.O. Borgstahl, H.E. Parge, M.J. Hickey, W.F. Beyer, R.A. Hallewell, J.A. Tainer, Cell 71 (1992) 107–118;
(b) M.M. Dixon, K.A. Pattridge, W.C. Stallings, J.A. Fee, M.L. Ludwig, Biochemistry 34 (1995) 1646–1660.
[16] I.A. Abreu, D.E. Cabelli, Biochim. Biophys. Acta 1804 (2010) 263–274.
[17] Y. Guan, M.J. Hickey, G.E.O. Borgstahl, R.A. Hallewell, J.R. Lepock, D. O'Connor, Y. Hsieh, H.S. Nick, D.N. Silverman, J.A. Tainer, Biochemistry 37 (1998) 4722–4730.
[18] A.S. Hearn, M.E. Stroupe, D.E. Cabelli, C.A. Ramilo, J.P. Luba, J.A. Tainer, H.S. Nick, D.N. Silverman, Biochemistry 42 (2003) 2781–2789.
[19] V.J. Leveque, M.E. Stroupe, J.R. Lepock, D.E. Cabelli, J.A. Tainer, H.S. Nick, D.N. Silverman, Biochemistry 39 (2000) 7131–7137.
[20] Y. Sheng, E.B. Gralla, M. Schumacher, D. Cascio, D.E. Cabelli, J.S. Valentine, Proc. Natl. Acad. Sci. U.S.A. 109 (2012) 14314–14319.
[21] (a) P. Chelikani, I. Fita, P.C. Loewen, Cell. Mol. Life Sci. 61 (2004) 192–208;
(b) B.I. Kruft, R.S. Magliozzo, A.A. Jarzęcki, J. Phys. Chem. A 119 (2015) 6850–6866;
(c) V.L. Pecoraro (Ed.), Manganese Redox Enzymes, VCH, New York, 1992.
[22] (a) S.V. Khangulov, V.V. Barynin, S.V. Antonyuk-Barynina, Biochim. Biophys. Acta Bioinerg. 1020 (1990) 25–33;
(b) G.S. Waldo, J.E. Penner-Hahn, Biochemistry 34 (1995) 1507–1512.
[23] (a) J.W. de Boer, W.R. Browne, B.L. Feringa, R. Hage, C.R. Acad Sci. Ser. II C: Chim. 10 (2007) 341–354;
(b) T. Stich, J. Whittaker, R. Britt, J. Phys. Chem. B 114 (2010) 14178–14188.
[24] V.V. Barynin, M.M. Whittaker, S.V. Antonyuk, V.S. Lamzin, P.M. Harrison, P.J. Artymiuk, J.W. Whittaker, Structure 9 (2001) 725–738.
[25] C.S. Coates, S. Milikisiyants, R. Chatterjee, M.M. Whittaker, J.W. Whittaker, K. V. Lakshmi, J. Phys. Chem. B 119 (2015) 4905–4916.
[26] N.J. Beal, P.J. O'Malley, J. Am. Chem. Soc. 138 (2016) 4358–4361.
[27] (a) B. Day, Biochem. Pharmacol. 77 (2009) 285–296;
(b) Y. Rong, S.R. Doctrow, G. Tocco, M. Baudry, Proc. Natl. Acad. Sci. U. S. A. 96 (1999) 9897–9902.
[28] S.R. Doctrow, M. Liesa, S. Melov, O.S. Shirihai, P. Tofil, Curr. Inorg. Chem. 2 (2012) 325–334.
[29] S.R. Doctrow, M. Baudry, K. Huffmann, B. Malfroy, S. Melov, in: J. S. Sessler, S. R. Doctrow, T. J. McMurray, S. J. Lippard (Eds.), Medicinal Inorganic Chemistry, American Chemical Society Symposium Series, 903, ACS and Oxford Press, 2005, Ch 18, pp. 319–347.
[30] S.R. Doctrow, K. Huffman, C. Bucay Marcus, G. Tocco, E. Malfroy, C.A. Adinolfi, H. Kruk, K. Baker, N. Lazarowych, J. Mascarenhas, B. Malfroy, J. Med. Chem. 45 (2002) 4549–4558.
[31] (a) S. Durot, C. Policar, F. Cisnetti, F. Lambert, J.-P. Renault, G. Pelosi, G. Blain, H.K. Youssoufi, J.-P. Mahy, Eur. J. Inorg. Chem. (2005) 3513–3523;
(b) Z.R. Liao, X.F. Zheng, B.S. Luo, L.R. Shen, D.F. Li, H.L. Liu, W. Zhao, Polyhedron 20 (2001) 2813–2821;
(c) J. Shearer, L.M. Long, Inorg. Chem. 45 (2006) 2358–2360;
(d) S. Dutta, S. Padhye, F. Ahmed, F. Sarkar, Inorg. Chim. Acta 358 (2005) 3617–3624;
(e) J.M. McCord, I. Fridovich, J. Biol. Chem. 244 (1969) 6049–6055;
(f) H.J. Forman, I. Fridovich, Arch. Biochem. Biophys. 158 (1973) 396–400;
(g) J. Butler, W.H. Koppenol, E. Margoliash, J. Biol. Chem. 257 (1982) 10747–10750.
[32] F.C. Friedel, D. Lieb, I. Ivanović-Burmazović, J. Inorg. Biochem. 109 (2012) 26–32.
[33] R. Li, J. Tian, H. Liu, S. Yan, S. Guo, J. Zhang, Trans. Met. Chem. 36 (2011) 811–817.
[34] Y. Noritake, N. Umezawa, N. Kato, T. Higuchi, Inorg. Chem. 52 (2013) 3653–3662.
[35] Y. Watanabe, A. Namba, N. Umezawa, M. Kawahata, K. Yamaguchi, T. Higuchi, Chem. Commun. (2006) 4958–4960.
[36] N.H. Khan, N. Pandya, M. Kumar, P.K. Bera, R.I. Kureshy, S.H.R. Abdi, H.C. Bajaj, Org. Biomol. Chem. 8 (2010) 4297–4307.
[37] N. Pandya, N.-U.H. Khan, K.J. Prathap, R.I. Kureshy, S.H.R. Abdi, S. Mishra, H.C. Bajaj, Chirality 24 (2012) 1063–1073.
[38] (a) R. Liu, I.Y. Liu, X. Bi, R.F. Thompson, S.R. Doctrow, B. Malfroy, M. Baudry, Proc. Natl. Acad. Sci. U.S.A. 100 (2003) 8526–8531;
(b) M. Zhou, M. Baudry, Brain Res. 1247 (2009) 28–37;
(c) S.R. Doctrow, A. López, A. Schock, N.E. Duncan, M.M. Jourdan, E.B. Olasz, J. E. Moulder, B.L. Fish, M. Mäder, J. Lazar, Z. Lazarova, J. Invest. Dermatol. 133 (2013) 1088–1096.
[39] W. Park, D. Lim, Bioorg. Med. Chem. Lett. 19 (2009) 614–617.
[40] (a) M.A. Vázquez-Fernández, M.R. Bermejo, M.I. Fernández-García, G. González-Riopedre, M.J. Rodríguez-Doutón, M. Maneiro, J. Inorg. Biochem. 105 (2011) 1538–1547;
(b) M. Maneiro, M.R. Bermejo, A. Sousa, M. Fondo, A.M. González, A. Sousa-Pedrares, C.A. McAuliffe, Polyhedron 19 (2000) 47–54.
[41] C. Palopoli, G. Gómez, A. Foi, F. Doctorovich, S. Mallet-Ladeira, C. Hureau, S. Signorella, J. Inorg. Biochem. 167 (2017) 49–59.
[42] N. Sarkar, P.K. Bhaumik, S. Chattopadhyay, Polyhedron 115 (2016) 37–46.
[43] D. Moreno, V. Daier, C. Palopoli, J.-P. Tuchagues, S. Signorella, J. Inorg. Biochem. 104 (2010) 496–502.
[44] (a) F. Bellia, D. La Mendola, C. Pedone, E. Rizzarelli, M. Saviano, G. Vecchio, Chem. Soc. Rev. 38 (2009) 2756–2781;
(b) V. Lanza, G. Vecchio, J. Inorg. Biochem. 103 (2009) 381–388.

[45] V. Oliveri, A. Puglisi, G. Vecchio, Dalton Trans. 40 (2011) 2913–2919.
[46] V. Oliveri, G. Vecchio, Eur. J. Med. Chem. 46 (2011) 961–965.
[47] H.-D. Bian, J. Wang, Y. Wei, J. Tang, F.-P. Huang, D. Yao, Q. Yu, H. Liang, Polyhedron 90 (2015) 147–153.
[48] X.-M. Zhang, J. Tang, L.-N. Wang, D. Yao, Q. Yu, F.-P. Huang, H.-D. Bian, Polyhedron 133 (2017) 433–440.
[49] J. Yu, L. Ge, S. Liu, P. Dai, S. Ge, W. Zheng, Biosensors Bioelectronics 26 (2011) 1936–1941.
[50] V. Daier, D. Moreno, C. Duhayon, J.-P. Tuchagues, S. Signorella, Eur. J. Inorg. Chem. (2010) 965–974.
[51] S. Signorella, V. Daier, G. Ledesma, C. Palopoli, D. Fernando Back, E.S. Lang, C. Rossini Kopp, P. Ebani, M. Brum Pereira, C. Giacomelli, P.C. Piquini, Polyhedron 102 (2015) 176–184.
[52] E.M. McGarrigle, D.G. Gilheany, Chem. Rev. 105 (2005) 1563–1602.
[53] (a) Y.G. Abashkin, S.K. Burt, Inorg. Chem. 44 (2005) 1425–1432;
(b) Y.G. Abashkin, S.K. Burt, J. Phys. Chem. B 108 (2004) 2708–2711.
[54] S.-Y. Liu, J.D. Soper, J.Y. Yang, E.V. Rybak-Akimova, D.G. Nocera, Inorg. Chem. 45 (2006) 7572–7574.
[55] J.I. Yang, D.G. Nocera, J. Am. Chem. Soc. 129 (2007) 8192–8198.
[56] V.R. Mundlapati, P. Jena, A.N. Acharya, A.K. Kar, A.C. Dash, H.S. Biswal, RSC Adv. 6 (2016) 111739–111746.
[57] M.A. Sharpe, R. Ollosson, V.C. Stewart, J.B. Clark, Biochem. J. 366 (2002) 97–107.
[58] T. Kurahashi, Inorg. Chem. 54 (2015) 8356–8366.
[59] E.J. Larson, V.L. Pecoraro, J. Am. Chem. Soc. 113 (1991) 7809–7810.
[60] J.A. Lessa, A. Horn Jr., E.S. Bull, M.R. Rocha, M. Benassi, R.R. Catharino, M.N. Eberlin, A. Casellato, C.J. Noble, G.R. Hanson, G. Schenk, G.C. Silva, O.A.C. Antunes, C. Fernandes, Inorg. Chem. 48 (2009) 4569–4579.
[61] Q.-X. Li, Q.-H. Luo, Y.-Z. Li, Z.-Q. Pan, M.-C. Shen, Eur. J. Inorg. Chem. (2004) 4447–4456.
[62] (a) M. Maneiro, M.R. Bermejo, M. Fondo, A.M. González, J. Sanmartín, J.C. García- Monteagudo, R.G. Pritchard, A.M. Tyryshkin, Polyhedron 20 (2001) 711–719;
(b) N.A. Law, J.W. Kampf, V.L. Pecoraro, Inorg. Chim. Acta 297 (2000) 252–264;
(c) H. Torayama, T. Nishide, H. Asada, M. Fujiwara, T. Matsushita, Polyhedron 17 (1998) 105–118;
(d) N. Aurangzeb, C.A. McAuliffe, R.G. Pritchard, M. Watkinson, M.R. Bermejo, A. Garcia-Deibe, A. Sousa, Acta Cryst C 49 (1993) 1945–1947.
[63] E.J. Larson, V.L. Pecoraro, J. Am. Chem. Soc. 113 (1991) 3810–3818.
[64] S. Durot, F. Lambert, J.-P. Renault, C. Policar, Eur. J. Inorg. Chem. (2005) 2789–2793.
[65] F. Cisnetti, G. Pelosi, C. Policar, Inorg. Chim. Acta 360 (2007) 557–562.
[66] J.S. Pap, B. Kripli, I. Bors, D. Bogáth, M. Giorgi, J. Kaizer, G. Speier, J. Inorg. Biochem. 117 (2012) 60–70.
[67] E.R. Milaeva, D.B. Shpakovsky, Y.A. Gracheva, S.I. Orlova, V.V. Maduar, B.N. Tarasevich, N.N. Meleshonkova, L.G. Dubovab, E.F. Shevtsova, Dalton Trans. 42 (2013) 6817–6828.
[68] H. Wu, Y. Zhang, J. Zhang, Z. Yang, C. Chen, H. Peng, F. Wang, Trans. Met Chem 40 (2015) 145–152.
[69] L. Dubois, J. Pécaut, M.-F. Charlot, C. Baffert, M.-N. Collomb, A. Deronzier, J.-M. Latour, Chem. Eur. J. 14 (2008) 3013–3025.
[70] D.-F. Zhou, Q.-Y. Chen, Y. Qi, H.-J. Fu, Z. Li, K.-D. Zhao, J. Gao, Inorg. Chem. 50 (2011) 6929–6937.
[71] B.K. Shin, M. Kim, J. Han, Polyhedron 29 (2010) 2560–2568.
[72] T.P. Ribeiro, C. Fernandes, K.V. Melo, S.S. Ferreira, J.A. Lessa, R.W.A. Franco, G. Schenk, M.D. Pereira, A. Horn Jr., Free Radical Biol. Med. 80 (2015) 67–76.
[73] G. Berggren, P. Huang, L. Eriksson, S. Styring, M.F. Anderlund, A. Thapper, Dalton Trans. 39 (2010) 11035–11044.
[74] C. Hureau, G. Blondin, M.-F. Charlot, C. Philouze, M. Nierlich, M. Césario, E. Anxolabéhère-Mallart, Inorg. Chem. 44 (2005) 3669–3683.
[75] G. Berggren, A. Thapper, P. Huang, P. Kurz, L. Eriksson, S. Styring, M.F. Anderlund, Dalton Trans. (2009) 10044–10054.
[76] F. Cisnetti, A.-S. Lefèvre, R. Guillot, F. Lambert, G. Blain, E. Anxolabéhère-Mallart, C. Policar, Eur. J. Inorg. Chem. (2007) 4472–4480.
[77] A.S. Bernard, C. Giroud, H.Y.V. Ching, A. Meunier, V. Ambike, C. Amatore, M.G. Collignon, F. Lemaître, C. Policar, Dalton Trans. 41 (2012) 6399–6403.
[78] E. Mathieu, A.-S. Bernard, N. Delsuc, E. Quévrain, G. Gazzah, B. Lai, F. Chain, P. Langella, M. Bachelet, J. Masliah, P. Seksik, C. Policar, Inorg. Chem. 56 (2017) 2545–2555.
[79] H.Y.V. Ching, E. Anxolabéhère-Mallart, H.E. Colmer, C. Costentin, P. Dorlet, T. A. Jackson, C. Policar, M. Robert, Chem. Sci. 5 (2014) 2304–2310.
[80] S. Groni, G. Blain, R. Guillot, C. Policar, E. Anxolabéhère-Mallart, Inorg. Chem. 46 (2007) 1951–1953.
[81] R.A. Geiger, D.F. Leto, S. Chattopadhyay, P. Dorlet, E. Anxolabéhère-Mallart, T. A. Jackson, Inorg. Chem. 50 (2011) 10190–10203.
[82] D.F. Leto, S. Chattopadhyay, V.W. Day, T.A. Jackson, Dalton Trans. 42 (2013) 13014–13025.
[83] H.Y.V. Ching, I. Kenkel, N. Delsuc, E. Mathieu, I. Ivanović-Burmazović, C. Policar, J. Inorg. Biochem. 160 (2016) 172–179.
[84] M. Yu, R.J. Beyers, J.D. Gorden, J.N. Cross, C.R. Goldsmith, Inorg. Chem. 51 (2012) 9153–9155.
[85] M. Yu, S.L. Ambrose, Z.L. Whaley, S. Fan, J.D. Gorden, R.J. Beyers, D.D. Schwartz, C.R. Goldsmith, J. Am. Chem. Soc. 136 (2014) 12836–12839.
[86] I. Kenkel, A. Franke, M. Dürr, A. Zahl, C. Dücker-Benfer, J. Langer, M.R. Filipović, M. Yu, R. Puchta, S.R. Fiedler, M.P. Shores, C.R. Goldsmith, I. Ivanović-Burmazović, J. Am. Chem. Soc. 139 (2017) 1472–1484.
[87] G.N. Ledesma, S.R. Signorella, Tetrahedron Lett. 53 (2012) 5699–5702.
[88] G.N. Ledesma, H. Eury, E. Anxolabéhère-Mallart, C. Hureau, S.R. Signorella, J. Inorg. Biochem. 146 (2015) 69–76.
[89] G.N. Ledesma, E. Anxolabéhère-Mallart, E. Rivière, S. Mallet-Ladeira, C. Hureau, S.R. Signorella, Inorg. Chem. 53 (2014) 2545–2553.
[90] D.P. Riley, O.F. Schall, Adv. Inorg. Chem. 59 (2007) 233–263.
[91] D.P. Riley, R.H. Weiss, J. Am. Chem. Soc. 116 (1994) 387–388.
[92] D.P. Riley, P.J. Lennon, W.L. Neumann, R.H. Weiss, J. Am. Chem. Soc. 119 (28) (1997) 6522–6528.
[93] D.P. Riley, S.L. Henke, P.L. Lennon, R.H. Weiss, W.L. Neumann, W.J. Jr, K.W. Rivers, K.R. Aston, H. Sample, C.-S. Rahman, J.J.-J. Ling, D.H. Shieh, W. Szulbinski Busch, Inorg. Chem. 35 (1996) 5213–5231.
[94] D.P. Riley, Adv. Supramol. Chem. 6 (2000) 217–244.
[95] (a) D. Salvemini, Z.Q. Wang, J.L. Zweier, A. Samouilov, H. Macarthur, T.P. Misko, M.G. Currie, S. Cuzzocrea, J.A. Sikorski, D.P. Riley, Science 286 (1999) 304–306;
(b) D. Salvemini, D.P. Riley, Cell Mol. Life Sci. 57 (2000) 1489–1492;
(c) K.W. Aston, N. Rath, A. Naik, U. Slomczynski, O.F. Schall, D.P. Riley, Inorg. Chem. 40 (2001) 1779–1789.
[96] C.M. Anderson, B.G. Allen, W. Sun, C.M. Lee, S. Agarwala, M. Venigalla, L. Greenberg, D. Adkins, Y. Chen, W. Zhen, D. Mould, J. Holmlund, J. Brill, S. Sonis, J. Buatti, Int. J. Radiat. Oncol., Biol., Phys. 94 (2016) 869–870.
[97] A. Maroz, G.F. Kelso, R.A.J. Smith, D.C. Ware, R.F. Anderson, J. Phys. Chem. A 112 (2008) 4929–4935.
[98] A. Dees, A. Zahl, R. Puchta, N.J.R. van Eikema Hommes, F.W. Heinemann, I. Ivanovic-Burmazovic, Inorg. Chem. 46 (2007) 2459–2470.
[99] I. Ivanović-Burmazović, R. van Eldik, Dalton Trans. (2008) 5259–5275.
[100] I. Ivanović-Burmazović, Adv. Inorg. Chem. 60 (2008) 59–100.
[101] G.-F. Liu, M. Filipovic, F.W. Heinemann, I. Ivanovic-Burmazovic, Inorg. Chem. 46 (2007) 8825–8835.
[102] G.-F. Liu, K. Dürr, R. Puchta, F.W. Heinemann, R. van Eldik, I. Ivanović-Burmazović, Dalton Trans. (2009) 6292–6295.
[103] M. Kose, P. Goring, P. Lucas, V. Mckee, Inorg. Chim. Acta 435 (2015) 232–238.
[104] D. Lieb, F.C. Friedel, M. Yawer, A. Zahl, M.M. Khusniyarov, F.W. Heinemann, I. Ivanović-Burmazović, Inorg. Chem. 52 (2013) 222–236.
[105] H. Lee, W. Park, D. Lim, Bioorg. Med. Chem. Lett. 20 (2010) 2421–2424.
[106] D. Lieb, I. Kenkell, J.L. Miljković, D. Moldenhauer, N. Weber, M.R. Filipović, F. Gröhn, I. Ivanović-Burmazović, Inorg. Chem. 53 (2014) 1009–1020.
[107] (a) I. Spasojević, I. Batinić-Haberle, R.D. Stevens, P. Hambright, A.N. Thorpe, J. Grodkowski, P. Neta, I. Fridovich, Inorg. Chem. 40 (2001) 726–739;
(b) K. Barnese, E.B. Gralla, D.E. Cabelli, J.S. Valentine, J. Am. Chem. Soc. 130 (2008) 4604–4606.
[108] C.M. Weekley, I. Kenkel, R. Lippert, S. Wei, D. Lieb, T. Cranwell, J.L. Wedding, A.S. Zillmann, R. Rohr, M.R. Filipovic, I. Ivanović-Burmazović, H.H. Harris, Inorg. Chem. 56 (2017) 6076–6093.
[109] (a) M.R. Filipović, K. Duerr, M. Mojović, V. Simeunović, R. Zimmermann, V. Niketić, I. Ivanović-Burmazović, Angew. Chem., Int. Ed. 47 (2008) 8735–8739;
(b) M.R. Filipović, A.C.W. Koh, S. Arbault, V. Niketić, A. Debus, U. Schleicher, C. Bogdan, M. Guille, F. Lemaître, C. Amatore, I. Ivanović-Burmazović, Angew. Chem., Int. Ed. 49 (2010) 4228–4232.
[110] W.-T. Lee, S.B. Muñoz III, D.A. Dickie, J.M. Smith, Angew. Chem. Int. Ed. 53 (2014) 9856–9859.
[111] (a) W.-T. Lee, S. Xu, D.A. Dickie, J.M. Smith, Eur. J. Inorg. Chem. (2013) 3867–3873;
(b) S. Xu, L. Bucinsky, M. Breza, J. Krzystek, C.-H. Chen, M. Pink, J. Telser, J.M. Smith, Inorg. Chem. 56 (2017) 14315–14325.
[112] M.P. Clares, S. Blasco, M. Inclán, L. del Castillo-Agudo, B. Verdejo, A. Doménech, C. Soriano, E. García-España, Chem. Commun. 47 (2011) 5988–5990.
[113] M.P. Clares, C. Serena, S. Blasco, A. Nebot, L. del Castillo, C. Soriano, A. Domènech, A.V. Sánchez-Sánchez, L. Soler-Calero, J.L. Mullor, A. García-España, E. García-España, J. Inorg. Biochem. 143 (2015) 1–8.
[114] P. Failli, D. Bani, A. Bencini, M. Cantore, L. Di Cesare Mannelli, C. Ghelardini, C. Giorgi, M. Innocenti, F. Rugi, A. Spepi, R. Udisti, B. Valtancoli, J. Med. Chem. 52 (2009) 7273–7283.
[115] R.F. Pasternack, B. Halliwell, J. Am. Chem. Soc. 101 (1979) 1026–1031.
[116] R.F. Pasternack, A. Banth, J.M. Pasternack, C.S. Johnson, J. Inorg. Biochem. 15 (1981) 261–267.
[117] A. Tovmasyan, C.G. Maia, T. Weitner, S. Carballal, R.S. Sampaio, D. Lieb, R. Ghazaryan, I. Ivanovic-Burmazovic, G. Ferrer-Sueta, R. Radi, J.S. Reboucas, I. Spasojevic, L. Benov, I. Batinic-Haberle, Free Radical Biol. Med. 86 (2015) 308–321.
[118] S. Miriyala, I. Spasojevic, A. Tovmasyan, D. Salvemini, Z. Vujaskovic, D. St. Clair, I. Batinic-Haberle, Biochem. Biophys. Acta 1822 (2012) 794–814.
[119] J.J. Perry, D.S. Shin, E.D. Getzoff, J.A. Tainer, Biochim. Biophys. Acta 2010 (1804) 245–262.
[120] (a) I. Batinic-Haberle, L. Benov, I. Spasojevic, I. Fridovich, J. Biol. Chem. 273 (1998) 24521–24528;
(b) I. Batinic-Haberle, I. Spasojevic, P. Hambright, L. Benov, A.L. Crumbliss, I. Fridovich, Inorg. Chem. 38 (1999) 4011–4022.
[121] J.S. Rebouças, G. DeFreitas-Silva, I. Spasojević, Y.M. Idemori, L. Benov, I. Batinić-Haberle, Free Radical Biol. Med. 45 (2008) 201–210.
[122] B.J. Day, I. Fridovich, J.D. Crapo, Arch. Biochem. Biophys. 347 (1997) 256–262.
[123] M.P. Trova, P.J.F. Gauuan, A.J. Pechulis, S.M. Bubb, S.B. Bocckino, J.D. Crapo, B.J. Day, Bioorg. Med. Chem. 11 (2003) 2695–2707.

[124] P.J.F. Gauuan, M.P. Trova, L. Gregor-Boros, S.B. Bocckino, J.D. Crapo, B.J. Day, Bioorg. Med. Chem. 10 (2002) 3013–3021.
[125] J.S. Reboucas, I. Spasojevic, I. Batinic-Haberle, J. Biol. Inorg. Chem. 13 (2008) 289–302.
[126] T-.J. Wu, N.H. Khoo, F. Zhou, B.J. Day, D.A. Parks, Free Radical Res. 41 (2007) 127–134.
[127] R.A. Rosenthal, K.D. Huffman, L.W. Fisette, C.A. Damphousse, W.B. Callaway, B. Malfroy, S.R. Doctrow, J. Biol. Inorg. Chem. 14 (2009) 979–991.
[128] B. Meunier, F. Cosledan, UPatent 2006/0241095 A1, October 2006.
[129] E. Vorotnikova, R.A. Rosenthal, M. Tries, S.R. Doctrow, S.R. Braunhut, Radiat. Res. 173 (2010) 748–759.
[130] Z. Fucks, R.S. Persuad, A. Alfieri, M. McLoughlin, D. Ehleiter, J.L. Schwartz, A.P. Seddon, C. Cordon-Cardo, A. Haitmovitz-Friedman, Cancer Res. 54 (1994) 2582–2590.
[131] H.B. Stone, J.E. Moulder, C.N. Coleman, K.K. Ang, M.S. Anscher, M.H. Barcellos-Hoff, W.S. Dynan, J.R. Fike, D.J. Grdina, J.S. Greenberger, M. Hauer-Jensen, R.P. Hill, R.N. Kolesnick, T.J. Macvittie, C. Marks, W.H. McBride, N. Metting, T. Pellmar, M. Purucker, M.E. Robbins, R.H. Schiestl, T.M. Seed, J.E. Tomaszewski, E.L. Travis, P.E. Wallner, M. Wolpert, D. Zaharevitz, Radiat. Res. 162 (2004) 711–728.
[132] S. Kubota, S. Imamura, T. Shimizu, S. Asayama, H. Kawakami, ACS Med. Chem. Lett. 5 (2014) 639–643.
[133] R. Kubota, S. Asayama, H. Kawakami, Chem. Commun. 50 (2014) 15909–15912.
[134] B. Li, X. Dong, N. Li, J. Gao, Q. Yuan, S. Fang, X. Gong, S. Wang, F. Wang, Exp. Biol. Med. (Maywood) 239 (2014) 1366–1379.
[135] (a) B. Li, S. Fang, X. Dong, N. Li, J. Gao, G. Yang, X. Gong, S. Wang, F. Wang, Eur. J. Drug Metab. Pharmacokinet. 38 (2013) 245–253;
(b) B. Li, X. Dong, G. Yang, N. Li, J. Gao, S. Fang, X. Gong, S. Wang, F. Wang, Lat. Am. J. Pharm. 32 (2013) 257–262.
[136] R.F. Beers, I.W. Sizer, J. Biol. Chem. 195 (1952) 133–140.
[137] A. Squarcina, A. Sorarú, F. Rigodanza, M. Carraro, G. Brancatelli, T. Carofiglio, S. Geremia, V. Larosa, T. Morosinotto, M. Bonchio, ACS Catal. 7 (2017) 1971–1976.
[138] N. Jin, D.E. Lahaye, J.T. Groves, Inorg. Chem. 49 (2010) 11516–11524.
[139] N. Jin, J.T. Groves, J. Am. Chem. Soc. 121 (1999) 2923–2924.
[140] M.K. Evans, A. Tovmasyan, I. Batinic-Haberle, G.R. Devi, Free Radical Biol. Med. 68 (2014) 302–314.
[141] I. Batinic-Haberle, A. Tovmasyan, I. Spasojevic, Redox Biol. 5 (2015) 43–65.
[142] R.A. Baglia, J.P.T. Zaragoza, D.P. Goldberg, Chem. Rev. 117 (2017) 13320–13352.
[143] I. Batinic-Haberle, A. Tovmasyan, in: Donald Armstrong, Robert D. Stratton (Eds.), Oxidative Stress and Antioxidant Protection: The Science of Free Radical Biology and Disease, John Wiley & Sons, 2016, chapter 27.
[144] A. Haber, Z. Gross, Chem. Commun. 51 (2015) 5812–5827.
[145] M. Eckshtain, I. Zilbermann, A. Mahammed, I. Saltsman, Z. Okun, E. Maimon, H. Cohen, D. Meyerstein, Z. Gross, DaltonTrans. (2009) 7879–7882.
[146] Z. Okun, Z. Gross, Inorg. Chem. 51 (2012) 8083–8090.
[147] A. Mahammed, Z. Gross, Chem. Commun. 46 (2010) 7040–7042.
[148] A. Mahammed, Z. Gross, J. Am. Chem. Soc. 127 (2005) 2883–2887.
[149] (a) R. Csonka, G. Speier, J. Kaizer, RSC Adv. (2015) 18401–18419;
(b) J.S. Pap, B. Kripli, T. Varadi, M. Giorgi, J. Kaizer, G. Speier, J. Inorg. Biochem. 105 (2011) 911–918.
[150] J. Kaizer, G. Barath, G. Speier, M. Reglier, M. Giorgi, Inorg. Chem. Commun. 10 (2007) 292–294.
[151] J. Kaizer, T. Csay, P. Kövári, G. Speier, L. Párkányi, J. Mol. Catal. A-Chem. 280 (2008) 203–209.
[152] J. Kaizer, B. Kripli, G. Speier, L. Párkányi, Polyhedron 28 (2009) 933–936.
[153] H. Wu, F. Shi, X. Wang, Y. Zhang, Y. Bai, J. Kong, C. Wang, Trans. Met Chem. 39 (2014) 261–270.
[154] K. Ghosh, N. Tyagi, P. Kumar, U.P. Singh, N. Goel, J. Inorg. Biochem. 104 (2010) 9–18.
[155] G. Lupidi, F. Marchetti, N. Masciocchi, D.L. Reger, S. Tabassum, P. Astolfi, E. Damiani, C. Pettinari, J. Inorg. Biochem. 104 (2010) 820–830.
[156] M. Kose, V. McKee, Polyhedron 75 (2014) 30–39.
[157] M. Grau, F. Rigodanza, A.J.P. White, A. Sorarù, M. Carraro, M. Bonchio, G.J.P. Britovsek, Chem. Commun. 50 (2014) 4607–4609.
[158] M. Zienkiewicz, A. Jabłońska-Wawrzycka, J. Szlachetko, Y. Kayser, K. Stadnicka, W. Sawka-Dobrowolska, J. Jezierska, B. Barszcz, J. Sá, Dalton Trans. 43 (2014) 8599–8608.
[159] M. Zienkiewicz, J. Szlachetko, C. Lothschütz, M. Hodorowicz, A. Jabłońska-Wawrzycka, J. Sá, B. Barszcz, Dalton Trans. 42 (2013) 7761–7767.
[160] R. Joshi, Radiat. Phys. Chem. 139 (2017) 74–82.